INTERROGATION OF BIOMOLECULAR INTERACTIONS UTILIZING

BACKSCATTERING INTERFEROMETRY

By

Amanda K. Kussrow

Dissertation

Submitted to the Faculty of the

Graduate School of Vanderbilt University

in partial fulfillment of the requirements

for the degree of

DOCTOR OF PHILOSOPHY

in

CHEMISTRY

December, 2009

Nashville, Tennessee

Approved:

Professor Darryl J. Bornhop

Professor Walter J. Chazin

Professor David E. Cliffel

Professor Sandra J. Rosenthal

To My Parents:
For all their love and support

ACKNOWLEDGEMENTS

TABLE OF CONTENTS

LIST OF TABLES

LIST OF FIGURES

CHAPTER 1

INTRODUCTION AND BACKGROUND

Importance of Molecular Interactions:

Proteins are the molecular machines that carry out the basic biological functions in cells and are therefore a major research focus for biologists, chemists, and biochemists.[1-6] In order to make novel advances in the medical field, it is necessary to identify target proteins involved in disease pathogenesis and to determine how these proteins interact with other molecules.[7] However, binding to proteins can be a complex process with multiple aspects to consider, including the mechanism of the binding process, the structural basis of the binding, and the functional outcomes. Factors that may complicate interaction studies include multi-step binding, influences from post-translational modifications, and sensitivity to the physical and chemical environment. Specifically, changes in environmental factors such as pH, temperature, and ionic strength may significantly reduce or completely inhibit binding to proteins. Monitoring of binding interactions can be impacted by the stoichiometric ratio of protein to ligand, as well as the binding affinity. Binding studies may also be complicated when the protein of interest must first be produced via expression in cells, an often difficult and time-consuming process that may produce only a miniscule amount of the protein for analysis or screening. The development of biosensing tools that can accommodate and overcome these challenges is critical to the study of molecular interactions. The work

presented in this thesis will focus on the detection of interactions and the measurement of the strength of these interactions through the calculation of the dissociation constant (K_D).

Methods to Study Molecular Interactions:

A number of methods are currently available to monitor binding of ligands to proteins, including fluorescence spectroscopy, isothermal titration calorimetry (ITC), nuclear magnetic resonance (NMR) spectroscopy, surface plasmon resonance (SPR), quartz crystal microbalance (QCM), analytical ultracentrifugation (AUC) and interferometry. Although each is effective for specific applications, these methods also possess certain limitations. Several approaches require a label of some type (e.g. fluorescent); some involve complicated surface chemistry (e.g. SPR, QCM), while others have low sensitivity and require large sample quantities (e.g., ITC, NMR). Therefore, there is a great need for an efficient detection method that will allow the experiments to be performed in small volumes, in free solution, and label-free. Also, having a single approach to the study of a binding system allows for better comparisons between measurements.

Fluorescence spectroscopy measures the light emitted from a molecule upon excitation by a light source. Fluorescence is a well-established technique used to measure binding with very high sensitivity, allowing for the detection of a single molecule.[8-10] However, fluorescence is often expensive to implement and can only be used in systems that are naturally fluorescent (very few) or that have been chemically modified with a fluorescent tag. Furthermore, the addition of a label can greatly affect affinity or binding due to an alteration in the protein structure.[1]

ITC takes advantage of the fact that heat is a universal signal that will always be absorbed or produced when compounds interact. ITC is performed by monitoring the heat change for a series of small injections of ligand. Many values of interest, such as ΔG, ΔH, and ΔS, as well as K_D, can be extracted from ITC experiments. However, despite the advantage of being able to calculate these constants, the disadvantages of ITC are that the assay typically requires long analysis times and significantly more material than other methods due to the large sample volumes and the high concentrations required.[11-14] Large sample quantities are particularly problematic when there is a limited amount of the protein available to perform the study.

NMR is another tool that has been widely used for the determination of dissociation constants, based either on the changes in the chemical shifts, the relaxation time measurements, or the diffusion measurements.[15-20] A major benefit of NMR is the ability to determine structural information about the binding site, given that the three-dimensional structure of the protein of interest and the NMR assignments of the protein backbone are known.[21] However the major limitation of NMR methodologies is low sensitivity, which results in the need for large amounts of sample. This results in NMR being best suited to studying mid to low affinity ligands.[21] Also, chemical shift changes are difficult to interpret because they are affected by many factors.[15-22]

SPR has also become a common technique for label-free monitoring of protein binding in small volumes.[23-28] SPR measures the localized change in the refractive index (RI) near the surface in order to detect binding[29-32] and has been used in a multiplex format.[33] SPR has the advantage of being able to determine forward and reverse reaction rates of the binding in order to calculate the dissociation constant. However, any

3

refractive index change between different solutions must be taken into account when using this technique. Also, SPR is a heterogeneous method that requires complicated surface chemistry and expensive gold-plated slides.[30,31,33] The attachment of a molecule to a surface can also change the protein structure which can affect the binding[23] and/or alter the affinity of the interaction,[13,27,28,34,35] especially if the molecule must be mutated in order to make the attachment possible.[36] Furthermore, the surface loading of the chip is critical to protein binding determinations as different methods of attachment can cause variations in the K_D values calculated. Finally, the SPR measurements are mass sensitive, which makes it difficult to monitor the binding of a small ligand to a large protein without immobilizing the ligand.[11,27,28,37,38]

QCM is comprised of a small crystal disc that is positioned between two electrodes. When a voltage is applied to the electrodes, the crystal is strained causing it to resonate at a unique frequency. The resonance frequency of the crystal is altered when there is a change in mass at the surface of the crystal. QCM can therefore be a very sensitive technique to study molecular interactions by immobilizing a receptor to the surface of the crystal; measuring the change in the resonance frequency of the crystal as the ligand binds.[39-41] Since the frequency of the crystal resonator is sensitive to any change at the surface, non-specific binding can be problematic and must be carefully accounted for. It is also necessary to thoroughly calibrate the system with the solutions to adjust for any affect the liquid may have on the resonance frequency.[42] QCM is also limited to a surface immobilized format, which can change the conformation of proteins and alter the measured affinities.[23,36]

AUC monitors the sedimentation of molecules in a centrifugal field in order to measure the binding of molecules by separating the bound and unbound molecules based on their size and shape.[43-45] AUC can measure interactions in free solution with modest requirements for sample quantity, but instrumentation can be difficult, requiring optical measurements to be taken while the sample is spinning at high speeds.[43,46] Additionally, common stabilizers, such as sugars, can hinder detection and must be carefully taken into account.[47]

Interferometric Methods:

When two or more light waves are superimposed, an interference pattern is created. By studying these patterns, the properties of the light waves and the material that they have been in contact with can be explored. This field, known as interferometry, has led to the development of some of the most sensitive optical techniques available and has been implemented for various applications, including astronomy, metrology, oceanography, seismology, and biological sciences.

Interferometry has also been applied to biological sciences as a tool to monitor and quantify molecular interactions.[48] Interferometry also offers the dual advantage of being a highly sensitive technique that does not require the use of expensive molecular labels. Therefore, molecular interactions may be characterized with both binding partners in their native states, eliciting quantitative, meaningful (i.e. unperturbed by labeling) affinity data in a cost-effective format. Here we describe several different types of interferometers which have been successfully utilized to study molecular interactions.

Mach-Zehnder Interferometer:

The Mach-Zehnder interferometer (MZI) utilizes a waveguiding method to monitor the difference in refractive index (RI) between the sample and the reference arm of the waveguide (Figure 1.1). A laser illuminates a single-mode waveguide which is then split into a sample and reference arm. The reference arm is coated with a thin cladding layer, while the sample arm has a window to allow the evanescent field to interact with the sample. The sensor and reference arms are then recombined, leading to beam interference. Any change in the sample's refractive index produces a phase shift in the sensor arm beam, which in turn results in a change in the output intensity when the two beams are recombined. Binding events are thereby measurable using photodetection. Intrinsically, the evanescent sensing approach of the MZI instrumental configuration requires a single polarization and single-mode illumination to prevent interference from cross-polarization and multimodal effects. The sensitivity of the MZI is typically correlated with the length of the sensing window, which makes it difficult to measure low concentrations of analytes without using large amounts of sample.

The MZI was first used for biosensing in 1993 and has since been utilized in a broad range of applications.[48-52] In 1997, Brosinger *et al.*, demonstrated the ability to resolve a refractive index change of 2×10^{-5} refractive index units (RIU) with their early MZI configuration.[49] Initial experiments to test the biosensing ability of the instrument were also reported, demonstrating that MZI can detect fetal calf serum binding nonspecifically to the sensor surface.[49] More recently, Prieto *et al.* used a Mach-Zehnder interferometer total internal reflection (MZI-TIR) configuration to achieve a minimum refractive index change of 7×10^{-6} at the sensor surface. The utility of the instrument
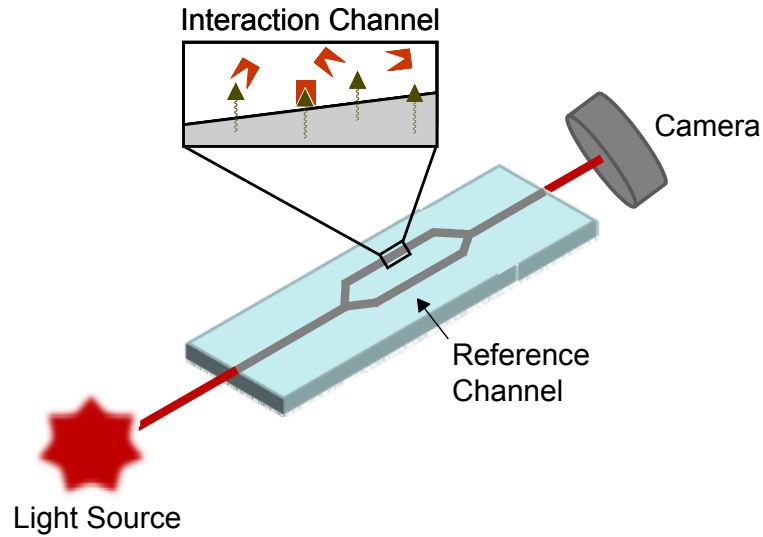
Figure 1.1: Block diagram of a Mach-Zehnder interferometer (MZI).

was demonstrated by detecting the interaction between a covalently immobilized pesticide and its antibody in PBST (phosphate buffered saline Tween).[50] The same group also constructed an MZI based on a rib anti-resonant reflecting optical waveguide (ARROW). The use of ARROW structures instead of conventional TIR waveguides allows for larger core and rib dimensions, making the instrument more compatible with mass-production, as well as lowering insertion losses. However, these advantages are accompanied by a loss in sensitivity as the minimum detectable refractive index change for the MZI-ARROW was found to be 2×10^{-5}.[51]

Young Interferometer:

Another waveguiding interferometer is the Young interferometer (YI). The YI configuration includes a single-mode laser illuminating a single-mode waveguide, which is then split into a sample and reference arm, as in the Mach-Zehnder interferometer
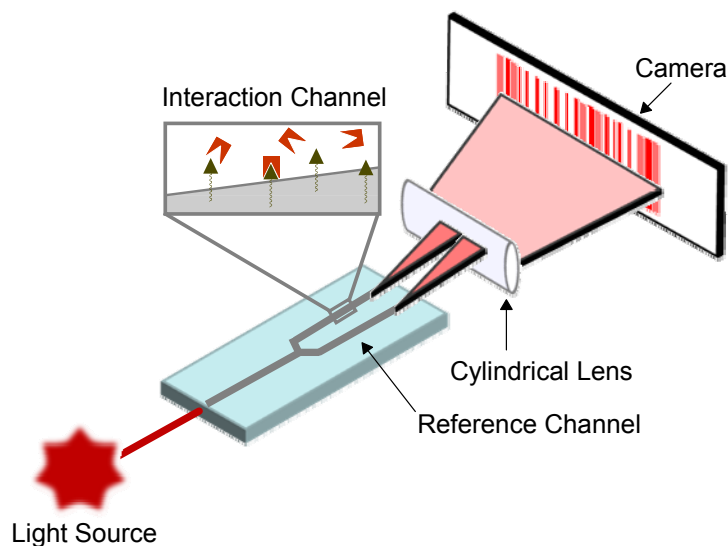
Figure 1.2: Block diagram of a Young interferometer (YI).

(Figure 1.2). However, instead of the interference being created when the waveguides recombine as in the MZI, in a YI the optical output of the waveguides interact in free space to create the interference fringes, which are displayed onto a CCD camera.

The YI was first used to measure molecular interactions in 1994[48] and has been widely published on thereafter.[53-55] In 2003, Ymeti *et al*. showed that their multi-channel YI configuration can measure four different analyte concentrations simultaneously, achieving a refractive index resolution of 8.5×10^{-8} RIU.[53] In 2006, Hradetzky *et al*. reported a refractive index detection limit of 0.9×10^{-6} for their single-cell YI, and detected the hybridization of 21-mer DNA with immobilized receptor DNA at the biosensor surface.[54] These finding suggest the detection limit of this DNA-DNA binding interaction to be in the picomolar range.

Hartman Interferometer:

The Hartman interferometer (HI) is also a waveguiding technique; however, in contrast with the MZI and YI, this approach utilizes a planar waveguide that is patterned with lines of immobilized molecules. Light is directed into the waveguide through a grating to create a single broad beam. The light then passes through parallel sensing regions which are coated with different receptors to create distinct binding and control regions. The light then travels though integrated optics that combine the light from neighboring regions to create interference. The interference signals then pass through another grating and to the detector. The phase shift of the interference patterns is measured to detect refractive index changes.

In 1997, Schneider *et al*. demonstrated the broad applications of the HI as a real-time detector of nucleic acid, protein, and pathogen analytes. Experiments were performed by immobilizing the receptor (anti-hCG antibody) to the sensor surface, allowing for real-time detection of human chorionic gonadotropin (hCG) with a direct detection limit of 2 ng/mL in phosphate buffered saline (PBS). DNA hybridization
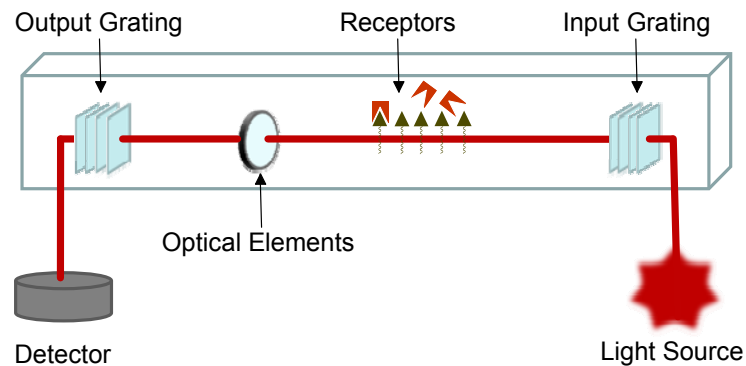
Figure 1.3: Block diagram of a Hartman interferometer (HI).

experiments detected a four-base mismatch in 50% formamide hybridization buffer, and a nucleic acid detection capability of 10^{11} copies per mL was achieved.[56] In early 2000, the same group expanded on these applications, demonstrating the ability of their configuration to detect hCG in human serum at clinically relevant levels of 0.1 ng/mL. Extensive studies of the nonspecific binding associated with serum samples were also performed, which concluded that the HI can overcome this particular setback using a reference region and controlled surface chemistry.[57] Later that year, Schneider *et al*. took their studies a step further by detecting hCG in whole blood; despite significantly higher background levels than buffer or serum systems, a clinically relevant detection limit of 0.5 ng/mL hCG was achieved.[58]

Diffraction Optics:

Diffraction-based sensing employs a similar technique of immobilizing the probe molecules into a pattern that will diffract the incoming laser light to create an interference pattern (Figure 1.4). This pattern has been shown to change as sample is introduced and binding occurs on the stripes of capture species, resulting in a change in the height and refractive index of the diffraction grating. The intensity of the refractive spots is measured using a photodectector, allowing any changes within the sample to be measured. While many applications of diffraction optics offer enhanced performance when used in conjunction with labeling strategies, the following examples focus primarily on label-free applications of the technique.

Early studies by St. John *et al*. demonstrated that diffraction optics can be used to detect whole bacteria cells captured using an antibody grating stamped on a silicon
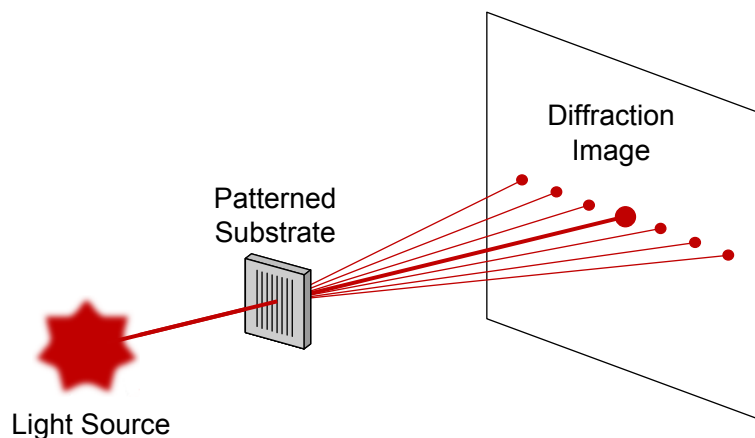
Figure 1.4: Block diagram of diffraction optics.

surface.[59] Goh *et al.* demonstrated the ability of diffraction optics to measure two different binding interactions simultaneously without the use of labels. To achieve this, receptor molecules mouse IgG and rabbit IgG were immobilized in two different patterns via PDMS stamping on the same 2D surface. Anti-mouse IgG and anti-rabbit IgG were then introduced into the cell sequentially and the binding observed for each pattern indicated specific binding of the target analyte exclusively to its receptor antibody. These findings carry implications for diagnostic applications involving multiple markers and/or competition assays.[60] Currently, Axela Biosensors offers a commercialized diffraction-based sensor known as the dotLab™ System which enables multiplexing of immunoassays over a broad dynamic range. They demonstrated the ability to simultaneously measure binding of two similar sets of antibody/analyte pairs with concentrations which differed by 6 orders of magnitude; however, labeling strategies were implemented to measure the analyte of lower concentration.[61] Savran *et al*. has used diffraction optics coupled with a magnetic bead labeling system to quantify

11

biomarkers S-adenosyl homocysteine (in solution) and folate receptor (in serum) with sensitivities of 24.5 pg/mL and 20 pg/mL, respectively.[62,63]

Dual Polarization:

The dual polarization interferometer (DPI) is another waveguide method for studying molecular interactions. This technique utilizes two waveguides, a sample and reference waveguide, which are stacked together, so they may be illuminated by a single laser with the resultant light exiting the waveguides form an interference pattern in the far field (Figure 1.5). In contrast with other waveguide sensors, the polarization of the laser in the DPI is alternated so that two polarization modes of the waveguides are excited in succession in order to modulate the signal and increase sensitivity. Using the information from the measurements of both polarization states, the refractive index and the thickness of the adsorbed protein layer can be calculated.

Swann *et al.* measured the binding and surface loading of streptavidin to the biotin-functionalized surface of their DPI to monitor nonspecific binding, thickness, and
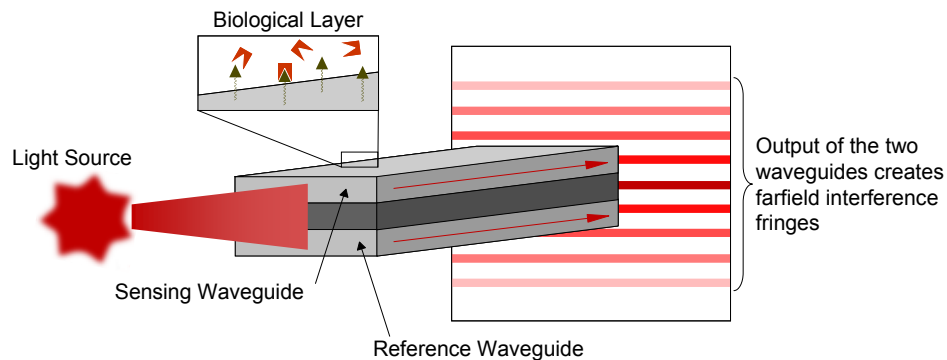
Figure 1.5: Block diagram of a dual polarization interferometer (DPI).

density changes of protein layers as well as other structural aspects of the streptavidin-biotin system.[64] In 2006, Lin *et al.* used DPI to derive dissociation constants (K_D) for homopolyvalent pentameric C-reactive protein (CRP) with monoclonal anti-CRP IgG; these values were in close agreement with those previously derived using enzyme-linked immunosorbent assays (ELISA).[65] That same year, Ricard-Blum *et al.* measured the interaction of immobilized heparin with heparin binding protein HepV. Exploring the stochiometric and kinetic parameters of this binding system using DPI lent insight into collagen V interaction with proteoglycans in tissues, a process which affects collagen fibril formation.[66] Wang *et al.* utilized DPI to measure the structural changes of electrostatically immobilized DNA upon binding to small molecules ethidium bromide and spermine in real time. Changes in mass, thickness, and refractive index of the DNA sample layer (consisting of either native or denatured DNA) were monitored upon small molecule binding. These studies harnessed the ability of DPI to measure structure and kinetics simultaneously and the flexibility of the technology to interrogate binding interactions over a large molecular size range.[67] Farfield Sensors, Ltd has been commercializing DPI-based biosensing systems since 2000 with the introduction of the AnaLight® 250, and has most recently released the AnaLight® 4D which enables the measurement of structural changes within lipid bilayers.[68,69]

Porous Si Sensors:

Porous silicon sensors have been developed using the principles of the Fabry-Perot interferometer on thin films of porous silicon etched in a silicon substrate (Figure 1.6). The porous Si film acts as the interferometer, creating fringes from reflections off
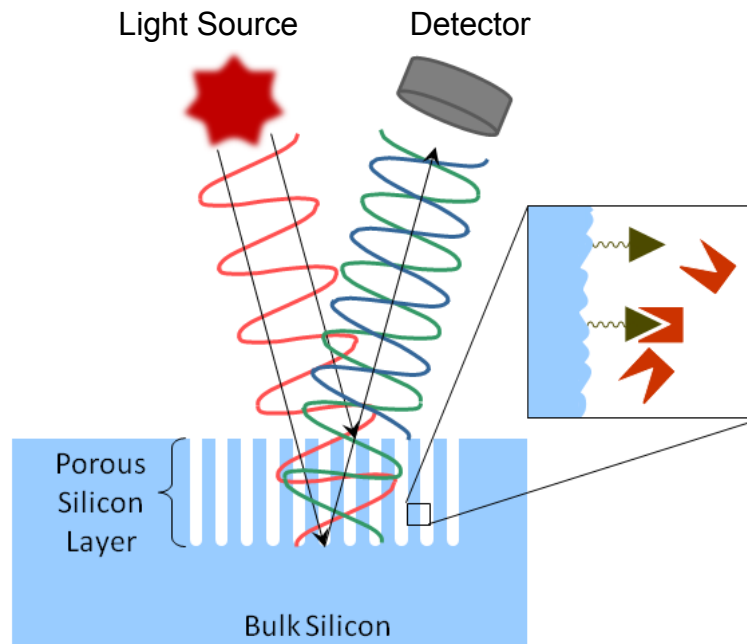
Figure 1.6: Block diagram of a porous silicon sensor.

the top and bottom of the pores. As demonstrated by Sailor, *et al*., this technique can overcome typical penetration depth limitations because the entire volume of the sample within the film is utilized for the measurement.[70,71]   Limited penetration depth, or the inability to measure interactions which occur above the sensor surface, is a significant shortcoming present in other surface-based techniques.

Lin, *et al*. reported the ability of a porous silicon-based optical interferometric bionsensor to detect the binding of small molecules, DNA oligomers, and proteins with unprecedented sensitivity (pico- and femtomolar concentrations).[70] Dancil *et al*. studied protein A and IgG binding via porous silicon biosensing. This report highlighted the reversibility and stability of the system, as well as the ability to render the sensor insensitive to nonspecific binding.[71]   Li *et al*. demonstrated that porous silicon can serve

14

as a template for the construction of complex optical structures comprising of organic polymers or biopolymers in biosensor applications. These more recent findings are of particular interest to drug delivery applications.[72]

BioCD:

The biological compact disk (BioCD) utilizes patterns of immobilized capture proteins on a disk with a mirrored surface to create periodic reflective interference spectra which are measurably altered by binding.[73,74] The interference signal is interrogated before and after the disk has been incubated with the sample, and the difference is correlated to the amount of binding that has occurred. Unfortunately, because the BioCD discretely measures the relative difference in the reflectance patterns of surface immobilized proteins before and after binding, the tool is not readily applicable for real-time monitoring, rendering kinetics studies problematic.

Detection limits as low as 10^5 molecules has been achieved using the BioCD, which was employed to measure specific binding between anti-mouse IgG and mouse IgG using rabbit IgG as a control.[73,74] In an expanded effort, it was shown that binding measurements are concentration-dependent, illustrating the potential of the technique for quantitative analyses.[75] Wang *et al*. expanded applications of the technique further by employing the BioCD to perform multiplexed prostate specific antigen (PSA) detection in human serum.[76]

Other Reflective Interferometric Platforms:

Recently, the principles of reflectance interferometry used in porous silicon and BioCD methods have been applied to other biosensor variations with increased

15

multiplexing abilities. In particular, Ozkumer *et al.* have introduced a multiplex platform known as the spectral reflectance imaging biosensor (SRIB) designed for high throughput use. SRIB is based on the optical phase difference rendered by the binding of biological species to probes on a transparent layered surface. This technique enables the collection of reflectance spectra for hundreds of spots on the array simultaneously.[77,78] Gauglitz *et al.* have used reflective interferometric spectroscopy (RIfS), a similar platform based on multiple white light reflections at thin transduction layers, to characterize biomolecule interactions in a multiplexed, high throughput format by attaching 96- and 384-well plates to the transducer slide.[79] The applications of this RIfS platform include use a screening tool for thrombin inhibitors and antibodies against triazine libraries.[79,80]

Backscattering Interferometry:

A new technique, backscattering interferometry (BSI), was originally used to measure small refractive index changes in fused-silica capillaries[81] and has been developed in multiple configurations and for a wide array of applications, including a highly sensitive universal solute detector in capillary electrophoresis,[82-84] a non-invasive nanoliter temperature probe,[84,85] a highly accurate flow sensor,[86,87] as well as an ultra-sensitive method for the detection of proteins.[88-90] BSI has more recently been employed to study molecular interactions in a label-free method[91] and has proven to be a versatile sensing technique; BSI can investigate binding events in both a surface immobilized scheme and in free solution. This ability to measure interactions in a free-solution format makes BSI unique among interferometric techniques. The free-solution advantage not only eliminates the time and monetary costs related to immobilization strategies, but also
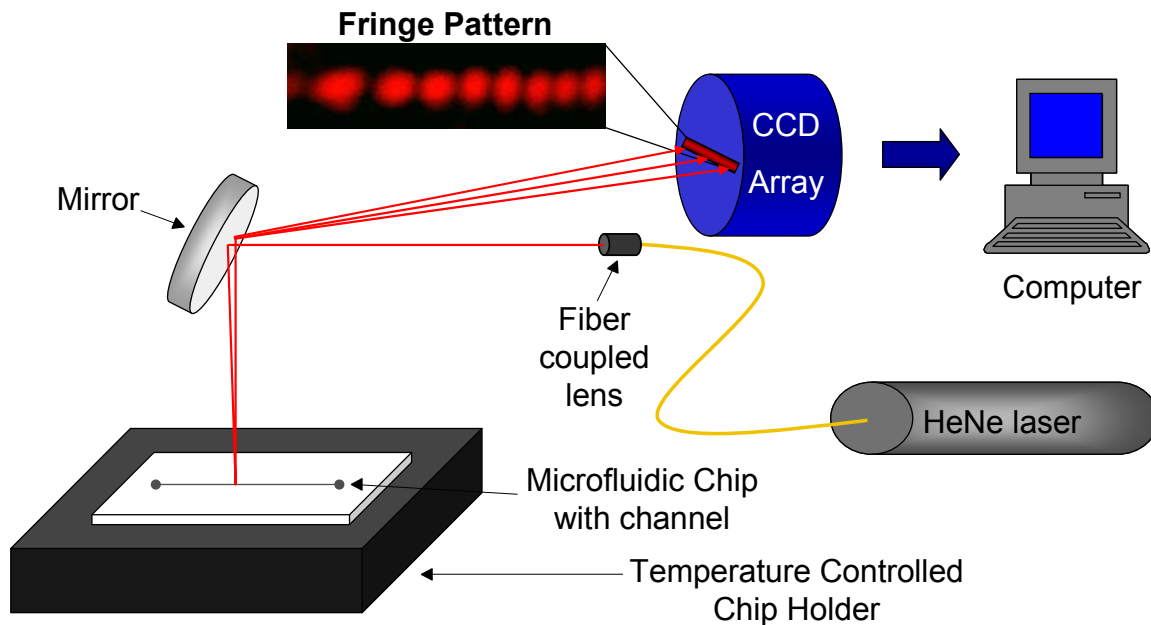
Figure 1.7: Block diagram of Backscattering Interferometry (BSI).

allows binding partners to be monitored entirely in their native state. As BSI is dually amenable to free-solution and surface-immobilized formats, any contribution of immobilization to binding perturbation may be measured directly. Perhaps surprisingly in light of the platform's unmatched versatility is that BSI maintains an extremely simple optical train, requiring only a collimated coherent light source, a capillary or microfluidic chip (hemispherical or rectangular), and a detector.

In the latest configuration of BSI, a microfluidic chip molded in polydimethylsulfoxide (PDMS) or etched in glass is employed. BSI utilizes a red helium-neon (HeNe) laser (λ = 632.8 nm) to illuminate the microfluidic channel in a simple optical train (Figure 1.7). Specifically, the laser is coupled to a collimating lens through a single-mode fiber, producing a 100 μm diameter beam and yielding probe
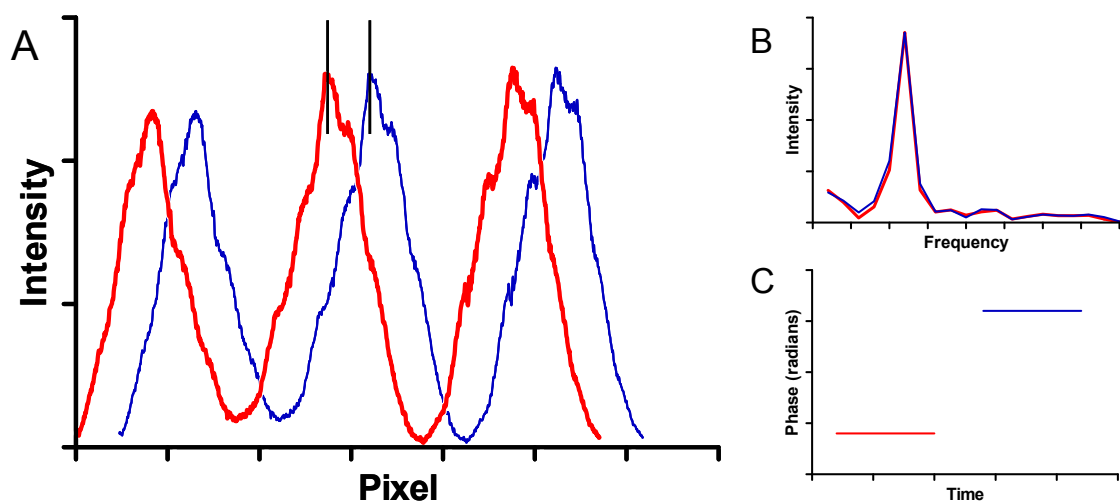
Figure 1.8: A. Line profile of the fringes produced with a shift illustrated. B. Fourier analysis of the two fringe patterns, showing the same frequency. C. Phase versus time plot illustrating the signal change observed for the fringe shift shown in A.

volumes in the 300 picoliter range. Subsequently, when the laser beam impinges the channel and interacts with the fluid contained in the channel, a set of high contrast interference fringes is produced and monitored in direct backscatter region at relatively shallow angles. The spatial position of these fringes depends upon the refractive index (RI) of the fluid within the channel (Figure 1.8). The change in fringe position is monitored using a CCD array in combination with Fourier analysis,[92] enabling the quantification of this positional shift as a change in spatial phase, calculated in the Fourier domain.

Originally BSI facilitated interaction assays in the heterogeneous mode, or utilized the immobilization of one binding partner onto the surface of a microfluidic chip molded in PDMS.[90,93] In early experiments, streptavadin was immobilized onto the

channel surface and the fringe pattern was measured before and after introducing biotin into the channel. A good correlation was found between the BSI molecular interaction signal and fluorescence signal reported in a similar experiment. Next, a biotinylated protein-A (P_A) surface allowed the monitoring of reversible IgG-P_A interactions with femtomole detection limits.[90] New surface chemistry enabled a two-fold improvement on detection limits of the protein A-IgG interaction without the use of a fluorescent label, and also allowed monitoring of the hybridization of complimentary strain of DNA at concentrations ranging from 5nM to 500 mM to a 30-mer of mActin. Assuming 100% surface coverage, the 3σ limit of quantification was found to be 36 attomoles of DNA in the 500 pL detection volume. Further experiments showed that a 3 base pair mismatch could be detected, evidenced by a marked decrease in binding signal from that of the original complimentary strand – only 7 % of the signal generated by the binding of the complimentary strands was observed for the mismatched strand.[93]

The most novel aspect of BSI is that it can be used to measure free-solution molecular interactions. Using a channel with a serpentine mixer and a restriction to mix the two interacting species on-chip, a stop-flow experiment can be performed label-free and in free solution to elicit real-time kinetic data. Solutions may also be pre-mixed off chip, enabling the determination of kinetic information using an end-point format.[91] Using these methods, systems reported were Protein A (P_A) which binds with high affinity to the F_C region of several immunoglobulin G (IgG) species, including human and rabbit; calmodulin (CaM), the ubiquitous calcium-binding protein that can bind to and regulate a multitude of different protein targets; and the interaction between IL-2 and a monoclonal antibody, in this case in buffer and in cell-free media.   Recent

advancements of BSI have shown that molecular interaction assays can be performed utilizing exceedingly small amounts of sample at physiologically relevant concentrations, without the use of labels or surface immobilization, and in complex matrices. For example, the entire CaM study (i.e., CaM-Ca^{2+}, CaM-TFP, CaM-M13 peptide, and CaM-calcineurin) required the consumption of only about 200 picomoles or 3 mg of CaM, and each binding event only required one minute for analysis.[91]

The broad range of unique applications that BSI is capable of will be reported in this thesis. The limits of BSI for the use in binding affinity determinations will be expanded to the pM range (Chapter II) through the study of the interaction between interleukin-2 (IL-2) and its monoclonal antibody (IL-Ab). IL-2 is a well-studied protein[94,95] that is secreted by activated T-cells and is involved in the regulation of the immune response. The interaction between IL-2 and IL-Ab has a high binding affinity (10 – 60 pM),[96] making it a difficult pair to study with most traditional methods.

Another system of particular interest is protein – carbohydrate binding (Chapter III), which is involved in many cellular recognition pathways such as immune response, cell agglutination and aggregation, as well as the initiation of numerous diseases.[97-100] Due to this fact, carbohydrates have become a target for the development of inhibitors that would be applicable to a broad variety of diseases.[100,101] The primary difficulty in studying the protein-carbohydrate system is that there is significant difference in the size of the binding pair.

Another prime area of investigation is the implementation of BSI for use in disease detection (Chapter IV). Current methods for the detection of many diseases, include cell cultures, ELISA (enzyme-linked immunosorbent assays), nucleic acid

amplification tests (PCR and LCR), and direct immunofluorescence (DIF). These methods often require the patient samples to be sent off to a lab for analysis, which may take several days. This procedure causes a delay in treatment and, in some instances, the patient does not even return for treatment. The lack of a rapid test often results in the empirical use of antibiotics, which may be prescribed to a patient in error. If a method were available to accurately diagnose a disease in the doctor's office instead of having to send it off to a lab, the correct treatment could begin immediately. To test the applicability of BSI for disease diagnosis and therapy monitoring, syphilis will be used as an example through a collaboration with the Sexually Transmitted Disease (STD) division of the Centers for Disease Control and Prevention (CDC).

BSI is also uniquely applicable to the study of membrane bound proteins (Chapter V). Membrane-associated proteins are integral components of many cellular processes and disease pathogeneses. Direct and quantitative observations of ligand-protein interactions are notoriously difficult to perform due to the associated membrane. Though assays exist to examine this class of molecular interactions, targets of interest must typically undergo covalent modification and removal from the native membrane environment prior to observation. Here BSI will be used to observe ligand-receptor binding events in a solution-based, native membrane environment.

Various other applications of BSI are currently being explored (Chapter VI), including antibody interactions for an array of small molecules and encapsulated RNA aptamer interactions.

CHAPTER II

PROBING HIGH-AFFINITY INTERACTIONS WITH
BACK-SCATTERING INTERFEROMETRY

Background and Significance:

Molecular interactions, such as protein-protein binding or protein-small molecule

binding, are fundamental to basic cellular function. Valuable insight to these functions is

provided by the ability to study these interactions and to determine the affinity and rate.

Such investigations provide the foundation for many diagnostic techniques and critically

aid in the development of therapeutics. For many of these interaction measurements to

be performed, very low concentrations must be utilized, often necessitating the

attachment of labels (such as fluorescent tags) to at least one of the binding partners.

Techniques designed to avoid labeling have traditionally been accompanied by other

disadvantages; for example, label-free measurements have been performed using

calorimetric methods, such as isothermal titration calorimetry (ITC) are carried out in

free solution and have become relatively well accepted.[102-104] However, there are

limitations to calorimetry, including large sample volumes, relatively low sensitivity, and

low throughput. The enthalpic array has been developed to overcome some of the

limitations of calorimetry, allowing measurements to be performed in 500 nL of sample

and in a high-throughput format.[105] Nevertheless, the method is still limited by its

sensitivity, with concentration detection limits around 50 μM,[105] thus constraining the

measurable range of binding affinities. Label-free techniques that have the necessary

sensitivity however often rely on surface immobilization, which can be expensive and

time consuming as well as having reduced activity over time.[23] In addition, immobilizing one of the binding pair to a surface can alter how the molecules interact.[106]

Backscattering interferometry (BSI) has previously been used with surface immobilization methods[90,93] and has recently been applied to free solution molecular interaction assays.[91] Here we show that BSI has the sensitivity necessary to probe high affinity (pM) binding events, expanding the molecular interaction dynamic range of the instrument to six decades.[91] To test the limits of BSI for use in binding affinity determinations, the binding between interleukin-2 (IL-2) and its antibody (IL-Ab) will be quantified in free-solution and label-free. IL-2 is a well-characterized protein that is secreted by activated T-cells and is involved in the regulation of the immune response, directing the proliferation and differentiation of immune cells.[94,95] The interaction between IL-2 and IL-Ab have been shown to bind with high affinity (10 – 60 pM),[96] making this pair difficult to study with most traditional methods.

IL-2 Calibration:

A calibration curve of the protein in solution (4 mM HCl with 0.1% FBS) was first performed using a concentration range from 10 – 100 pM. In these studies, a rectangular microfluidic channel (90 μm × 50 μm) molded in poly(dimethyl)siloxane (PDMS) was used, representing a probe volume of 450 pL. These were prepared utilizing standard photolithography and replica molding techniques.[107,108] Approximately 4 μL of solution was introduced into the inlet well and was subsequently loaded into the channel by applying a vacuum to the waste outlet. After allowing the solution to equilibrate to temperature and pressure, the phase shift was recorded using a program

23

previously developed in our group.[92] The experiment was repeated in triplicate. The

resulting calibration curve for IL-2 proved, as expected, to be linear (R^2 = 0.985) and

produced a 3σ detection limit of 40.2 pM (Figure 2.1), equivalent to 10,900 molecules or

278 ag of protein within the probe volume.

$y = 1.43 \cdot 10^{-3}\, x + 5.81$
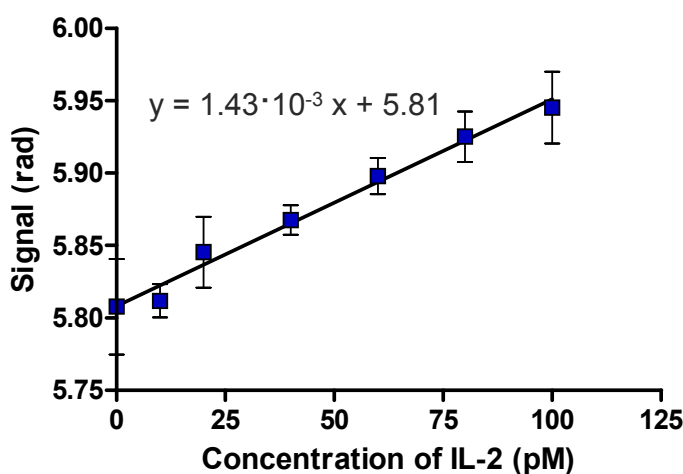
Figure 2.1: Calibration curve of IL-2, error bars represent the three run standard deviation.

Free Solution Binding:

A chip with a serpentine mixer molded in PDMS was used for the binding

experiments (Figure 2.2). The antibody solution was introduced into one inlet well and

the IL-2 solution was introduced into the other inlet well. A vacuum was applied to the

waste outlet to draw the samples through the serpentine, mixing the samples on the chip.

The vacuum was then removed, stopping the flow and the binding between IL-2 and

IL-Ab was monitored. An example of a real-time trace of the signal before and after the
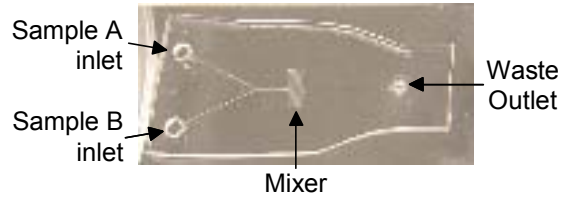
Figure 2.2: Image of the serpentine mixer chip utilized in the free-solution binding experiments.

flow is stopped in shown in Figure 2.3. Here the time scale is arbitrarily set to zero at the time that the vacuum is released and the flow is stopped. Before this point (at negative times), there are freshly mixed reactants that have not yet bound flowing in the channel. When performing the binding assay, the concentration of IL-Ab was held constant at 2 nM (in PBS, pH 7.4), while the concentration of IL-2 was varied from 10 – 100 pM (in 4 mM HCl with 0.1% FBS). The reaction was monitored for three minutes, at which time
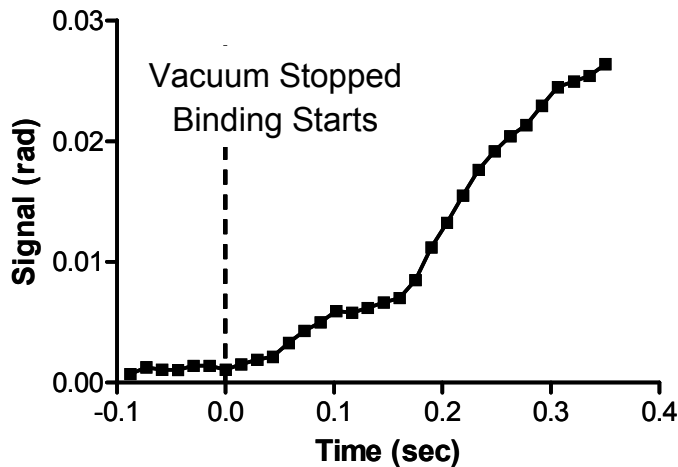
Figure 2.3: Time-dependent BSI signal before (t < 0) and after (t > 0) flow of reactants is stopped by removing vacuum nozzle from the chip outlet port. Total time shown is ½ second from a reaction lasting several seconds under these conditions.

the signal remained relatively stable, indicating that the reaction was complete (Figure 2.4). Due to the different solvents used for the protein and the antibody, three separate control runs were performed. The solvents of each molecule were mixed first (black), followed by the highest concentration of IL-2 mixed with the antibody buffer (red), and, finally, the antibody in the absence of the protein (blue). There was a slight signal produced by all of the blanks, however the change was consistent for all three controls, demonstrating that this change is simply the result of the mixing and any environmental perturbations.

The free-solution binding experiment was then repeated in cell media (RPMI 1640 with 1% fetal bovine serum (FBS) and 10 µg/mL Cipro) to closer mimic the native environment of the interaction. The IL-Ab concentration was again held constant at 2nM
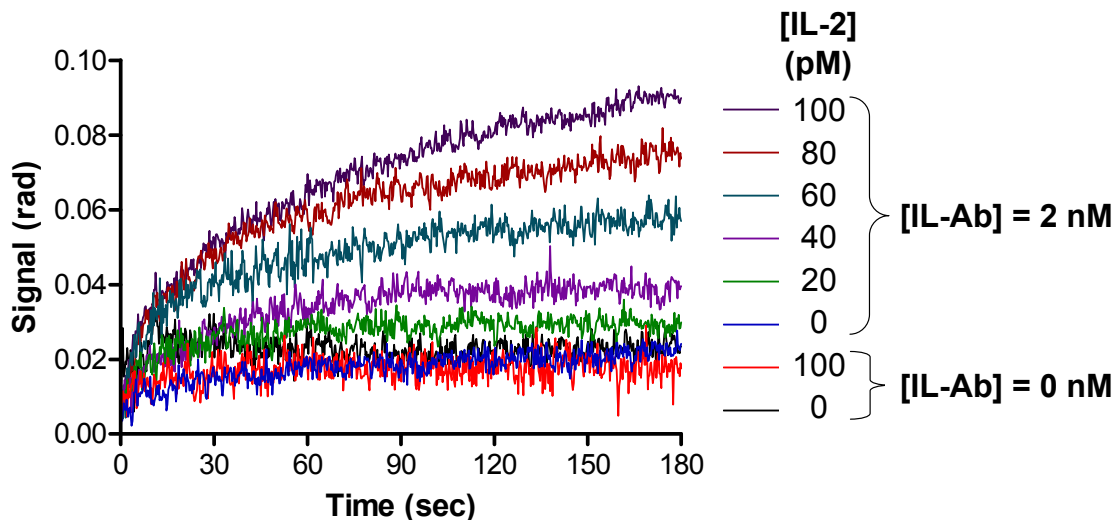
Figure 2.4: Real-time IL-2 – Ab binding curves with interaction assay performed in free solution. Note: no signal change observed in 3 control experiments (Black: IL-2 buffer mixed with Ab buffer, Red: max IL-2 concentration mixed with Ab buffer, and Blue: IL-2 buffer mixed with 2nM Ab).
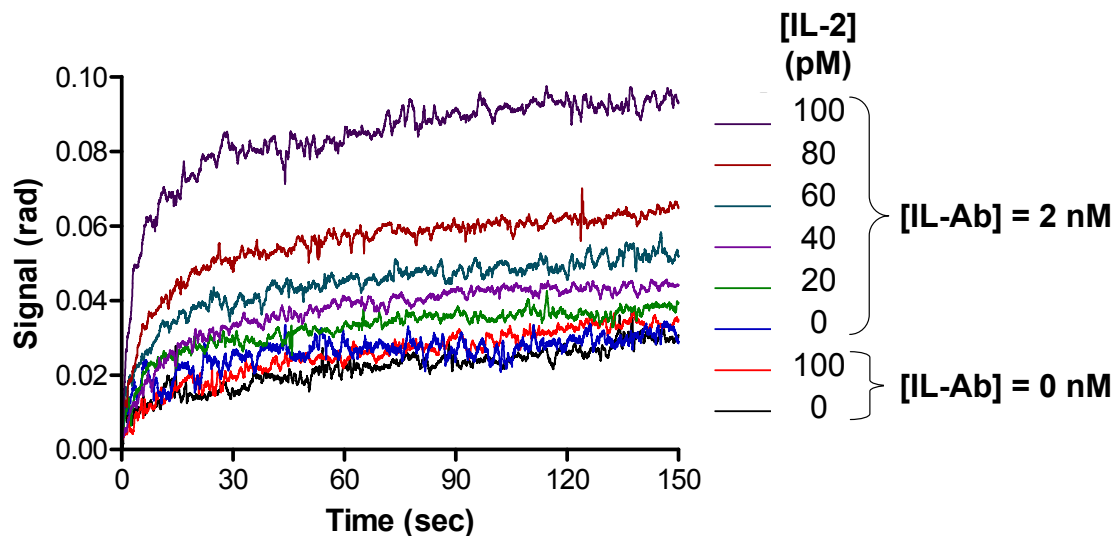
Figure 2.5: IL-2 – Ab binding curves with interaction assay performed in cell media. The IL-Ab concentration was held constant at 2 nM. Both the IL-2 and IL-Ab solutions were made utilizing RPMI 1640 cell media with 1% FBS and 10 µg/mL Cipro. A blank [0 M of both IL-2 and IL-Ab, (black)], as well as two controls [0 pM IL-2 reacted with 2 nM IL-Ab (blue); 100 pM IL-2 mixed on chip with 0 nM IL-Ab (red)] were evaluated.

and the IL-2 concentration was varied from 10 – 100 pM. Similar results were seen for the reaction in cell media as were seen in buffer solutions (Figure 2.5).

Data Analysis:

The binding reaction between a receptor (R) and a ligand (L) (Equation 1) have been shown to have kinetics with first order exponential association.[91]

$$R + L \underset{k_{reverse}}{\overset{k_{forward}}{\rightleftharpoons}} RL$$

(1)

Therefore the trace of the association between the binding partners was fitted with a one-phase exponential association (Equation 2) using SigmaPlot^{TM} software.

$$y = y_{max}\left(1 - e^{-k_{obs}x}\right)$$

(2)

Here k_{obs} is the observed rate constant of the reaction. A plot of k_{obs} versus concentration can then be generated and fitted with linear regression. The slope (m) of this line corresponds to the $k_{forward}$ and the y-intercept (b) is $k_{reverse}$, the rate constants in the forward and reverse reactions (Equation 1).

The K_D can then be determined from the ratio of $k_{reverse}$ to $k_{forward}$ (Equation 3).

$$K_D = k_{reverse}\Big/ k_{forward} = b\Big/ m$$

(3)

This calculation of K_D provides a straightforward method of determining the K_D of the system based on the kinetic data of the binding event.[91]

The K_D determination was performed from the binding curves in cell media (Figure 2.6) and yielded a value of 25.9 ± 5.2 pM.[91] This value falls within the published
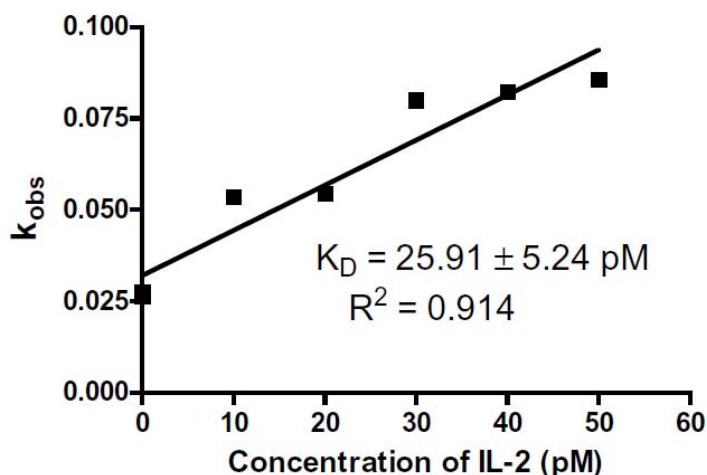
Figure 2.6: Observed rates determined by exponential fits of kinetic traces for the IL-2 – IL-Ab binding assay in cell media.

28

literature values (10 – 60 pM).[96]   This experiment verifies that BSI can be used to quantify binding affinities for a range spanning six orders of magnitude (μM to pM).[91]

Conclusions:

It has been shown the BSI can now be used to measure molecular interactions with picomolar binding affinities. This expands the dynamic range of K_D values that BSI is capable of measuring to span six orders of magnitude.[91]   The instrument provides excellent sensitivity, being able to monitor picomolar affinity interactions and to detect tens of thousands of molecules, while still maintaining a free-solution, label-free format. These benefits make BSI unique, enabling previously impossible molecular interactions studies.   Perhaps BSI will shift the paradigm when attempting to quantify affinity, determine labeling perturbation, or screen for binding.

CHAPTER III

MEASUREMENT OF MONO- AND POLYVALENT CARBOHYDRATE-LECTIN
BINDING BY BACK-SCATTERING INTERFEROMETRY

Background and Significance:

Carbohydrate-protein interactions transmit an immense amount of information during intracellular and extracellular processes.[97,98,109-113] As a result, functional glycomics has taken its place among genomics and proteomics as a vital area of investigation for the understanding and treatment of cellular biology and disease.[114] A fundamental datum in the study of any carbohydrate-protein interaction is the binding constant. Because of the size mismatch in the binding partners and the fact that carbohydrates do not usually contain functional groups that induce large changes in protein absorbance or fluorescence, quantitative determinations of binding affinities are often quite difficult to obtain. The installation of labels (fluorophores, spin labels, crosslinking agents) on the carbohydrate, while necessary in many cases, runs the risk of distorting the binding function that is being studied. The most popular label-free technique in recent years has been surface plasmon resonance (SPR),[27,28,115-121] with quartz crystal microbalance (QCM) technology emerging as a promising alternative at lower cost.[119,122-124] Both methods require the immobilization of one of the binding components on a chip, with the other partner incubated with or flowed over the chip surface. The only method in common use for label-free quantitation of binding constants in solution is isothermal titration calorimetry (ITC).[125-128] However, ITC is relatively insensitive, time-consuming, and often requires large amounts of sample.

Because both SPR and QCM techniques detect changes in mass upon binding, the small carbohydrate is usually immobilized and the large protein binding partner presented in solution.[28,115,121] Several examples of the reverse format (addition of free sugar to immobilized lectin) have appeared,[37,129-132] but sensitivity and accuracy are generally limited.[133] One attempt has been made to address this problem for carbohydrates with a heavy linker to enhance the mass-sensitive SPR signal upon binding.[134]

Described here is the use of a fundamentally different technique, backscattering interferometry (BSI), for the quantitation of binding constants of carbohydrate-lectin interactions. BSI is highly sensitive and can be used on surface-tethered species[90,93] or on binding events that take place in free solution.[91] BSI has been previously described for its use in the detection of IgG-protein A interactions and DNA hybridization[93] and recently reported the quantification of binding affinities over six decades (μM – pM) with small molecule-protein, protein-ion, protein-protein, protein-peptide, and antibody-antigen systems.[91] It is shown in this chapter that BSI can now be used to obtain highly reproducible binding constants for the interactions of both monovalent and polyvalent carbohydrates with lectins that have been immobilized in a very mild manner so as to support their native structure and function.

Experimental Procedure:

Surface Immobilization of Lectins:

BSI chips were manufactured by Micronit, Inc and were isotropically etched in borosilicate glass to give a cross section described by two quarter-circles of 40 μm radius

connected by a 10 μm flat region. A layer of avidin was first immobilized, to which biotinylated lectins were attached by simple mixing (Figure 3.1), by the method of Matsunaga and coworkers.[135] In preparation, the channel surface was cleaned with 10%
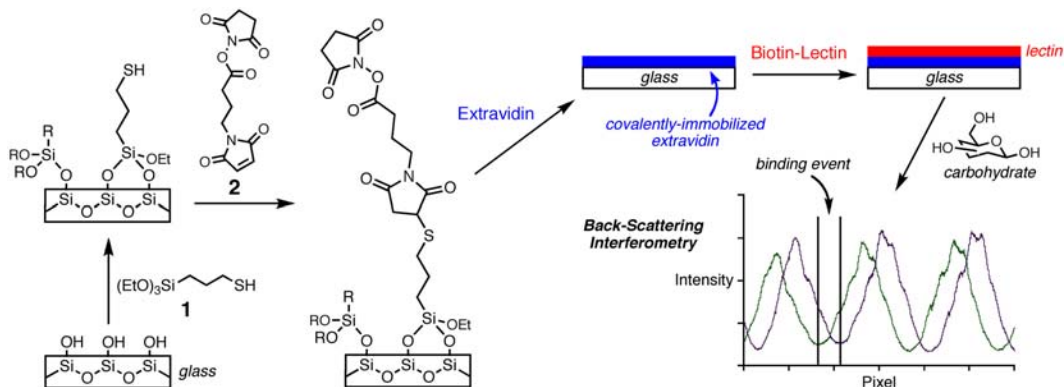
Figure 3.1: Functional preparation of immobilized lectins in for BSI measurements.

KOH in methanol for 30 minutes, then rinsed with deionized water and dried in air. The channel was then filled with a solution of 3-mercaptopropyl triethoxysilane (**1**, 2% in toluene) for 60 minutes to introduce surface thiol groups, then rinsed again with deionized water air dried. The surface was condensed with a bifunctional linker by filling the channel with *N*-[γ-maleimidobutyryloxy]succinimide ester (**2**, 1mM in absolute ethanol) for 30 minutes. The channel was again rinsed and air dried. The surface-tethered N-hydroxysuccinimide ester groups were used to capture extravidin by soaking the channel in a solution of extravidin (1 mg/mL in PBS) overnight, as indicated by wash-resistant changes in surface wetting and interferometry. The channel was thoroughly rinsed with PBST (PBS with 0.05% Tween-20) and PBS to remove any
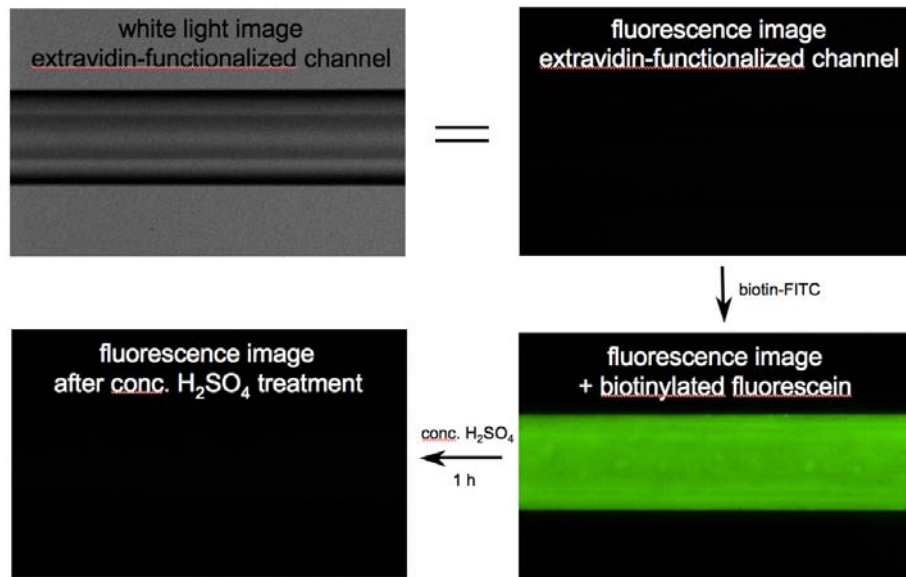
Figure 3.2: Microscope images of a representative BSI channel following surface functionalization and extravidin attachment, followed by treatment with biotinylated fluorescein, and then removal by treatment with concentrated sulfuric acid, which strips all attached material from the surface so the channels can be re-used.

excess avidin. The activity of the immobilized avidin was independently verified by fluorescent labeling of the channels using biotinylated fluorescein (Figure 3.2).[136]

Biotinylated lectins (1 mg/mL) were then introduced to arrive at the fully charged channel and soaked for 60 minutes, followed by washing with sodium acetate buffer. The use of an extravidin layer was designed to make the system as modular as possible, and also to install the binding protein of interest in a less denaturing environment than it would experience if tethered directly to the glass surface.

For the experiment with different surface coverages, conA was biotinylated by mixing it with a 10-fold molar excess of *N*-hydroxysuccinimidobiotin for one hour at room temperature, followed by filtration three times through 10,000 MW cutoff

microcentrifuge filtration tubes to remove the excess reagent, rinsing with 50 mM sodium acetate buffer containing 1 mM Ca^{2+} and Mn^{2+} (pH = 6.8).

Backscattering Interferometry Measurements:

BSI has been described in detail previously;[90,91] a brief summary of the apparatus and method are shown here. The instrument consists of a red helium-neon (HeNe) laser (λ = 632.8 nm) to illuminate the microfluidic channel and a camera for transduction of the signal contained in the fringe pattern. In a simple optical train, the laser is coupled to a collimating lens through a single-mode fiber, producing a 100 μm diameter beam and a probe volume of approximately 300 picoliters. When the laser beam impinges the channel and interacts with its surface, a set of high-contrast interference fringes is produced. The spatial position of these fringes depends upon the refractive index of the fluid within the channel and is monitored in the direct backscatter region. The change in the fringe position is quantified using a CCD array in combination with Fourier analysis methodology that allows the positional shift to be interpreted as a change in phase, calculated in the Fourier domain. All data was collected in real-time utilizing an in-house program written in LabView™.

To perform the binding studies, the lectin was immobilized onto the surface of the channel utilizing the scheme outlined above. A reference solution of sodium acetate buffer was introduced into the channel by pipetting 1 μL of solution into the inlet reservoir and applying a vacuum to the outlet well. Once the solution had filled the channel, the flow was stopped and the backscatter signal, or binding event, was monitored for one minute. This process was repeated iteratively for increasing

concentrations of the carbohydrate from 10–100 μM. The channel was rinsed with sodium acetate buffer between each analyte sample to remove any bound sugar from the Con A; the BSI signal was always observed to return to the baseline value after such rinsing. The same experiments were performed with CPMV particles (0–40 nM in capsids, 0–8 μM in attached sugar), Qβ virus-like particles (0–5 nM in capsids, 0–2.5 μM in attached sugar), generation-4 PAMAM dendrimers (0–2.5 μM in dendrimer, 0–100 μM in attached sugar), and generation-6 PAMAM dendrimers (0–60 nM in dendrimer, 0–5 μM in attached sugar). Wild-type CPMV and Qβ particles, as well as G4 and G6 dendrimers bearing only galactose, were used as controls in order to rule out contributions from non-specific adsorption.

The competition data shown in Figure 3.9A, B were obtained from the following procedure. A 32 nM solution of particle **11** was incubated in a standard extravidin/conA-derivatized channel for one minute, during which time the signal stabilized at approximately 0.03. The value indicated by the horizontal black line in each plot represents the average of these measurements throughout the experiment (standard deviation = 0.005). A solution of conA or mannose, starting with the most dilute concentration, was flowed into the channel, displacing the solution of **11**. The change in signal was monitored for one minute; it reached the indicated value within 15 seconds. The channel was then rinsed extensively with buffer and the process was started again with a fresh 32 nM solution of **11**, and the next highest concentration of reagent.

Data Analysis:

A correction must be made for the bulk refractive index change due to the presence of different concentrations of ligand in solution. This is accomplished by recording a calibration curve for the ligand in the absence of immobilized protein (data not shown). For each experiment, the observed phase change (corrected for bulk ligand effects) was plotted versus concentration in order to create a saturation binding curve. This endpoint analysis plot was then fitted to the square hyperbolic function (Langmuir isotherm) shown in Equation 1 using Prism^{TM} software to obtain a value for ($1/K_{ads}$).

$$(S - S_0) = \frac{(S_{max} - S_0)[L]}{(1/K_{ads}) + [L]} \tag{1}$$

where S = corrected phase change in the presence of carbohydrate ligand, S_0 = corrected phase change in the absence of ligand (buffer only), S_{max} = maximum corrected phase change in the presence of ligand (assumed to represent full binding to the immobilized protein), and $[L]$ = concentration of carbohydrate ligand in solution. Use of the Frumkin isotherm equation as described by Kiessling and coworkers[27] gave no indication of attractive or repulsive interactions between the adsorbing molecules.

Polymer Carbohydrate Adduct Preparation:

Cowpea mosaic virus (CPMV)[137,138] and bacteriophage Qβ virus-like particles,[139,140] both approximately 30 nm in diameter but very different in their structural details,[141,142] were decorated with monosaccharides, as shown in Figure 3.3, by Eiton Kaltgrad at The Scripps Research Institute. CPMV displays 240 lysine amine side chains on its exterior surface in solvent-accessible positions.[143,144] Two forms of Qβ were used: the wild-type assembly domain sequence of the coat protein which displays up to 900

conjugate	scaffold	linker	R-N$_3$	glycan	ratio	glycans per particle
7	CPMV		3	Man		212 ± 20
8	CPMV		3	Man		217 ± 20
9	Qβ-WT		3	Man		470 ± 50
10	Qβ-K16M		3	Man		450 ± 50
11	CPMV		3	Man		192 ± 20
12	CPMV		3 + 4	Man/Gal	3 : 1	192 ± 20
13	CPMV		3 + 4	Man/Gal	1 : 1	192 ± 20
14	CPMV		3 + 4	Man/Gal	1 : 3	192 ± 20
15	CPMV		4	Gal		192 ± 20

conjugate	Gen	glycans per particle		conjugate	Gen	glycans per particle	
		Man	Gal			Man	Gal
16	G4	42	0	21	G6	111	0
17	G4	38	9	22	G6	86	33
18	G4	31	10	23	G6	53	33
19	G4	18	31	24	G6	31	88
20	G4	0	42				

Figure 3.3: Polymer virus- and dendrimer-carbohydrate adducts.

amine groups per particle, and the K16M mutation of this sequence which eliminates the most accessible lysine and therefore bears 720 surface amines.[145] In both Qβ structures, some steric hindrance exists among sets of symmetry-related residues, diminishing the maximum number of carbohydrates that can be attached. Polyvalent CPMV-glycan structures **7**, **8**, and **11** were prepared, bearing approximately equal numbers of α-

mannose molecules but with different linkers. CPMV particles (**11** – **15**) bearing different ratios of mannose and galactose, with the same overall loading of sugar, were also synthesized. These structures were prepared using different ratios of mannose and galactose azides **3** and **4**, assuming that the rates of the reaction are insensitive to the identity of the monosaccharide (Figure 3.3A). In addition, Qβ structures **9** and **10** were made to test higher densities of sugar loading on the shortest linker arm. Details of the virus particle preparation are in appendix A.

Generation 4 (G4) and generation 6 (G6) PAMAM dendrimers decorated with varying numbers of α-linked mannose and galactose units were prepared as previously described (Figure 3.3B).[146]

Results and Discussion:

Monovalent Interactions:

The interaction of biotinylated concanavalin A (conA), immobilized in the above manner, with its natural ligands was measured as a function of concentration, with the results shown in Figure 3.4A. The phase change in the interferometry signal was found to vary in a manner consistent with dose-dependent saturation of a single binding site. The apparent Langmuir adsorption coefficients calculated from these curves (K_{ads} = 2.4 ± 0.3 x $10^4\,M^{-1}$, $1/K_{ads}$ = 42 ± 5 μM for D-mannose; K_{ads} = 6.5 ± 5.4 x $10^3\,M^{-1}$, $1/K_{ads}$ = 155 ± 88 μM for D-glucose)[136] show the same relative trend, but stronger apparent binding, than true solution-phase equilibria (K_D) that have been measured by ITC for the free sugars (K_d = approx. 450 μM for mannose and 1800 μM for glucose at room
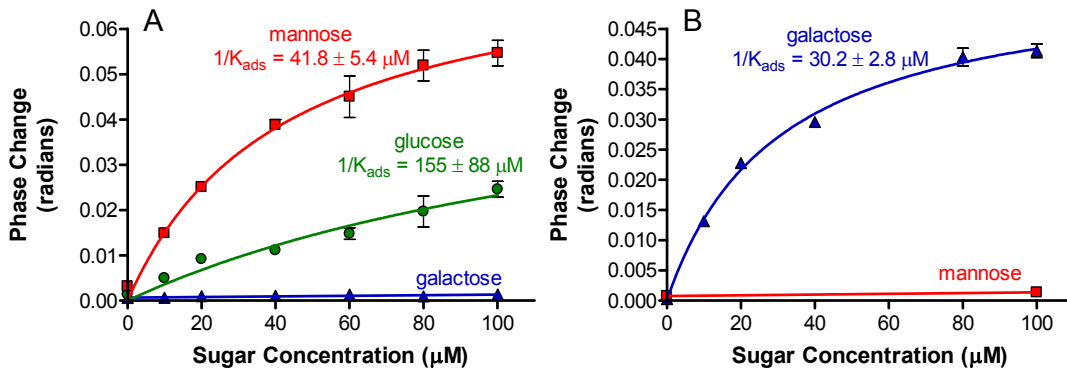
Figure 3.4: Measurement of monovalent carbohydrate binding to immobilized biotin-conA. (A) Comparison of sugars on immobilized commercial biotin-conA. (B) Comparison of sugars on immobilized biotin-BS-1. Error bars on all plots are derived from three independent experiments using different chips, showing a high degree of reproducibility.

temperature).[13,27,28,34,35] The same type of discrepancy (but to a greater degree, 1000-fold vs. 10-fold) has been observed by Kiessling, Corn, and coworkers for immobilized glycosides in SPR measurements ($1/K_{ads} = 0.18\pm0.06$ μM *vs.* $K_d = 100\text{-}200$ μM for α-Me-mannose).[27] Galactose induced no change in interferometry signal, consistent with its inability to bind to conA (Figure 3.4A). In contrast, biotinylated BS-1 lectin used in the same manner responded to added galactose ($1/K_{ads} = 30.2 \pm 2.8$ μM),[136] but not mannose, consistent with its known glycan affinities (Figure 3.4B).[147-150]

The observed K_{ads} for the conA-mannose interaction was independent of both the source of the biotinylated lectin and its loading on the channel surface (Figure 3.5). The binding of mannose to a surface of conA that was biotinylated in-house was compared to the binding to a surface of commercially purchased biotin-conA and very similar binding curves that produced the same affinty. The number of conA molecules immobilized on the channel was reduced by treating the avidin-coated chip with a 1:1 mixture of biotin-
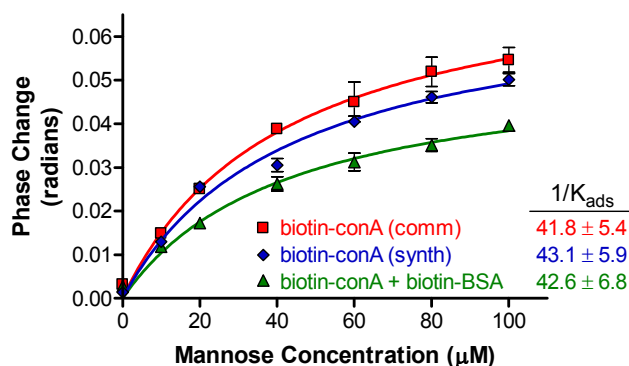
Figure 3.5: Comparison of mannose binding to different sources of biotinylated conA (deposited at the same concentration): red squares = commercially available material; blue diamonds = conA biotinylated in-house; green triangles = an equimolar mixture of commercial biotin-conA and biotin-BSA.

conA and biotinylated bovine serum albumin (BSA). BSI analysis of mannose binding in the two cases gave a diminished maximum signal in the mixed conA/BSA case, reflecting the expected dilution of glycan-binding protein on the surface. However, the same binding constant was found in both cases, suggesting that each molecule of immobilized protein acts independently from the others, although the existence of binding sites having different affinities within each conA tetramer[151] cannot be discerned from these data. It is also noteworthy that once the channel is charged with lectin, the BSI measurements are made within minutes and are highly reproducible. Added carbohydrate can be washed out with buffer and the immobilized lectins reused with no loss in signal or change in observed binding constant over at least 30 repetitions.

Polyvalent Interactions:

As with any surface-based technique, BSI lends itself to measurements of polyvalent binding.[116] To demonstrate this, icosahedral virus particles that have been previously employed for the presentation of polyvalent glycans to lectins, cell surfaces, and the avian immune system,[152-154] as well as polyamidoamine (PAMAM) dendrimers decorated with monosaccharides, known to have a strong generational (size and valency) dependence on interactions with cognate lectins[146,155,156] were studied.

Polyvalent CPMV-glycan structures **7**, **8**, and **11** have approximately the same number of α-mannose molecules, but with different linkers. In addition, Qβ structures **9** and **10** have higher densities of sugar loading utilizing the shortest linker arm. The binding of these particles to immobilized conA was measured by BSI, with the results shown in Figure 3.6.[136] The unmodified wild-type virions showed no interaction with the conA-derivatized surfaces, whereas the mannosylated particles were tightly bound. On a per-mannose basis, the measured average adsorption coefficients were approximately 60 times better for the CPMV-displayed sugar (Figure 3.6A) than for free mannose in solution (and thus likely to be 20-30 times better than α-Me-mannoside, which binds conA 2-3 times more tightly than mannose[13,27,28,34,35]). On a per-particle basis, the virus adducts achieved avidities in the low nanomolar range. For the same surface glycan density, the use of different linkers made no difference. When displayed at a significantly higher density on the Qβ scaffold (Figure 3.6B), binding was further improved, with affinity approximately 200 times that of free mannose on a per-sugar basis, and sub-nM in terms of particle concentrations.
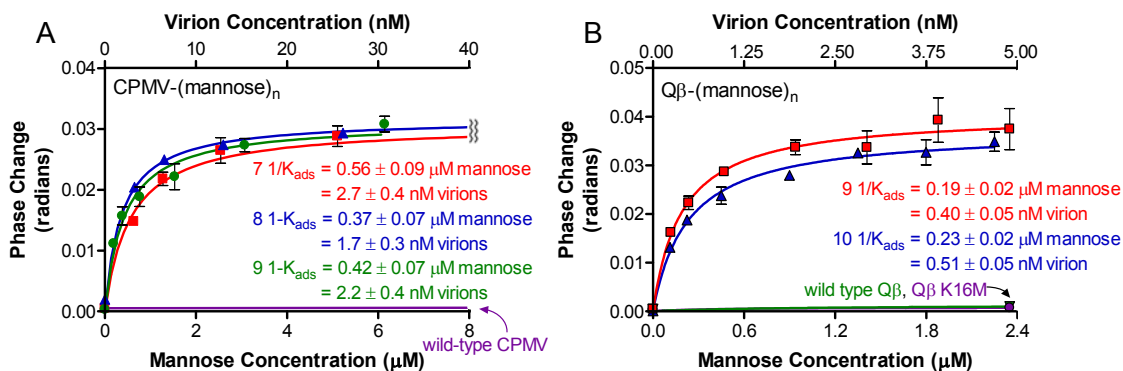
Figure 3.6: Measurement of polyvalent virus-carbohydrate binding to immobilized biotin-conA.

Changes in polyvalent affinity were also conveniently determined by BSI for CPMV particles bearing different ratios of mannose and galactose, with the same overall loading of sugar.[136] As shown in Figure 3.7A-B, particles **11** (bearing only mannose) and **15** (bearing only galactose) were not bound by immobilized BS-1 and conA lectins, respectively, ruling out contributions from nonspecific adsorption by the linker and triazole moieties added to the coat proteins in the bioconjugation process. In each case, the installation of mannose or galactose at 25% of the approximately 200 virus surface sites gave rise to highly potent binding to conA and BS-1, respectively, with modest increases in avidity of the particles observed as the percentage of active glycan was increased (Figure 3.7C-D, blue). On a per-glycan basis, however, the affinities (while still much higher than the free sugars) were found to either decrease throughout the series for mannose-conA or decrease to an approximate plateau for galactose-BS-1 (Figure 3.7C-D, black) as the loading of the active sugar on the virus surface was increased. The magnitude of the increase in per-glycan affinity (60-200 times) suggests that true polyvalent binding (simultaneous multipoint interactions with more than one anchored

42
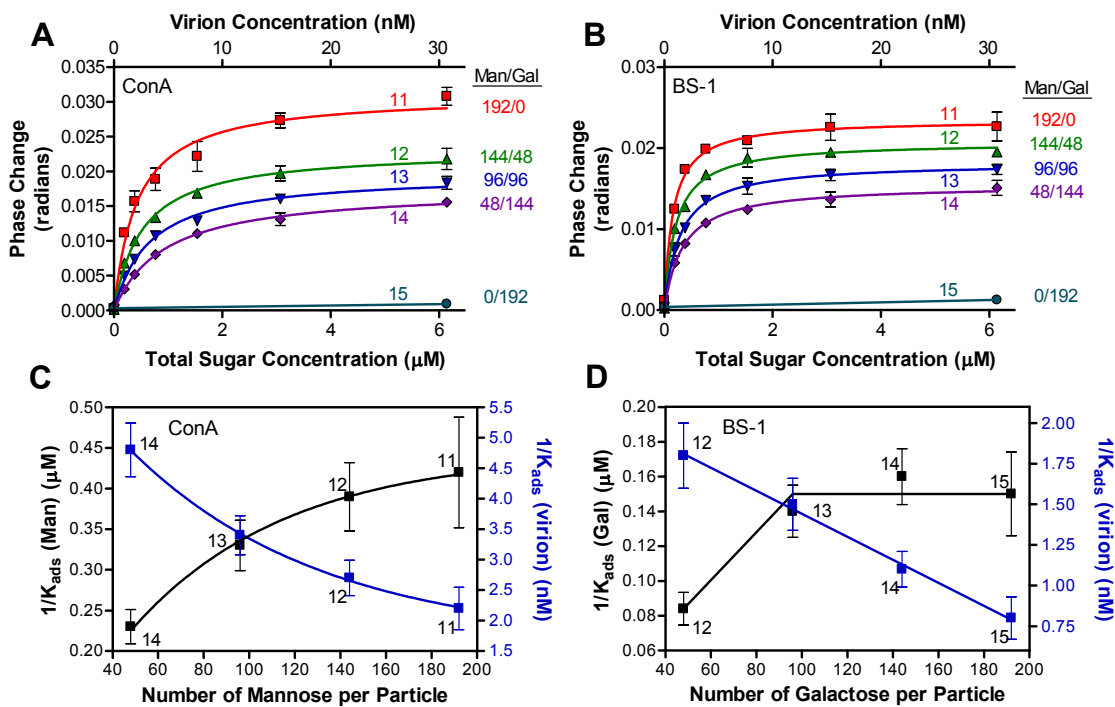
Figure 3.7: Binding of mixed mannose-galactose virus particles to immobilized conA and BS-1 lectins. (A, B) BSI measurements of the binding of the indicated CPMV-(sugar)$_{192}$ particles to immobilized conA and BS-1. (C, D) Plots of values of $1/K_{ads}$ derived from A and B, in terms of the overall concentrations of the indicated glycan presented on the virus surface (black) and the concentrations of the virus particles (blue). In all cases, $1/K_{ads}$ values were calculated from each curve independently, ignoring the relative differences in signal magnitudes between curves.

receptor) is taking place.[155,156] A summary of the measured binding constants used in Figure 3.7 C-D are shown in Table 3.1.[136] It is noteworthy that the binding avidities measured for the galactose-labeled particles to BS-1 are on the same order as mannose particles to conA, in spite of the fact that the weaker-binding β-anomer of galactose was used on the particles.[149] This also supports the assignment of polyvalency to these interactions of virus-glycans with surface-tethered lectins.

Table 3.1: Measured binding constants of polyvalent glycan virus particles

Polyvalent Glycan	$1/K_{ads}$ of particles to conA (nM)	$1/K_{ads}$ per mannose to conA (µM)	$1/K_{ads}$ of particles to BS-1 (nM)	$1/K_{ads}$ of per galactose to BS-1 (µM)
11	2.2 ± 0.35	0.42 ± 0.068	no binding	no binding
12	2.7 ± 0.29	0.39 ± 0.042	1.8 ± 0.20	0.084 ± 0.0094
13	3.4 ± 0.32	0.33 ± 0.031	1.5 ± 0.16	0.14 ± 0.015
14	4.8 ± 0.44	0.23 ± 0.021	1.1 ± 0.11	0.16 ± 0.016
15	no binding	no binding	0.80 ± 0.13	0.15 ± 0.024

To extend the observation of polyvalent binding, generation 4 (G4) and generation 6 (G6) PAMAM dendrimers decorated with varying numbers of α-linked mannose and galactose units were studied. BSI measurements with immobilized conA were again sensitive and highly reproducible, with signal magnitude depending on the number of mannose units loaded onto each dendrimer, and the measured adsorption coefficients sensitive to dendrimer size (Figure 3.8).[136] The G4-based particles showed per-mannose affinities ($1/K_{ads} \approx 20$ µM) approximately twice the measured values for mannose alone, and thus exactly what one would expect for monovalent α-alkylmannoside. Neither the per-mannose nor the per-particle affinity ($1/K_{ads} \approx 0.5$ µM) changed appreciably with variation in mannose loading from 18 to 42 per dendrimer (Figure 3.8C). In contrast, the G6 dendrons did show a modest improvement in per-mannose adsorption coefficient from 10.0 ± 3.4 µM (for **24**, with 31 mannoses) to 2.8 ± 0.4 µM (for **21**, with 111 mannoses) as mannose loading increased. Similarly, the per-dendrimer association constants improved through the G6 series (Figure 3.8D; **24**, $1/K_{ads}$ = 84 ± 29 nM, to **21**, $1/K_{ads}$ = 25.8 ± 4.1 nM). The "proximity effect" from the presentation of high local concentrations of glycan ligands on the dendrimer surface to
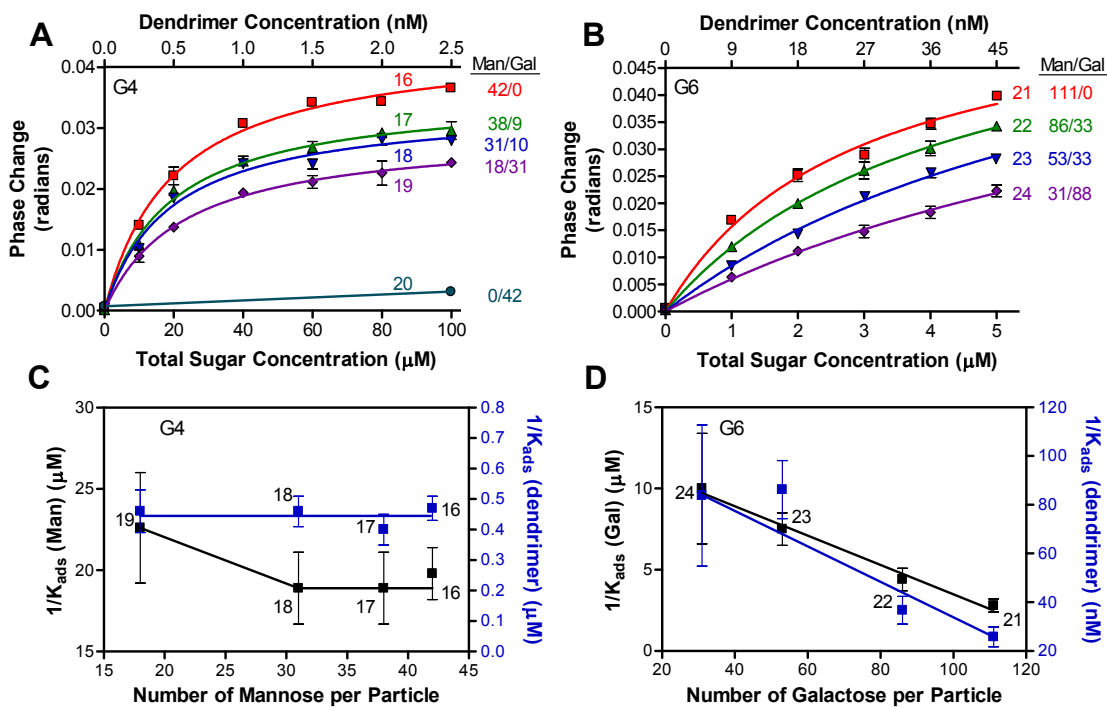
Figure 3.8: Binding of mixed mannose-galactose dendrimers to immobilized conA and BS-1 lectins. (A, B) BSI measurements of the binding of the indicated G4 and G6 dendrimer-(sugar)$_n$ particles to immobilized conA. (C, D) Plots of $1/K_{ads}$ derived from E and F. In all cases, $1/K_{ads}$ values were calculated from each curve independently, ignoring the relative differences in signal magnitudes between curves.

individual immobilized lectins can be expected to contribute to the improved avidity of dendrimer-glycan conjugates.[100,146,157] However, the fact that even the most lightly-loaded G6 structure shows better binding than the G4 dendrimers that are more densely decorated with glycan suggests that the G6 particles interact with the immobilized conA in a different manner than G4. Such interactions are presumably bi- or polyvalent, either with individual conA lectins (G6 being able to reach two binding sites better than G4) or with adjacent conA molecules. A summary of the measured binding constants used in Figure 3.8 C-D are shown in Table 3.2.[136]

Table 3.2: Measured binding constants of polyvalent glycan dendrimer particles

Polyvalent Glycan	$1/K_{ads}$ of particles to conA (nM)	$1/K_{ads}$ per mannose to conA (μM)
16	470 ± 40	19.8 ± 1.6
17	400 ± 50	18.9 ± 2.2
18	460 ± 50	18.9 ± 2.2
19	460 ± 70	22.6 ± 3.4
21	25.8 ± 4.1	2.8 ± 0.4
22	36.7 ± 5.7	4.4 ± 0.7
23	86.2 ± 11.9	7.5 ± 1.0
24	83.8 ± 29.0	10.0 ± 3.4

It has previously been demonstrated by agglutination and precipitation assays that both the G4 and G6 dendrimers used here, but not G3 or smaller structures, are able to engage conA units in polyvalent binding interactions in solution.[146] In the BSI measurements described above, however, G4 glycan dendrimers are monovalent binders and G6 dendrimers only begin to show polyvalent-style affinities, whereas the virus-based structures bind much more tightly. The most obvious distinguishing characteristic among these polyvalent ligands is their size: G4 dendrimers, G6 dendrimers, and the virus capsids have approximate diameters of 5, 7, and 30 nm, respectively. The avidin tetramer occupies a volume of approximately 5 x 5 x 6 nm,[158] and is likely to be affixed to the glass-NHS ester surface in an orientation that blocks at least two of its biotin binding sites from solution.[159] The density of surface attachment points for biotinylated lectin should therefore be quite low, and adjacent lectins would be reachable for polyvalent binding only by the larger glycosylated structures. Multivalent binding to individual adsorbed conA tetramers will be difficult for these dendrimers and virus particles which have short tethers connecting the sugar to the platform.[146]

The most important difference between the BSI technique and methods such as SPR and QCM concerns the nature of the signal: BSI detects changes in refractive index,[91] and is thus sensitive to the number of binding events rather than the change in mass brought about by binding. For example, the maximum (saturation) signal for polyvalent particles, such as viruses and dendrimers, was found to be proportional to the number of binding ligands attached to the scaffold (mannose vs. galactose, for example, in Figures 3.7A, B and 3.8A, B), even though the maximum number and mass of particles that can access the surface was the same for all members of the series. In contrast, one could not distinguish by SPR at surface saturation between particles bearing different numbers of binding ligands. The mass change in such a measurement would be equal in all such cases, regardless of how many receptor-ligand binding events occur, except for water displaced from each protein binding site upon interaction with the ligand. Because BSI detects changes in refractive index, it is sensitive to that water displacement. For this reason, the magnitudes of the phase changes observed for the saturation of the immobilized proteins with monovalent sugars are *greater* than those observed for binding of the massive virus- or dendrimer- displayed structures (Figures 3.4 and 3.5 vs. Figures 3.6, 3.7, and 3.8).[136]

This difference in the nature of the signal also manifests itself when species are removed from the surface. If one washes a large molecule off an SPR chip, the signal invariably decreases due to the loss of attached mass. With BSI detection, the signal depends on which species is used to do the washing, as shown in Figure 3.9. When soluble conA was used to remove CPMV-mannose (**11**) from the standard extravidin-conA channel, a dose-dependent decrease in signal was observed, consistent with the
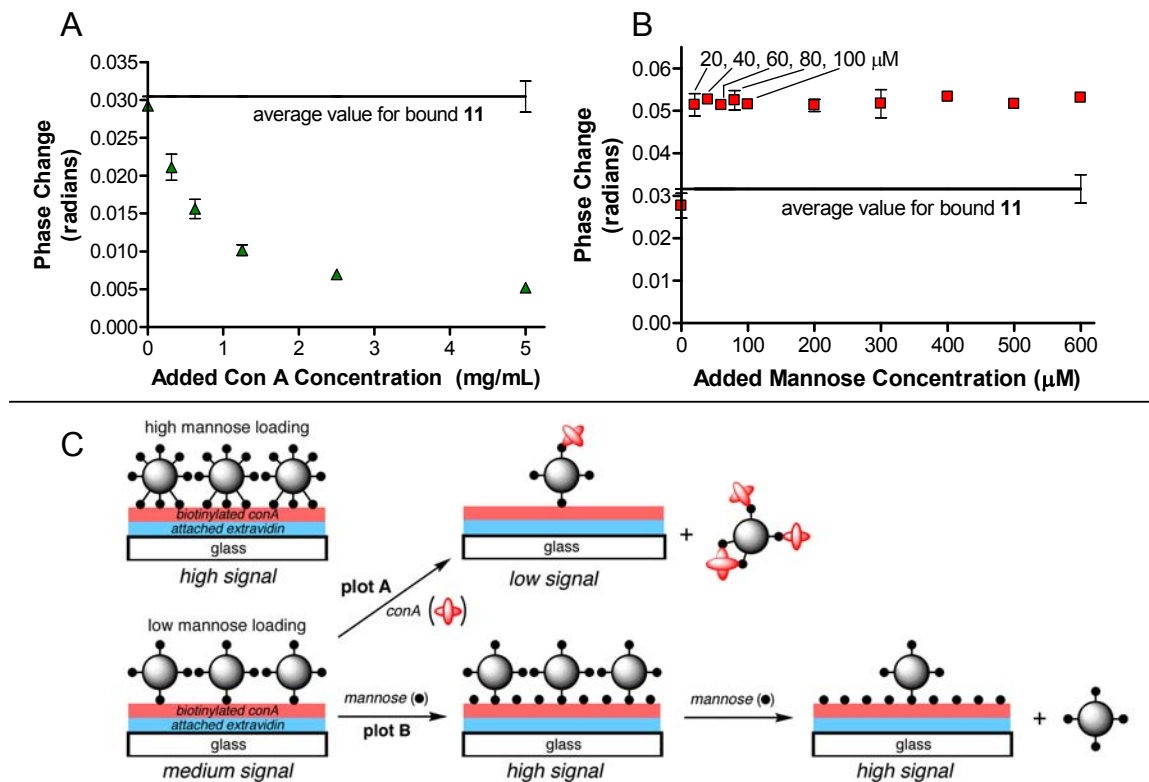
Figure 3.9: BSI measurement of the treatment of CPMV-mannose particle **11** bound to an extravidin-conA channel with increasing concentrations of (A) soluble conA and (B) mannose. (C) Cartoon representation of experiments measuring binding and competition with free sugar and receptor. For particles bearing different numbers of sugars, saturation is reached with approximately the same number of virions bound, and yet the signal intensities in the two cases are markedly different.

competitive stripping away of the virion from the surface by the soluble receptor (Figure 3.9A). One could in principle use this phenomenon to measure solution-phase association constants by competitive binding, as has been done with SPR imaging.[27] In contrast, the addition of soluble mannose (Figure 3.9B) gave rise to an invariant increase in signal, even when the mannose concentration (20 μM) was well below the K_D value for free mannose-conA binding (42 ± 6 μM). At that concentration (and probably higher concentrations as well), mannose cannot be expected to dislodge virus particles that bind

with much greater affinity (K_D = 2.2 ± 0.36 nM in virions; 0.42 ± 0.07 μM per mannose). The interferometry signal increases because mannose occupies empty conA binding sites that are underneath virus particles attached to the surface. In this case, it is impossible to tell when virus is outcompeted by added mannose for surface conA sites, since the signal does not change. Figure 3.9C summarizes in graphical form the various states achieved when large polyvalent ligand particles compete with soluble ligand or receptor for surface receptor sites, highlighting the dependence of BSI signal on the number of receptor-ligand binding events occurring at the surface of the channel.

Conclusions:

Back-scattering interferometry uses simple hardware to achieve highly sensitive measurements of protein binding events on very small amounts of material in a reusable format. Here its application to the quantitative determination of adsorption coefficients, and the relative determination of binding constants and polyvalent avidities, for glycan-lectin interactions, one of the most important classes of interactions in biochemistry, has been demonstrated. The receptor has been attached to the BSI channel by a general method involving complexation with an intervening layer of avidin, providing relatively large spacing between attachment sites and an environment conducive to the maintenance of native structure and function.

The interferometric response detects the act of complexation without direct regard to the size of the species doing the binding. This is consistent with BSI's known sensitivity to changes in refractive index.[91] It is presumed that conformational changes in the tethered binding partner and/or expulsion of bound water caused by ligand binding

contribute to refractive index modulation. The technique therefore gives rise to very different types of responses to polyvalent interactions, detecting the total number of binding events whereas SPR and QCM report on the fate of the polyvalent structure as a whole. Given its technical simplicity, high sensitivity, and label-free nature, it is expected that BSI will find use in the quantitative exploration of glycan-receptor interactions in a variety of contexts.

BACKSCATTERING INTERFEROMETRY FOR THE POTENTIAL USE IN
DISEASE DIAGNOSITICS UTILIZING SYPHILIS AS AN EXAMPLE

Background and Significance:

Backscattering interferometry (BSI) is a versatile sensing technique and has been developed for a wide array of applications.[81,84-87,89,160,161] BSI has most recently been employed to study molecular interactions in a label-free method and has been used to investigate binding events in both a surface-immobilized scheme and in free solution.[91,93,136,162] The ability of BSI to measure interactions rapidly using picoliter detection volumes in a free-solution format makes BSI unique among sensing techniques, eliminating time and monetary costs related to labeling and immobilization strategies. BSI will now be applied to disease-detection strategies with the potential application as a reactive serum detector. For these studies, syphilis serology will be used as a model for evaluating the diagnostic performance of BSI.

Current diagnostic tools rely heavily on labeling with signaling moieties to detect the presence of a particular antigen or antibody in a sample. Such chemical labeling not only consumes time and resources, but may also alter the conformations and/or behavior of binding partners, obscuring test results.[163] Introducing this variable necessitates that many common label-based diagnostic assays must be corroborated by additional testing methods, further increasing time, cost, and sample consumption.[164]

Current methods for the detection of many diseases, such as syphilis, include cell cultures, ELISA (enzyme-linked immunosorbent assays), nucleic acid amplification tests

(PCR and LCR), and direct immunofluorescence (DIF). These methods often require the patient samples to be sent off to a lab for analysis, which may take several days. This procedure causes a delay in treatment and, in some instances, the patient does not even return for treatment. The lack of a rapid test often results in the empirical use of antibiotics, which may be prescribed in error. If a method were available to diagnose a disease in the doctor's office, the correct treatment could begin immediately.

The enzyme-linked immunoassay (ELISA) is a widely-used diagnostic tool which relies heavily on signaling moieties to detect the presence of a particular antigen or antibody in a sample. This technique has become a standard diagnostic strategy for numerous critical diseases, including syphilis.[164-166] Syphilis diagnostics are particularly sensitive to time, cost, and sample volume considerations because of their heavy presence worldwide, including developing areas. Therefore, a label-free microfluidic diagnostic tool has the potential to revolutionize point-of-care diagnostics for these and other widespread diseases.

Of the available label-free techniques, BSI provides unmatched sensitivity and is the only tool that is fully compatible with microfluidics − critical advantages for diagnostic applications.[91] Using BSI to detect antigen-antibody interactions has the advantage of not only decreasing cost, time, and sample volume considerations, but also offering the unique potential to quantify antibody levels in clinical samples. Such an advantage may provide valuable information concerning disease status, severity, progression, and/or therapeutic efficacy. In order to explore BSI's capacity to detect syphilis infection in human sera, purified antigens will be used to detect antibodies in the sera raised against the infection (Figure 4.1). The ability to detect antigen-antibody
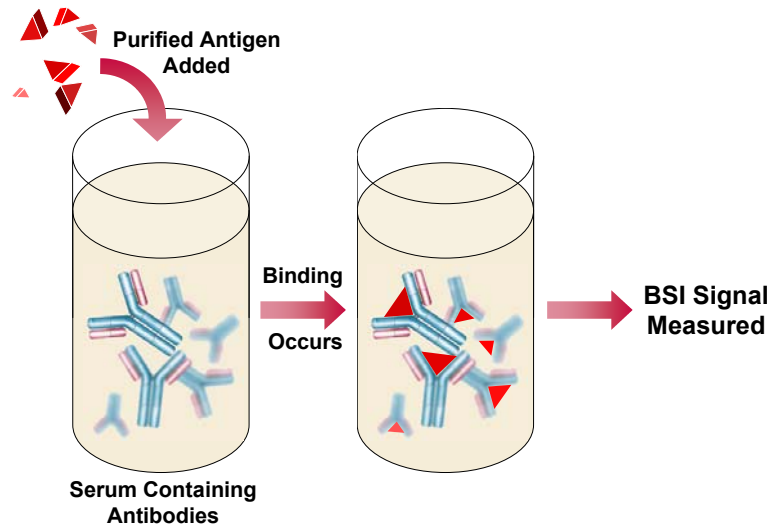
Figure 4.1: Illustration of the method used to detect the presence of disease in human serum samples.

interactions with BSI has previously been established by the Bornhop group.[91] Successful detection of syphilis infection in human specimens using BSI will not only provide innovative diagnostic approaches for this particular disease, but will serve as a benchmark in protein-based diagnostics, applicable to countless other diseases.

Syphilis is a sexually transmitted infectious disease caused by the bacterium *Treponema pallidum* for which no adequate *in vitro* culturing method has been developed.[167,168] Therefore, current syphilis diagnostic tests typically rely on the detection of anti-treponemal antibodies raised against the pathogen itself (i.e., treponemal tests) as well as nontreponemal tests for antibodies against lipoidal material released from damaged host cells and against lipoprotein-like secretions of the treponeme.[167,168] The most commonly used treponemal tests include fluorescent treponemal antibody absorption (FTA-ABS) and the treponemal pallidum particle agglutination test (TP-PA),

and current nontreponemal tests include the Venereal Disease Research Laboratory (VDRL) and the Rapid Plasma Reagin (RPR) tests.[167,168] While treponemal tests are highly specific, they give little or no indication of the status of the infection because anti-treponemal antibodies are retained for a lifetime. In contrast, nontreponemal tests are most reactive during active syphilis infection; when the disease is latent or has been effectively treated, the reactivity of the antiserum to these tests subsides.[167] However, nontreponemal tests have shown a high rate of false-positive results (i.e., are relatively nonspecific) because anti-cardiolipin antibodies may be generated as a result of conditions unrelated to syphilis, including autoimmune diseases, tuberculosis, pregnancy, and vaccinations.[169] Therefore, it is most informative to perform a treponemal and a nontreponemal diagnostic test in concert; a typical clinical diagnosis may be based upon an RPR or VDRL screening followed by a TP-PA or FTA-ABS confirmation.[168]

Each of these diagnostic tests relies on a visual interpretation of results and/or labeling. The FTA-ABS utilizes the reaction of fluorescently-labeled anti-IgG antibodies with anti-treponemal serum antibodies bound to an antigen-coated slide, detected using fluorescent microscopy. The TP-PA test employs antigen-coated colored gelatin particles to visualize the hemagglutination of reactive antiserum (Figure 4.2[170]). The VDRL test evaluates the level of clumping between antiserum and an antigen containing cardiolipin, lecithin, and cholesterol as seen under a visible light microscope.[167,168] The RPR test utilizes charcoal as a visualizing agent to detect this same clumping reaction with the naked eye (Figure 4.2[170]). The application of BSI to syphilis diagnostics would enable both treponemal and nontreponemal tests to be performed rapidly in a single low-volume

TP-PA   **RPR**
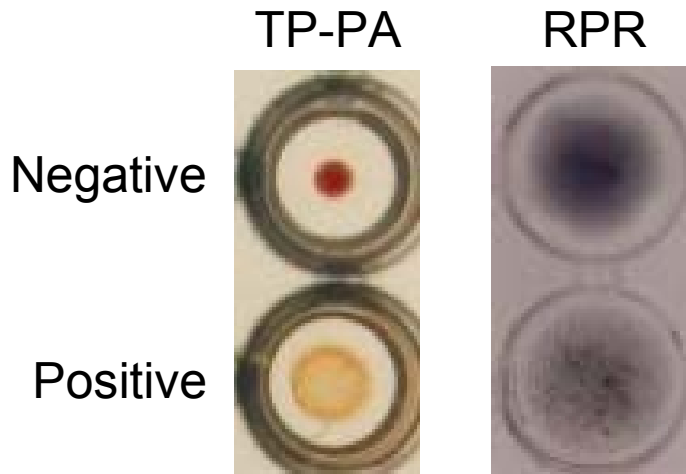
Negative

Positive

Figure 4.2: Images of positive and negative results using the TP-PA and RPR tests.

assay format without the use of fluorescent tags, visualizing agents, or microscopy, as well as decreasing time and cost considerations.

Blind Assay:

Through a collaboration with the Sexually Transmitted Disease (STD) division of the Centers for Disease Control and Prevention (CDC), samples for a blind assay, including four human serum samples (1 – 4) and four syphilis antigens (A – D), were received. The serum samples were from patients with different titer values (negative, low titer, medium titer, and high titer) based on the standard RPR test. The antigens were three different protein conjugated cardiolipin antigens and a treponemal antigen, all at a 10 µg/mL concentration. Cardiolipins are used as antigens to detect antibodies in the serum that are created as a result of the damage caused to the host cells.[167] The

treponemal antigen (r17) is a recombinant protein antigen with a molecular weight of 17 kDa that mimics the proteins found on the surface of the treponemes.

The initial experiment set up was an endpoint analysis of the combinations of the four serum samples with the four antigens, utilizing the borosilicate glass chips manufactured by Micronit previously described (Chapter III). The serum samples were first diluted with PBS in a 1:10 ratio (30 µL serum + 300 µL PBS). Equal amounts of the diluted serum and the antigen (15 µL diluted serum + 15 µL antigen) were then thoroughly mixed to yield a solution that had a final serum dilution of 1:20 and a final antigen concentration of 5 µg/mL. The mixture was then introduced into the channel and the BSI measurements were taken of all 16 samples and plotted versus serum number for each antigen.

The average phase values of the serum – antigen mixtures were plotted versus serum number and are shown in Figure 4.3. As expected, the trend of the serum samples was consistent for each antigen. The trend indicates the order of reactivity for the serum samples for the antigens; however, it is not possible to differentiate the sera samples or to determine which is the non-reactive serum and which is the high-reactive serum. Therefore the order according to reactivity is either serum 1 < serum 4 < serum 3 < serum 2 or serum 2 < serum 3 < serum 4 < serum 1.

This limitation is due to the fact that, without prior knowledge, the fringes can shift either to the left or to the right depending on the change in RI and that binding interactions can cause either an increase or decrease in RI. The source of the signal detected by BSI is still under investigation, but is thought to arise from changes in conformation, waters of hydration, and molecular dipoles.[91] The effects of binding on
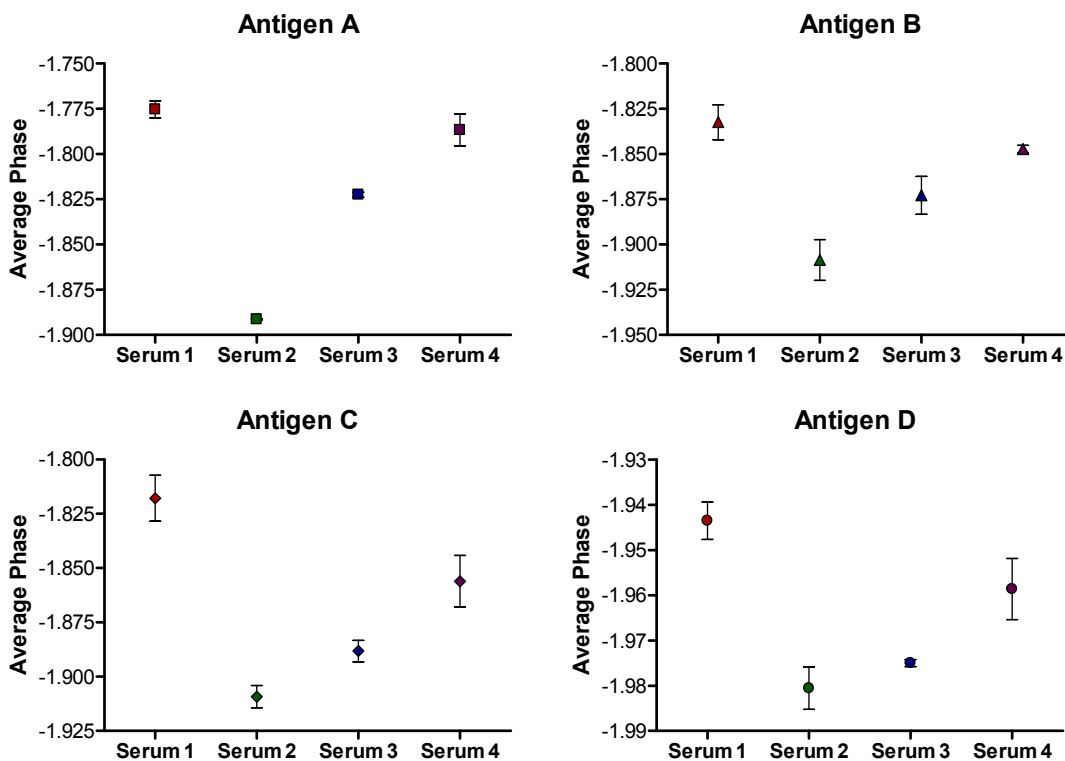
Figure 4.3: BSI measurements of the blind assay endpoint analysis.

these properties is not immediately predictable and can result in an increase or decrease in the BSI signal. In short, without previous knowledge of the binding system or a known blank sample, the phase change can be positive or negative as the reactivity of the sample increases. Of course, in a real assay, calibrations and controls would eliminate this limitation.

Utilizing the ability of BSI to perform real-time measurements, a kinetic analysis was performed in a manner similar to the interleukin-2 assay in Chapter II. This experiment utilized a chip, also manufactured by Micronit that had an on-chip serpentine mixer (Figure 4.4). The diluted serum was introduced into one inlet and the antigen was
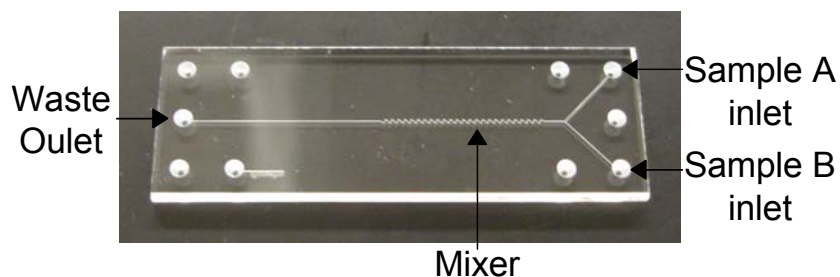
Figure 4.4: Microfluidic mixer chip used in the kinetic analysis experiments.

introduced into the second inlet. The samples were then drawn through the channel with a vacuum, mixing the pair and allowing the binding event to be observed in near-real time. By observing the magnitude and direction of the binding isotherm, this assay allowed for the assignment of the relative titer strengths of the samples. The serum sample that consistently showed the largest binding signal would have the highest relative concentration of antibody and, therefore, the highest titer.

The kinetic assay showed a consistent decrease in phase as the antibody and
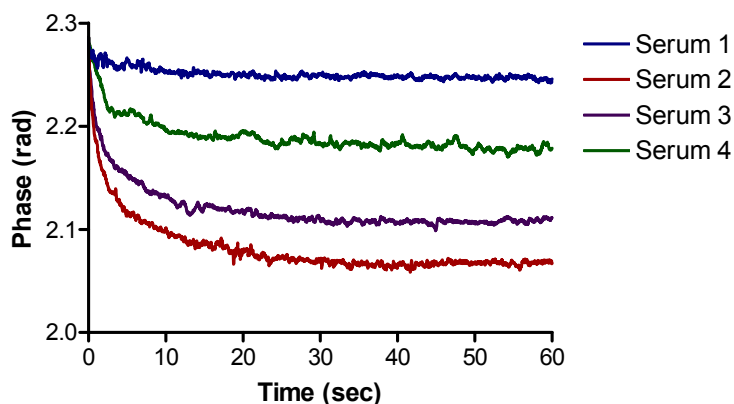
Figure 4.5: A sample of the real-time binding curves observed during the kinetic analysis.

antigen bound. A representative trace of the binding curves for all of the serum samples is shown in Figure 4.5. The magnitude of the change was confounded slightly by inconsistencies in the mixing due to the difference in viscosities of the serum and the antigen solution and by protein adhesion to the surface of the channel. However, the overall trend showed the largest binding signal for serum 2 indicating that it had the highest reactivity. The relative strength of the sera samples could then be determined from the trend observed in the endpoint assays resulting in the following assignments:

- Serum 1 = Non-Reactive

- Serum2 = High Reactive

- Serum 3 = Mid Reactive

- Serum 4 = Low Reactive

The results from BSI were compared to the known titers of the blinded serum samples based on the standard RPR test performed by the CDC (Figure 4.6). It was
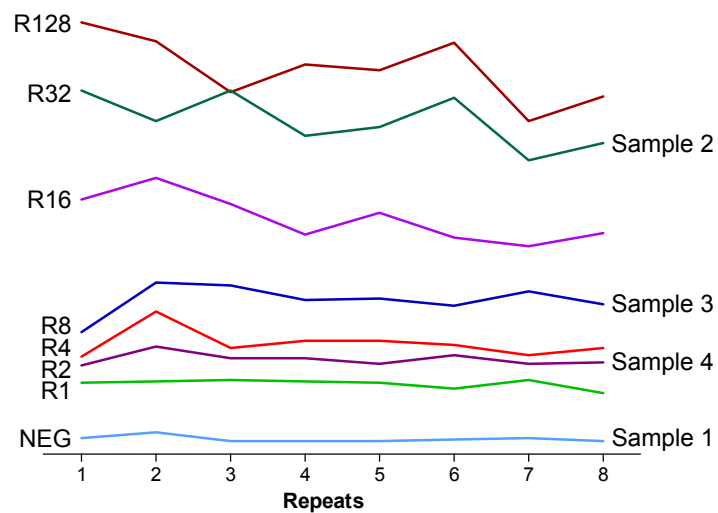
Figure 4.6: Results of the ELISA scan provided by the CDC.
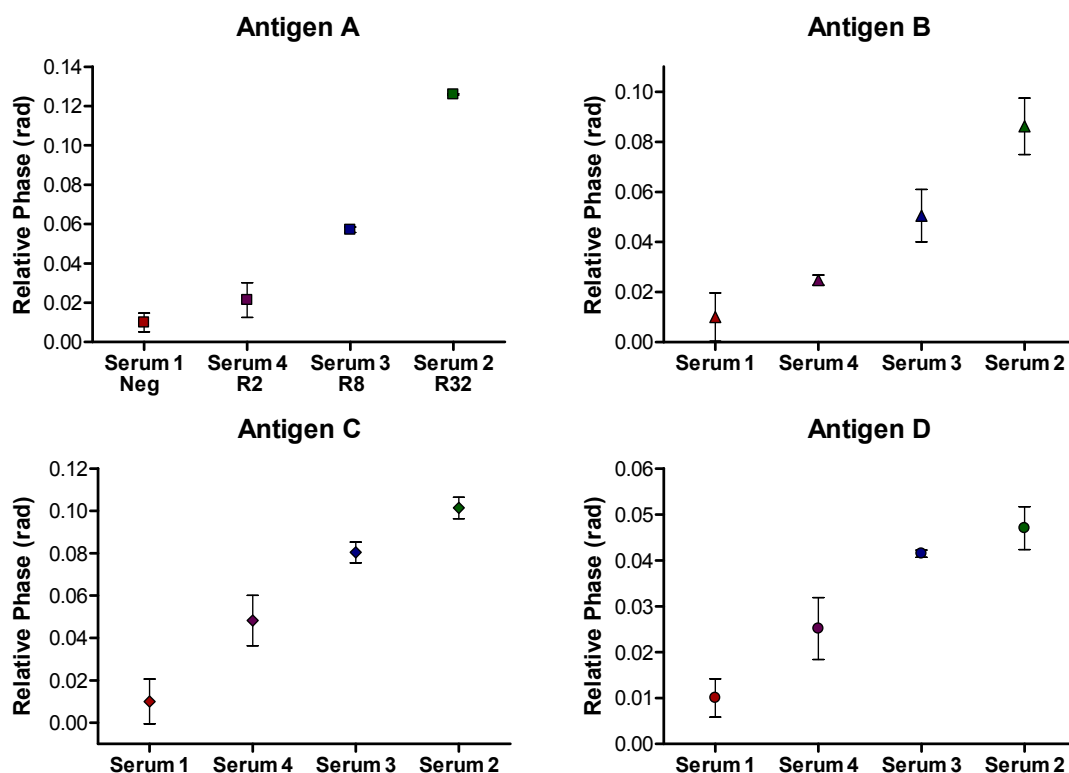
Figure 4.7: Adjusted BSI measurements of the blind assay endpoint analysis illustrating the consistent trend, in agreement with the ELISA results.

determined that our ranking of the sera samples was correct: serum 1 was a negative sample, serum 2 was an R32 sample, serum 3 was an R8 sample, and serum 4 was an R2 sample (Figure 4.7).

Micellar Cardiolipin Antigen:

A micelle is an aggregate formed by molecules with hydrophilic head regions and hydrophobic tail regions. The molecules arrange themselves in a typically spherical formation, so that the hydrophobic tails are protected from the aqueous environment by
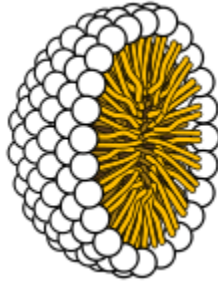
Figure 4.8: Image of a micelle.

the hydrophilic head groups (Figure 4.8). The micellar cardiolipin antigen is a synthetic antigen containing cardiolipin, cholesterol, and lechithin which is designed to mimic the lipoidal material secreted from damaged host cells and from the treponeme itself.[167] It has been developed by the CDC in order to increase the sensitivity of the non-treponemal agglutination tests. The next experiment tested the use of the micellar cardiolipin antigen for BSI measurements. The micellar antigen was diluted in a 1:500 ratio with PBS (1 µL antigen + 500 µL PBS) and mixed in even amounts with the diluted serum, yielding a solution that had a final serum dilution of 1:20 and a final antigen dilution of 1:1000. The results of the analysis had the same trend as the titer strength calculated using the standard RPR test with a traditional cardiolipin antigen (Figure 4.9). This analysis further shows that BSI has the potential to be a quantitative test for the presence of antibodies in clinical samples.

Treponemal Antigen:

In order to evaluate the performance of BSI in determining the reactivity of clinical samples, the treponemal antigen experiments were expanded to include multiple
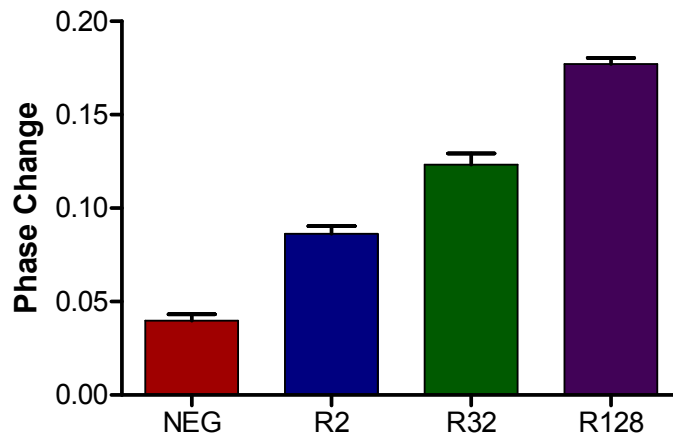
Figure 4.9: Results of the interaction of the serum with the micellar cardiolipin antigen; error bars represent the noise within the measurement. The results show a good correlation with the titers determined by the standard RPR test.

clinical samples. The samples used in this experiment were previously classified as positive or negative using the treponemal particle agglutination (TP-PA) test by the CDC. The serum samples were first diluted with PBS and were then mixed with the r17 treponemal antigen to yield a solution that had a final serum dilution of 1:20 and a final antigen concentration of 5 μg/mL. The samples were incubated for one hour at room temperature. The binding signal of the interaction was measured and plotted versus the serum classification (Figure 4.10). These results show a strong statistical difference (p = $2 \cdot 10^{-6}$) between signals for positive and negative samples using the treponemal r17 antigen. This data demonstrates that a signal threshold may be established for determining the reactivity of unclassified samples.
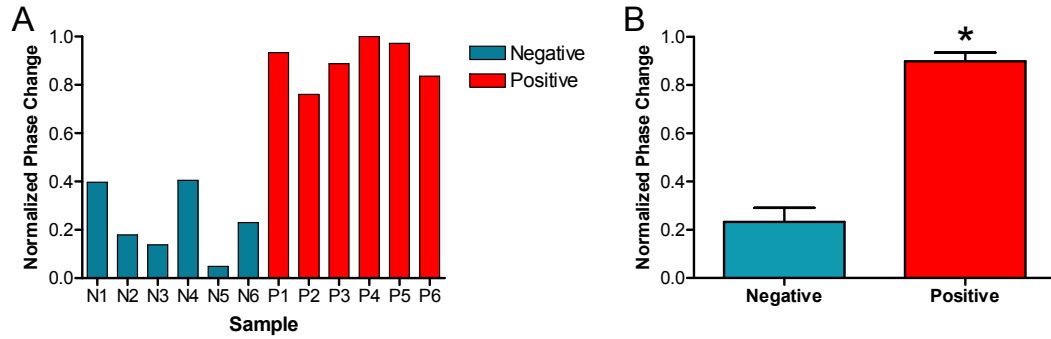
Figure 4.10: A. Treponemal results in twelve clinical samples. B. Average signal for positive and negative samples showing a clear separation ($p = 2 \cdot 10^{-6}$).

Conclusions:

The experiments performed using human serum samples demonstrate that BSI may be capable of serving as a reactive serum detector in a clinical setting. There was a clear threshold between reactive and nonreactive sera determined for a panel of samples using a treponemal antigen. Additionally, the BSI signal arising from the binding of the antiserum and the nontreponemal antigens shows a strong correlation with the semi-quantitative RPR test currently in practice. These results show promise for utilizing BSI to perform rapid serological tests using a variety of molecular probes, offering endless possibilities for multiplexed, quantitative assays to improve current clinical diagnostics and therapy monitoring applications.

CHAPTER V

MEMBRANE ASSOCIATED BINDING STUDIES PERFORMED UTILIZING
BACKSCATTERING INTERFEROMETRY

Background and Significance:

Lipid bilayer membranes are naturally-occurring, two-dimensional fluids comprised of stringently regulated combinations of molecules, such as phospholipids and proteins. This molecular architecture of membrane-associated proteins is ubiquitous within all living organisms. Molecular interactions occurring at or on these proteins occur only within the well-defined chemical environment afforded by the surrounding lipid bilayer membrane. This two-dimensional fluid not only serves to isolate a cell from its external environment, but also provides the spatial, temporal, and chemical control critical for these events to occur. The molecular interactions occurring at the membrane are constantly transformed into gross physiological phenotypes through a combination of spatially-regulated binding events and transduction of the resulting signal across the membrane barrier.[171] As a result, membrane-associated proteins and their interactions remain of great interest to the design of clinical therapies, accounting for almost 70% of existing drug candidate targets.[172] Though a plethora of assays exist to examine binding events, for this class of molecular interactions, the targets of interest must typically undergo covalent modification and removal from the native membrane environment prior to observation. Techniques such as direct labeling, surface coupling, and genetic modification, while necessary for quantitative analysis, are known to affect a target's function in unpredictable ways, pose experimental hazards, and are not uniformly

applicable to all targets.[173] BSI's ability to study homogeneous binding events[91] will now be employed to study membrane-associated interactions in a label-free solution-based format.

In the simplest case, optically compatible synthetic lipid membrane-based materials can be created that allow for well-defined display of chemical and biological moieties within the context of a fluid lipid bilayer.[174,175] By introducing a binding target into membranes during the organic mixing phase, a population of small, unilamellar vesicles (SUVs) containing a uniformly-distributed population of solution-accessible ligands was created. By controlling the incorporation of specific lipids in the organic phase, the population of created vesicles can be made to retain the characteristic fluidity of native membranes (Figure 5.1). In this case, the monosialoganglioside GM1 was used
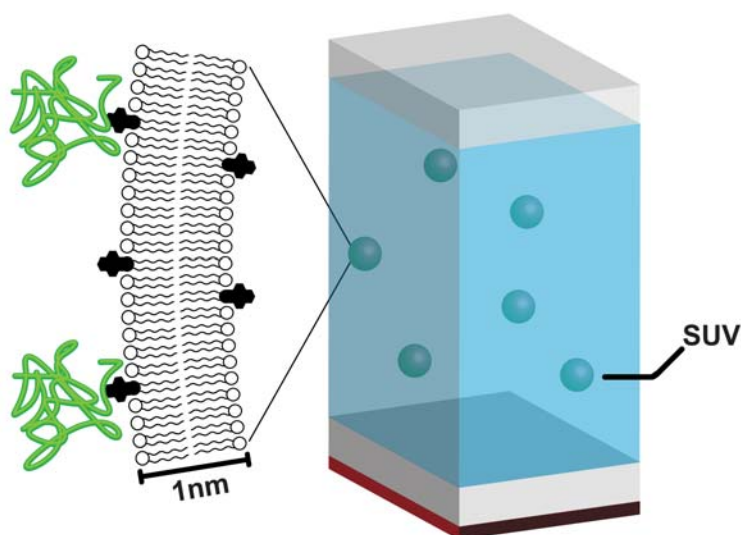
Figure 5.1: Schematic illustration of the SUVs containing the binding motifs within the lipid bilayer (black) incubated with the cognate ligands (green).

as the target molecule to be embedded into the membrane; GM1 is a target for the cholera toxin. The B subunits of the cholera toxin (CTB) bind to the pentasaccharide region of the GM1 and initiate the intoxication of the host cell.[176,177] This interaction is characteristic of most bacterial toxins and has been well studied in the testing of potential inhibitors.[176-178]

It is also possible to incorporate full-length, non-recombinant membrane proteins into membranes.[179,180] Through the detergent solubilization and dialysis, a population of proteins can be introduced into a lipid bilayer membrane of synthetic origin. The resulting materials have been shown to retain the *in vivo* characteristics of both ordered structure and fluidity, thus maintaining the activity of the associated proteins. Though deposited onto supported monolithic substrates is a common technique for observing purified membrane proteins, transmembrane proteins usually suffer from restricted movement with this strategy, presumably due to the interactions occurring with the underlying surface.[181-184] In fact, it is common to truncate such proteins by attaching a membrane-compatible insertion tag, such as a long-chain alkane, to preserve fluidity, thus conserving the functional elements of such proteins. By using SUVs in combination with full-length proteins, we can preserve the natural fluidity of the membrane and consequently allow the proteins unrestricted diffusive properties along the surface of the membrane. Additionally, we do not compromise the functionality of such proteins through biochemical alteration. For these experiments, the transmembrane protein Fatty Acid Amide Hydrolase (FAAH) was incorporated into the SUV bilayers and its binding to several inhibitors was studied. This particular catabolic enzyme has substantial roles

in many neurological phenotypes, primarily nociception.[185] FAAH inhibitors have shown promise as analgesics and as therapeutics for neuropsychiatric disorders.[186,187]

Since it is not always possible or efficient to extract proteins from all native cells, a common method of determining ligand binding to cell membrane-associated proteins is to study downstream cellular responses in whole cells or to use radioactive assays on cell lysates. Although considered to be the most suitable environments for the retention of correct membrane composition (and as a result, retention of membrane protein binding behavior) such assays cannot provide a method for examining binding directly and without labels. However, by separating the outer membranes of the cell from the intracellular components and converting the membranes into vesicle-like suspensions of uniform size (Figure 5.2), we can render the membranes, with all their constituents, compatible with the BSI instrument without the need for protein purification or alteration.[188,189] To investigate this possibility, a cell line genetically modified to express the G-protein-coupled receptor (GPCR) of B-form gamma-aminobutyric acid receptor (GABA-B) was utilized. This protein has been implicated in many neurological disease
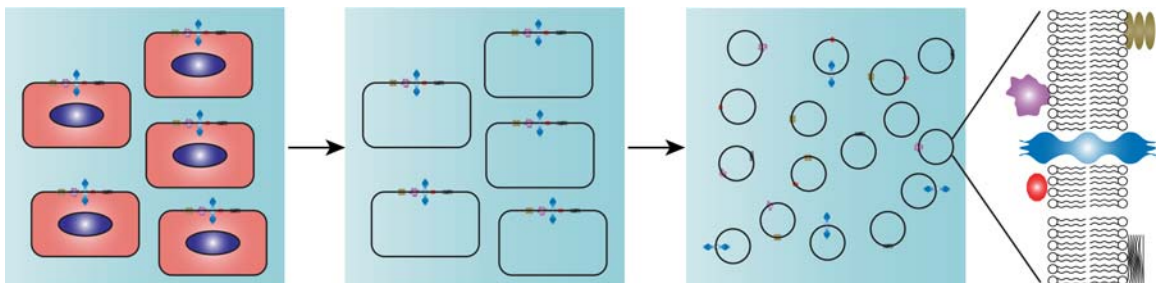
Figure 5.2: Schematic of creation of membrane SUVs. Cells are incubated in a hypotonic solution, gently lysed, and the internal components separated from the outer membranes through centrifugation. Outer membranes are then sonicated and centrifuged to create a uniform population of SUVs.
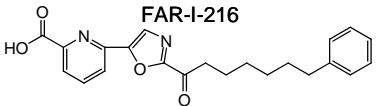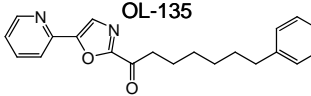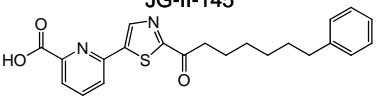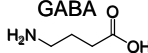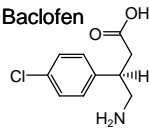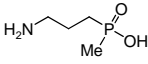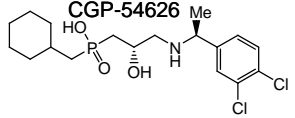
phenotypes and has become a promising drug target.[190-192] However, GABA-B retains the characteristic purification difficulties and low conformational stability that are common to all GPCRs that have been removed from the membrane. The binding of GABA-B to a variety of substrates, including the known binder of gamma-aminobutyric acid, two known agonists (SKF-97541, and R-Baclofen), and one known antagonist (CGP-54626), was interrogated.

Experimental Procedure:

SUVs were formed using standard techniques by Michael Baksh at the Scripps Research Institute (Appendix B). Ligand binding to the SUVs was accomplished by incubating a fixed amount of SUV suspension with varying concentrations of different ligands (Table 5.1). Control solution containing SUVs that did not contain the receptor were also prepared. Ligand and SUV solutions were mixed and allowed to bind for 8 hours at 4°C.

The BSI instrument was set up as previously described using a borosilicate glass chip manufactured by Micronit. The control SUV – ligand solution was introduced into the channel and the BSI signal was measured for 15 seconds. The receptor SUV – ligand solution was then introduced into the channel and the signal measured. The channel was then rinsed and the procedure was repeated iteratively for increasing ligand concentrations. The binding signal was calculated as the difference in phase between the control SUV – ligand solution and the receptor SUV – ligand complex (Figure 5.3). The background signal due to the presence of the SUVs was subtracted from all measurements. This corrected binding signal was then plotted versus concentration to

68

Table 5.1: Membrane-bound receptors and ligands studied.

Membrane Bound Receptor	Ligand	Concentration Range
GM1	CTB	100 pM – 100 nM
FAAH	FAR-I-216	1 pM – 30 nM
	OL-135	3 pM – 30 nM
	JG-II-145	10 pM – 300 µM
GABA-B	GABA	10 nM – 300 µM
	Baclofen	100 nM – 50 µM
	SKF-97541	5 nM – 2.5 µM
	CGP-54626	500 pM – 500 nM

form a saturation binding curve and fitted to a square hyperbolic function to calculate the K_D value.

Results and Discussions:

The interaction between CTB and membrane-bound GM1 was measured and the results are shown in Figure 5.4A. The data was fitted with a single-site binding model and dissociation constant (Table 5.2) was found to be 129 ± 27 pM ($R^2 = 0.94$). Tetanus
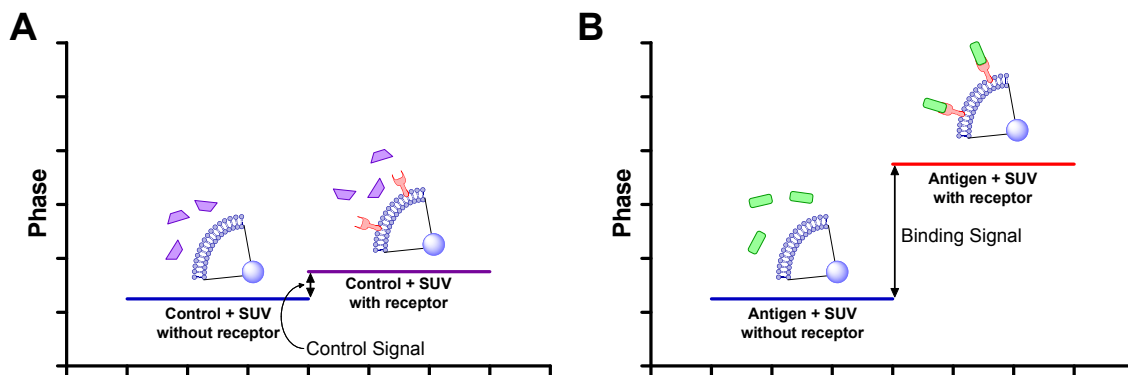
Figure 5.3: Illustration of the calculation of the (A) control signal and (B) binding signal of the ligand – membrane-bound receptor interactions.

toxin (TT) was used a control and showed little binding to the GM1 vesicles. This value is consistent with established measurements obtained from other experimental systems, such as SPR and supported lipid bilayers.[176,178]

The results of the measured interaction of FAAH with the inhibitor molecules are shown in Figure 5.4B-D. The K_D values determined (Table 5.2) for these interactions were: 128 ± 22 pM ($R^2 = 0.85$) for FAR-I-216, 264 ± 36 pM ($R^2 = 0.86$) for OL-135, and 4.1 ± 1.7 µM ($R^2 = 0.89$) for JG-II-145. Cholesterol was used as a control for all the pairs and showed little to no binding in all cases. It should be noted that our observed K_D's differ substantially from what has been demonstrated previously in the literature.[193] However, the difference may be due to the fact that these previous measurements were performed on a truncated version of FAAH and utilizing methods of analysis that involved mixtures of organic and aqueous solvents in an attempt to stabilize the protein. While it is possible to solubilize an amphipathic transmembrane protein in a combination of solvents, a two-solvent configuration is probably not representative of the native

70

membrane environment. Consequently, the protein will likely display binding characteristics that differ from those observed when the protein is in its native membrane environment. Additionally, our binding measurements are measured directly, without the
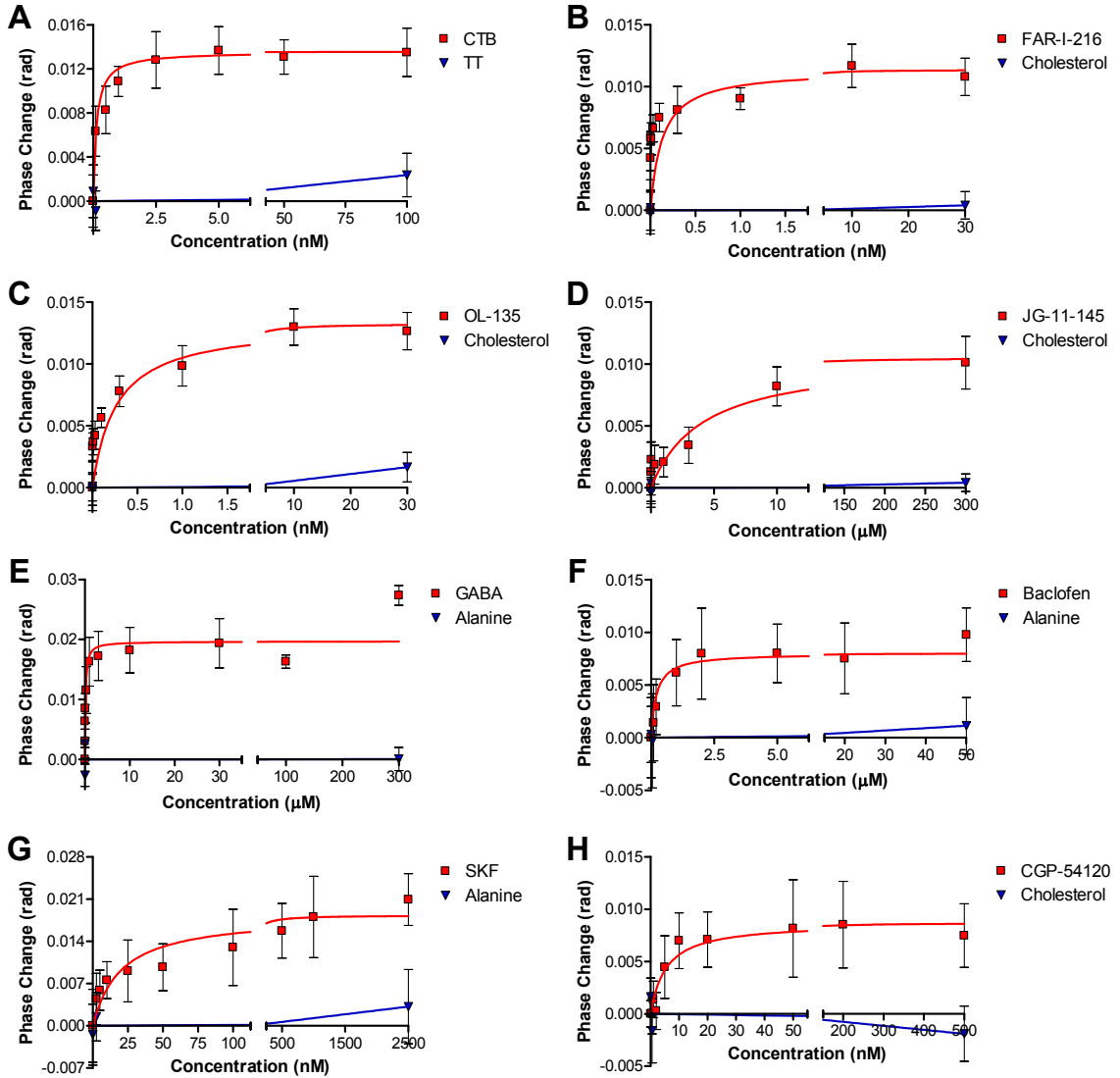
Figure 5.4: Binding curves obtained for all experiments (red squares). Description of binding partners: (A) GM1-CTB; (B) FAAH – FAR-1-216; (C) FAAH - OL-135; (D) FAAH – JGII-145; (E) GABA-B – GABA; (F) = GABA-B – Baclofen; (G) NCM – SKF-97541; (H)= NCM – CGP-54626. Controls showed little to no binding (blue triangles). Description of the controls: (A) TT; (B-D) cholesterol; (E-G) alanine; (H) cholesterol.

Table 5.2: Calculated K_D values and literature affinity measurements for the membrane-bound receptor interactions.

Membrane Bound Receptor	Ligand	K_D Determined	Literature Affinity
GM1	CTB	129 ± 27 pM	K_d = 4.61 pM[176] IC_{50} = 20 nM[178]
FAAH	FAR-I-216	128 ± 22 pM	K_i = 20 nM[193]
	OL-135	264 ± 36 pM	K_i = 4.7 nM[193]
	JG-II-145	4.1 ± 1.7 µM	K_i = 10 µM[193]
GABA-B	GABA	139 ± 65 nM	IC_{50} = 140 nM[195]
	Baclofen	208 ± 34 nM	IC_{50} = 210 - 250 nM[194,195]
	SKF-97541	20 ± 7.1 nM	IC_{50} = 66 nM[194]
	CGP-54626	5.4 ± 1.7 nM	IC_{50} = 2.2 nM[195]

use of labels, which are currently employed to characterize these binding systems. Furthermore, existing assays for FAAH-ligand binding measurements generally tend to rely on downstream signals, such as enzymatic activity, to determine binding affinities.

The reactions between the GABA-B contained in native cell membranes and several ligands were quantified and the results are shown in Figure 5.4E-G. The dissociation constants (Table 5.2) were calculated from the curves and found to be: 139 ± 65 nM (R^2 = 0.86) for GABA, 208 ± 34 nM (R^2 = 0.97) for baclofen, 20 ± 7.1 nM (R^2 = 0.88) for SKF-97541, and 5.4 ± 1.7 nM (R^2 = 0.92) for CGP-54626. Alanine was used as a control for GABA, baclofen, and SKF-97541 and cholesterol was a control for CGP-54626. In all cases, the control showed little to no binding. The calculated K_D values agree well with existing data of radioactive displacement and competitive binding assays.[194,195]

Conclusions:

The experiments presented in this chapter have shown that it is possible to measure ligand – receptor binding events in a solution-based, native membrane environment using backscattering interferometry in combination with synthetic and reconstituted membrane technology. This technique helps to maintain the native structure of the membrane-associated receptor and has the potential to address many applications. In particular, a high-throughput screening of ligand binding to cell surface proteins could serve to simplify the screening of new drug candidates, as well as enable the more direct examination of interactions at membrane surfaces. The chemical control imparted by synthetic membranes could very well serve to display ligands that might not be amenable to any other environment, as well as enhance the signal-to-noise present in such measurements due to factors such as lipid compressibility and consequent dynamic rearrangement of water.

CHAPTER VI

SMALL MOLECULE RECOGNITION ASSAYS USING
BACKSCATTERING INTERFEROMETRY

Antibody – Antigen Interactions:

Background and Significance:
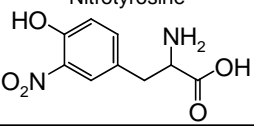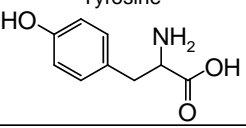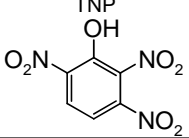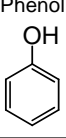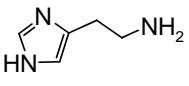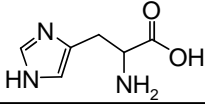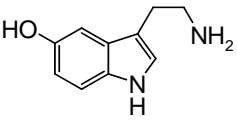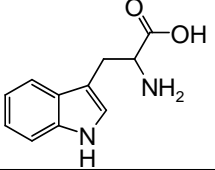
Billions of different a ntibodies are created in nature by the immune system in order to protect the body.[196] Antibodies have been used to detect analytes since the 1950's[197] and by 1975, with the development of the monoclonal antibody,[198] antibodies began to be produced in large quantities. Antibodies currently play a large role in biological and biochemical research as well as in medicine for both diagnostic and therapeutic purposes.[199-201] Antibodies are also fundamental to the determination of biomarkers that are central to the diagnosis of cancers and other diseases.[202-207] As antibody production methods have improved,[202,208,209] it has become possible to create numerous different antibodies faster than it is possible to perform the characterization of their binding.[199] There are several methods available for antibody characterization, however most rely on labeling or on surface immobilization.[196,200] As discussed in Chapter I, altering a molecule in any way can affect its ability to interact and bind; therefore, it is advantageous to have a quick, efficient, free-solution, label-free method to measure antibody interactions and to quantify the affinity of the interaction. BSI has the potential to fit this need and the work presented here demonstrates this potential.

74

Four systems have been chosen to illustrate BSI performance in the characterization of antibodies. These systems include four different small molecules (nitrotyrosine, 2,3,6-trinitrophenol (TNP), histamine, and serotonin) and their monoclonal antibodies. Nitrotyrosine is created in the body in the presence of nitric oxide and has been linked as a marker for various diseases and inflammatory processes.[210-212] TNP is a model for explosive materials, which would benefit from a quick detection method. Histamine is involved in many systems in the body, including the immune system, the gastrointestinal system, and the central nervous system, and works to regulate inflammation.[213-215] Serotonin is a well-studied neurotransmitter that is also involved in the cardiovascular and gastrointestinal systems.[216] These molecules were chosen because they represent a variety of molecules that are characteristic of antibody targets.

Experimental Procedure:

The BSI instrument was set up as previously described using a borosilicate glass chip manufactured by Micronit (Chapter III). Solutions of the antigen alone and the antigen − antibody mixture were prepared in Dulbecco's phosphate buffered saline (DPBS) over the concentration ranges outlined in Table 6.1. The solutions were allowed to bind and equilibrate overnight at 4°C. The antigen solution was introduced into the channel and the BSI signal was measured for 15 seconds. The solution with the same concentration of antigen with the antibody present was then introduced into the channel and the signal measured. The channel was then rinsed and the procedure was repeated iteratively for increasing antigen concentrations. The binding signal was calculated as the difference in phase between the antigen alone and the antigen − antibody complex

Table 6.1: Ligand and control molecules studied.

Ligand	Control	Concentration Range
Nitrotyrosine	Tyrosine	0 – 100 nM
TNP	Phenol	0 – 1000 nM
Histamine	Histidine	0 – 100 nM
Serotonin	Tryptophan	0 – 1000 nM

(Figure 6.1). The background signal due to the presence of the antibody was subtracted from all concentrations. The corrected binding signal was then plotted versus concentration to form a saturation binding curve and fitted to the square hyperbolic function using Prism^{TM} software to calculate the K_D value.

Results and Discussions:

The interaction between the four small molecules and their antibodies was measured and the results are shown in Figure 6.2. The corrected binding signal determined from the phase change in the interferometry signal was found to vary in a manner consistent with dose-dependent saturation of a single binding site. The
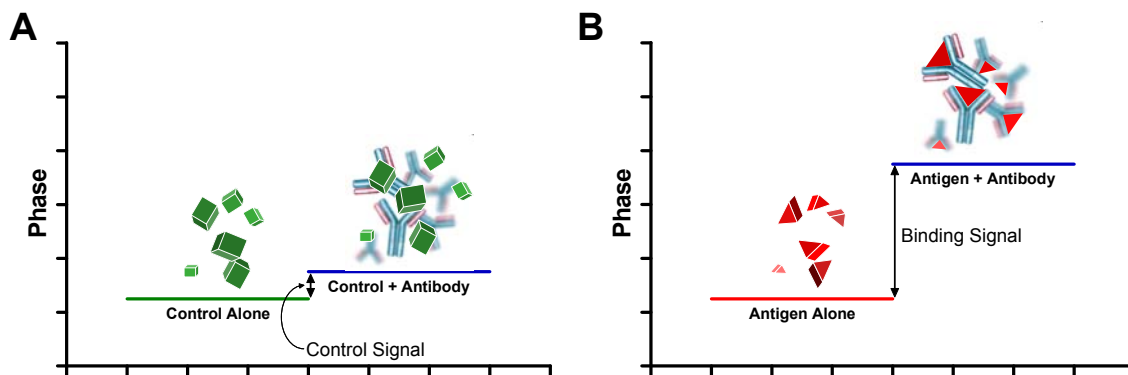
Figure 6.1: Illustration of the calculation of the (A) control signal and (B) binding signal of the antigen – antibody interaction.

dissociation constants calculated (Table 6.2) from these curves were: 1.34 ± 0.21 nM for nitrotyrosine ($r^2 = 0.99$), 21.9 ± 4.0 nM for TNP ($r^2 = 0.97$), 330 ± 109 pM for histamine ($r^2 = 0.93$), and 10.9 ± 1.4 nM for serotonin ($r^2 = 0.99$). In all cases, little to no BSI response was recorded for the controls, demonstrating the expected specificity of the antibody-based detection system. The controls were molecules with very similar structures: tyrosine for the nitrotyrosine antibody; phenol for the TNP antibody; histidine

Table 6.2: Summary of the measured affinities of the antibodies studied.

Antibody	Affinity (K_D)	Correlation (R^2)
Nitrotyrosine	1.34 ± 0.21 nM	0.99
TNP	21.9 ± 4.0 nM	0.97
Histamine	330 ± 109 pM	0.93
Serotonin	10.9 ± 1.4 nM	0.99
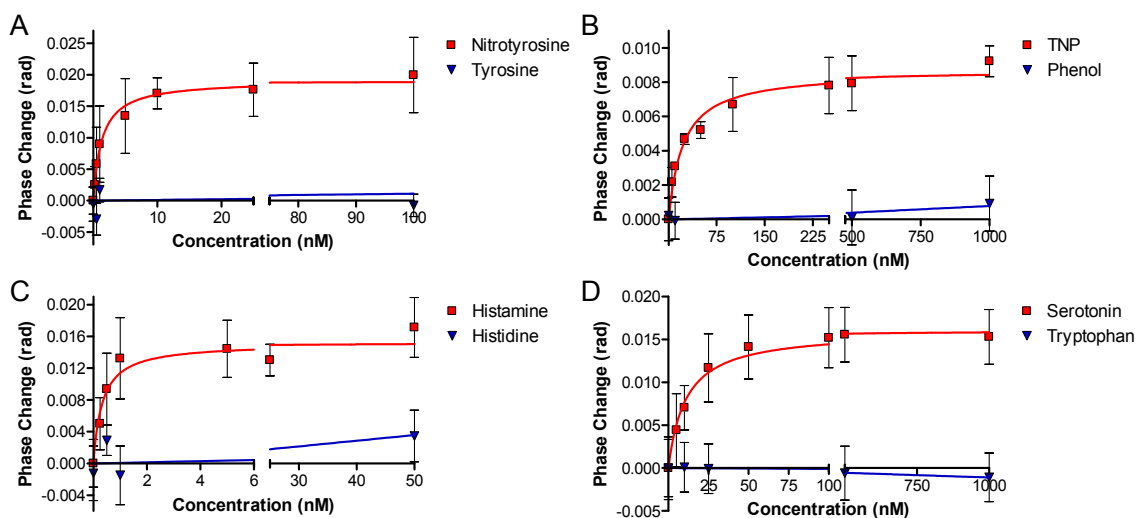
Figure 6.2: Endpoint analysis dose-response curves (red squares) for four small molecule antigens and their cognate antibodies: A. nitrotyrosine, B. trinitrophenol, C. histamine, and D. serotonin. Controls (blue triangles) using very similar molecules (A. tyrosine, B. phenol, C. histidine, and D. tryptophan) showed no binding and illustrated the specificity of the antibodies.

for the histamine antibody; and tryphtophan for the serotonin antibody (see Table 6.1). For these antibodies, no affinity measurement has previously been performed; however, the results are consistent with values typically seen for monoclonal antibodies and are in agreement with the recommended concentrations for the antibody for the use in immunohistochemistry experiments that detect the presence of the ligand.[217,218] Affinity measurements are not typically performed for every batch of antibody produced because the affinity is not necessary for most qualitative tests and it would require the consumption of too much antibody. This point illustrates the need for a quick, reliable method to measure the binding affinity of antibodies that does not use large amounts of sample. BSI required less than 3 µg of antibody for each determination, making it perfectly suited to meet this need.

Encapsidated Aptamer Interactions:

Background and Significance:

Aptamers are oligonucleotides and are emerging as an alternative for molecular recognition assays. Aptamers were first developed in 1990[219,220] and have become known for their specificity.[221] In fact, aptamers can be developed that are more selective than antibodies.[222] These molecules are developed and identified *in vitro*[221,223] so they do not depend on the animals or cells, which is a significant advantage over antibodies. This development process also creates the advantage of being able to change the properties of the aptamer as needed.[221] Aptamers can also be synthesized quickly and precisely, eliminating batch-to-batch variations. They are also very stable, so shipments can be at ambient temperatures and they can be stored long-term without loss of activity.[221] Because of these advantages, aptamers are quickly gaining widespread acceptance and have been used in place of antibodies for numerous applications, including chromatography, flow cytometry, electrophoresis, and several biosensors.[221,224,225]

Heteroaryl dihydropyrimidines (HAP, Figure 6.3A) are a class of molecules that are not found in nature; therefore, HAP molecules are good targets for aptamer development because the dissimilarity in structure should prevent off-target binding to other biological molecules. HAP has also been studied for non-nucleosidic inhibition of the hepatitis B virus replication.[226-228] Through *in vitro* selection[219,229] an RNA aptamer (clone 2-1) to a HAP was developed by the Finn lab at the Scripps Research Institute. The aptamer was then packaged into the coat protein of bacteriophage Qβ, which is expressed recombinantly to generate icosahedral virus-like particles (VLPs). A hairpin
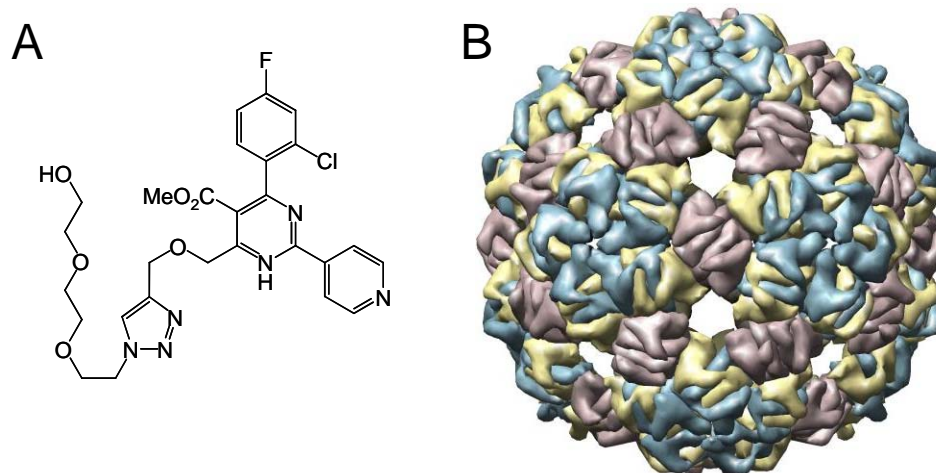
Figure 6.3: A. Structure of the Heteroaryl dihydropyrimidine (HAP) target. B. Structure of the Qβ capsid showing the prominent holes through which HAP can diffuse to the interior to bind the encapsidated aptamer.[137]

RNA sequence is specifically bound by the inside of the capsid and can direct the encapsidation of desired RNA molecules.[230] The protein capsid is stable to a variety of chemical and genetic modifications; therefore, when encapsidated, the aptamer is protected from nuclease degradation yet still retains its ability to bind HAP molecules that diffuse into the capsid interior. The Qβ capsid features several large openings in its structure[142] (Figure 6.3B) which allow small molecules, such as HAP, to easily access the interior.

Experimental Procedure:

The binding of HAP to four different RNA aptamer sequences packaged inside the Qβ capsid was measured in a similar manner as the antigen – antibody interactions. These aptamers included the original aptamer (Qβ 2-1), a single point mutant (Qβ A), a triple point mutant (Qβ E), and a mutant with the necessary hairpin (Qβ Δhp). For these
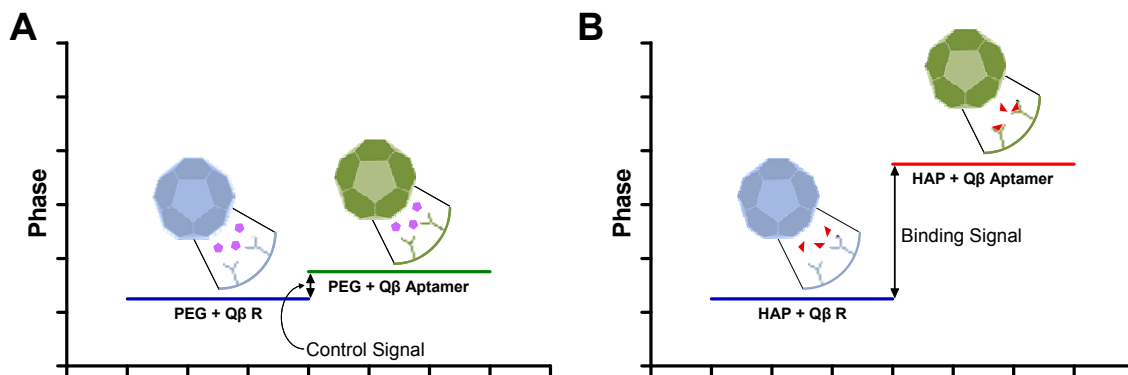
Figure 6.4: Illustration of the calculation of the (A) control signal and (B) binding signal of the encapsidated aptamer - HAP interaction.

measurements, the interactions of HAP and a control with an encapsidated nonsense RNA strand (Qβ R) was compared to the interactions of HAP and Qβ containing the aptamer in a similar manner to the antibody experiments (Figure 6.4). The solutions were made in 50 mM HEPES buffer with 150 mM NaCl and 5 mM MgCl$_2$ and were incubated for ~8 hours at 4°C. The control solution was introduced into the channel and the BSI signal was measured for 15 seconds. The solution with the same concentration of HAP with the aptamer present was then introduced into the channel and the signal measured. Subsequently, the channel was rinsed and the procedure was repeated iteratively for increasing HAP concentrations (10 pM to 15 nM). The corrected binding signal was determined, plotted versus concentration to form a saturation binding curve, and fitted with a square hyperbolic function using Prism^{TM} software to calculate the K$_D$ value.

Results and Discussions:

The interaction between HAP and the four encapsidated RNA aptamers was measured and the results are shown in Figure 6.5. Three of the aptamers were found to bind with curves consistent with a dose-dependent saturation of a single binding site. The dissociation constants calculated (Table 6.3) from these curves were: 31.4 ± 9.6 pM for Qβ 2-1 ($r^2 = 0.96$), 8.96 ± 1.95 pM for Qβ A ($r^2 = 0.98$), and 2.40 ± 0.61 nM for Qβ E ($r^2 = 0.98$). The fourth aptamer mutant, Qβ Δhp, which does not have the necessary hairpin to interact, did not show any binding (Figure 6.5D). For all aptamer mutants, little to no BSI response was seen using the control molecule, PEG, illustrating that the
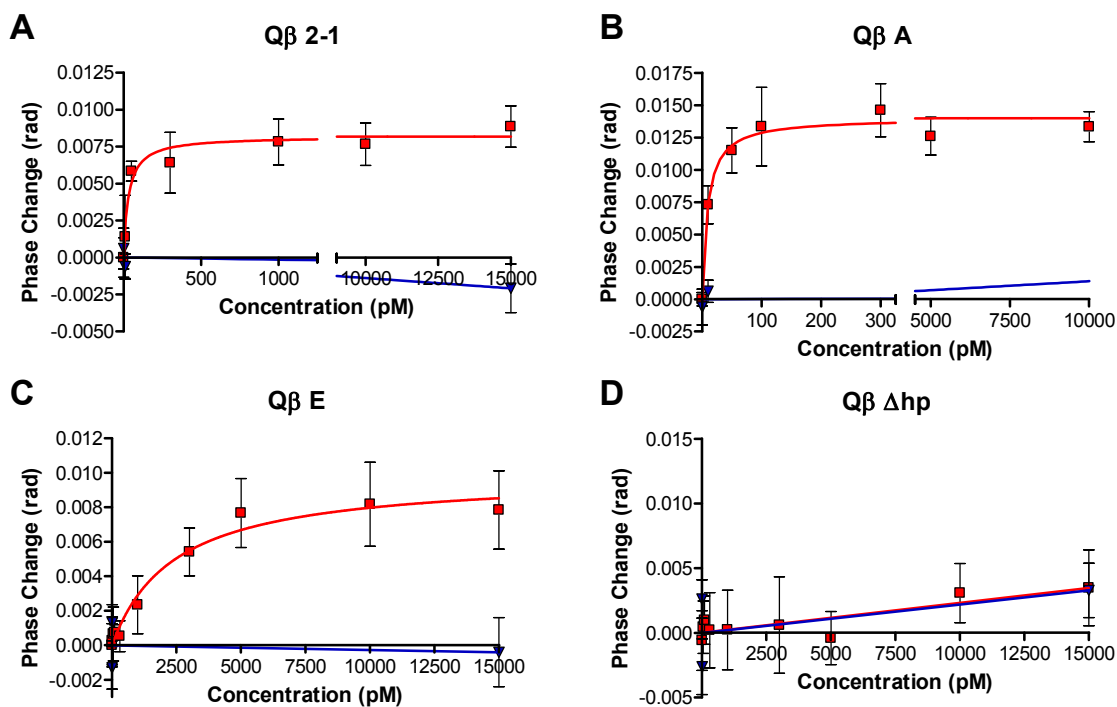
Figure 6.5: Endpoint analysis dose-response curves for heteroaryl dihydropyrimidine (HAP) against four mutations of the RNA apatmer packaged inside the Qβ capsid (red squares). PEG was used as a control (blue triangles) and showed little to no binding.

Table 6.3: Summary of the measured affinities of the aptamers studied.

Mutant	Affinity (K_D)	Correlation (R^2)
Qβ 2-1	31.4 ± 9.6 pM	0.96
Qβ A	8.96 ± 1.95 pM	0.98
Qβ E	2.40 ±0.61 nM	0.98
Qβ Δhp	non-binding	

binding is specific. These experiments illustrate the potential of BSI to be used to study aptamer binding, in both a traditional application and in an encapsulated manner. It would have been difficult to measure these interactions with another method because the affinities of these particles are very high which can make the measurements difficult to perform, as described in Chapter II. Labeling of the HAP would have created a considerable change in the ligand structure, giving rise to significantly different RNA binding properties. Additionally, measuring the encapsidated interactions would not have been possible using a surface immobilized technique, because the binding partners would not be able to get close enough to interact. The ability to package and protect a molecule has uses in vaccine development, cytotoxic drug delivery, and protect RNA sequences used to induce protein expression.[231-234] A method to characterize these particles in their encapsidated form is therefore an important task that BSI is uniquely capable of performing.

Conclusions:

It has been shown in this chapter that BSI is capable of quantifying the interactions of both antibodies and aptamers, two main types of molecular recognition molecules. Novel measurements of the affinity of four monoclonal antibodies were reported and the specificity of the antibodies was demonstrated using very similar molecules as controls. This has demonstrated that BSI is capable of measuring the affinities in an efficient, free-solution, label-free manner while only using a minute amount of sample. These unique properties of BSI makes it well suited for use in antibody characterization.

The affinities of several mutations of an RNA aptamer for HAP were also determined. This is an important system to measure because aptamers are becoming a prime area of investigation. These measurements were performed with the aptamer encapsidated inside the coat protein of the Qβ virus-like particle, making this a measurement that would have been difficult to impossible to measure with traditional methods, such as SPR. The encapsidation of molecules such as aptamers has shown great promise for many uses because of the protection that the capsid provides. These measurements also did not require modification, such as labeling or immobilization, of either of the binding partners, further demonstrating the unique abilities of BSI.

CHAPTER VII

CONCLUSIONS

Backscattering interferometry is distinctive and versatile instrument that employs a simple optical train to perform highly sensitive, label-free molecular interaction measurements. The unique design of BSI allows for measurements to be performed in either a heterogeneous (surface-immobilized) or homogeneous (free-solution) format.

Heterogeneous measurements performed in this dissertation (Chapter III) measured the relative binding affinities and polyvalent avidities of several glycan – lectin pairs. Because BSI is not a film thickness sensor, these measurements were performed with the lectin attached to the surface. Additionally, an intermediate layer of avidin provided spacing between the channel surface and the binding sites in order to create an environment more conducive to the maintenance of native structure and function. This study is significant because it demonstrates that BSI uniquely allows quantification of a binding event for less than one part in 1000 change in mass. Another unique aspect of BSI demonstrated in these findings is that the BSI response is correlated to the number of actual binding events rather than the size of the species that is involved in the binding. This is consistent with the theory that the signal is created from conformational changes and/or changes in the waters of hydration causing a change in the refractive index.

BSI has also shown exceptional sensitivity in the homogeneous format, detecting tens of thousands of molecules and monitoring interactions with picomolar affinities, without the use of any type of label (Chapter II, V, and VI). This work has expanded the

dynamic range of K_D values that BSI is capable of measuring to span six orders of magnitude.[91]   Additionally, BSI has made it possible to measure these interactions in complex matrices, such as cell media.

The ability of BSI to perform measurements in complex matrices makes it possible to use BSI as a reactive serum detector in a clinical setting. This potential use was tested using human serum samples from patients with syphilis (Chapter IV). A small panel of samples was tested using a treponemal antigen and showed sensitivity, selectivity, and accuracy when compared with traditional clinical tests. There was also a strong correlation of the BSI signal using nontreponemal antigens with the semi-quantitative tests currently in practice. While additional investigations are needed before BSI can be used in clinical testing, its potential for the use in performing rapid serological tests have been clearly demonstrated.

BSI was also applied to the study of membrane-associated proteins, a system that is notoriously difficult to study (Chapter V). Despite the fact that these proteins are the target for nearly 70% of drug candidates, current methods to study the interactions require some type of modification of one of the binding partners. Here we were able to quantify the interaction of several interactions in a solution-based native membrane environment. The ability to study membrane interactions in this format can provide accurate insight into this important class of molecules, and BSI has illustrated that this is now possible.

BSI has also been used to measure the interaction of several monoclonal antibodies and their small molecule ligands (Chapter VI). The binding affinities for the pairs were determined and the specificity of the antibodies was also demonstrated. In

conjunction with these experiments was the measurement of the affinities of several RNA aptamer mutants. The ability of BSI to measure aptamer interactions is important because of their growing applications. Antibody interactions currently play a large role in biological and biochemical research and the replacement of antibodies with aptamers in these fields is growing. Therefore a method to characterize the interactions between aptamers and target molecules quickly and efficiently is needed. BSI fits this need well, demonstrating the ability to accommodate free-solution, label-free binding assays using only a small amount of sample.

BSI is unique, powerful approach to biosensing and has enabled previously impossible molecular interactions studies. BSI works in free solution and with little *a priori* knowledge of the binding pair, allowing this technique to perform novel binding affinity determinations on uncharacterized molecules. BSI had already been shown to be a sensitive technique for quantifying molecular interactions and the work presented here extended the limits, showing that low picomolar binding affinities could be measured. The range of unique applications that BSI is capable of has also been broadened beyond expectations. The ability to monitor interactions with large particles such as micelles, liposomes, and viruses, was once speculation, but has now been proven possible as seen in the work reported in this thesis. Incredibly, it is even possible to quantify binding that occurs inside of such a particle. Further experimentation is needed to fully understand the source of the BSI signal with respect to the changes that occur within biomolecules during the binding process, though properties such as the dipole moment, waters of hydration, and confirmation are likely sources. BSI has the ability to shift the paradigm when attempting to quantify affinity, determine labeling perturbation, or screen for

binding. The process of commercialization of the technology is currently underway and will make BSI available to a wide array of researchers. As the technology continues to develop, the potential for BSI, whether used in a laboratory for the development of new and better drugs, in a doctor's office for the diagnosis of diseases, or in the field to study environmental contaminants, is extensive.

APPENDIX A

PREPARATION OF CARBOHYDRATE COATED VIRAL PARTICLES

Production and Isolation of Virus Particles:

CPMV particles were produced in cowpea plants and isolated using previously published procedures.[235] Briefly, CPMV was isolated from infected leaves of black-eye cowpea plants. Primary leaves from 10-day old cowpea plants were first dusted with carborundum and inoculated with homogenized infected leaves in phosphate buffer. Symptoms of infection appear within a week and a systemic infection is observed after three weeks. Leaves were collected, weighed and frozen for future purification of CPMV. Blended leaf tissue was separated from virus as previously described.[235] Expression of the Qβ coat protein from a recombinant plasmid has been previously reported;[139] we created our own vector to allow for more convenient genomic manipulation, as will be described in detail elsewhere. A 133-amino acid version of the Qβ coat protein gene was cloned into the vector pQE-60 and expressed under IPTG control in M15MA cells in SOB media. After expression, collected cells were lysed by sonication and lysozyme treatment and then centrifuged to remove insoluble cell components. Assembled particles were precipitated from the resulting supernatant using 8% PEG 8000. Following further centrifugation, the isolated pellet was resuspended in 0.1M potassium phosphate pH 7.0. The virus-like particles then underwent a final purification by ultracentrifugation through 10-40% sucrose gradients followed by ultrapelleting and resuspension in 0.1M potassium phosphate pH 7.0.

Final purification of all viruses was performed by ultracentrifugation through 10-40% sucrose gradients; we find that this is more reliable than size-exclusion "spin columns" previously employed (and still used for preliminary cleanup in some cases). It may be possible to improve upon the maximum recovery of 70-80% from sucrose gradients with the use of molecular weight cutoff filtration (resin or membranes), but this was not attempted in the studies described here. CPMV concentrations were determined by absorbance at 260 nm (0.1 mg/mL virus sample gives an absorbance of 0.8). Qβ concentrations were determined using the modified Lowry protein assay.[236] Unless otherwise indicated, all virus samples were handled in 0.1 M potassium phosphate buffer (pH 7.0).

Synthesis of Glycan Azides:

Compounds **3** and **4** were synthesized as previously described from α-mannose pentaacetate or β-galactose pentaacetate.[237] A solution of pentaacetate (316 mM) and 2 equiv (633 mM) 2-azidoethanol (CH_2Cl_2) was placed under dry nitrogen atmosphere, cooled to 0°C, and treated with freshly distilled $BF_3·Et_2O$ (2 equiv) in dropwise fashion. The mixture was stirred for 1 hour and the cooling bath was removed to allow stirring overnight at room temperature. The reaction was followed by silica gel thin layer chromatography (TLC, 2:3 EtOAc:hexanes), with the product showing R_f=0.4. The mixture was neutralized with solid sodium bicarbonate, filtered, and evaporated. The residue was purified by flash chromatography on silica gel (gradient of 10-50% EtOAc in hexanes) to obtain the intermediate pentaacetate azidoethyl adducts in 60-80% yields as colorless oils. EI-MS ($M+H^+$) 417.

Each protected azide-carbohydrate was dissolved in MeOH with 3Å molecular sieves under a nitrogen atmosphere. NaOMe (1% in MeOH, approximately 1 equiv with respect to acetate groups) was added dropwise and the reaction was stirred for 45 minutes at room temperature, with monitoring by TLC (2:3 EtOAc:hexanes, product R_f = 0.1). Dowex 50W x2-200 resin was added to neutralize the reaction, followed by filtration and concentration by rotatory evaporation. The product was purifed by flash chromatography on silica gel (9:1 CH_2Cl_2:MeOH) to obtain pure **3** or **4** in approximately 80% yield as a colorless oil. The NMR spectra of **3** matched the published data.[238] The α-anomer of azidoethylgalactose has been reported;[239] compound **4** is assigned as the β-configuration due to its very different anomeric proton chemical shift and coupling constant (4.22 ppm, J=10 Hz *vs.* 4.67 ppm, J=3.3 Hz for the α-anomer).

Derivatization of Virus Particle:

Each capsid particle was reacted with a large excess of an NHS ester-alkyne reagent to acylate most of the surface lysine side chains (Figure 2.3). The isolated alkyne-derivatized particles were then condensed with azidoethyl derivatives of α-mannose or β-galactose[150] (**3** and **4**, respectively) using complex **5** as a precatalyst for the copper-catalyzed azide-alkyne cycloaddition (CuAAC) "click" reaction that has been developed for the purpose.[154,240] This conjugation methodology allows for complete coverage of the alkyne groups with modest concentrations of the desired azide under mild conditions, irrespective of the other functional groups in the reaction partners. Particles were purified by sucrose-gradient ultracentrifugation. At each stage (acylation and

CuAAC coupling), only intact particles were observed, as characterized by sucrose gradient sedimentation and size-exclusion chromatography.

The numbers of attached glycans were estimated by performing reactions under identical conditions with the selenomethionine azide derivative **6** instead of a glycan-azide. Selenium, not present in detectable levels as background, can be quantified at sub-μM concentrations using inductively coupled plasma optical emission spectroscopy (ICP-OES). Along with the independent determination of protein concentration in each purified sample by a modified Lowry assay, this provides a measurement of the average number of attachments made per virion by the CuAAC reaction. An experimental error of 10% is typical for independent reactions under identical conditions. Compound **6** is designed to replace dyes such as fluorescein that we have previously used to determine loading on capsid scaffolds,[143,152] since **6** more closely resembles the hydrophilic character of carbohydrates and thereby provides a closer analogy to their attachment.

APPENDIX B

PREPARATION OF MEMBRANE VEXICLES

Synthetic Membranes:

A lipid solution containing 1,2-Dimyristoleoyl-*sn*-glycero-3-phosphocholine (DMOPC) and 1,2-dimyristoyl-*sn*-glycero-3-[phospho-L-serine] (sodium salt) (DMPS) in chloroform was evaporated onto small round-bottom flasks and hydrated for an hour at 4ºC in PBS to ~3.3 mg/mL. The lipids were probe-sonicated to clarity in an ice-water bath and transferred to a 100nm Millipore Ultrafree-MC centrifuge tube filter. Samples were centrifuged for 2 hr at 16,000 g and 4ºC. All solution that passed through the centrifuge tube filter was collected and stored at 4ºC for up to one week. Full-length FAAH was incorporated into synthetic lipid vesicles by mixing together FAAH and SUVs to a final concentration of 100 µg of protein per 1 ml of centrifuged SUV solution. The resulting mixture was then dialyzed extensively against PBS to facilitate complete removal of detergent and form proteoliposomes. Proteoliposomes were stored at 4ºC for up to one week.

Mammalian Cell Cultures:

Two different lines of adherent Chinese hamster ovary (CHO-K1) cells were used; one wild-type, and one engineered to express the full length transmembrane GABA-B. Cells were grown at 37ºC and 5% ambient CO_2 to near 100% confluence over three days from initial addition to 175 cm^2-area flasks. Cells were harvested by removing

all growth medium from the flask and incubating with 4ml of Detachin solution for 5 min at 37ºC. 48 mL of incubation buffer was then added to the flask and the contents removed and transferred to two 50ml centrifuge tubes. The cells and media were centrifuged for 5 min at 300g to pellet the cells. Following centrifugation, the media was removed from the centrifuge tubes, the cells were re-suspended in PBS, and the cell/PBS suspension was re-centrifuged. Cell pellets were rinsed three times in PBS and used immediately.

Native Membrane Vesicles:

A cell pellet containing approximately 1×10^9 cells (of either type) was re-suspended in 20 mL of ice-cold lysis buffer (2.5 mM NaCl, 1 mM Tris, 1x EDTA-free, broad-spectrum protease inhibitors, pH 8.0) and placed on a rotator for 45 minutes at 4ºC. The resulting solution was then centrifuged at 40,000g for 60 min at 4ºC. The supernatant was removed and re-suspended in 4 mL of ice-cold PBS and transferred to a 5 mL glass dram vial. The pellet and buffer were then probe-sonicated to clarity in an ice bath and transferred to a 220nm Millipore Ultrafree-MC centrifuge tube filter. The resulting solutions were centrifuged for 1 h at 16,000 g and 4ºC. All solution that passed through the centrifuge tube filter was collected and stored at 4ºC for up to two days.

REFERENCES:

1.   S. Fields, "Proteomics - Proteomics in genomeland," Science, vol. 291, pp. 1221-1222, 2001.

2.   S. Hu and N. J. Dovichi, "Capillary electrophoresis for the analysis of biopolymers," Analytical Chemistry, vol. 74, pp. 2833-2850, 2002.

3.   N. Lion, T. C. Rohner, L. Dayon, I. L. Arnaud, E. Damoc, N. Youhnovski, Z. Y. Wu, C. Roussel, J. Josserand, H. Jensen, J. S. Rossier, M. Przybylski, and H. H. Girault, "Microfluidic systems in proteomics," Electrophoresis, vol. 24, pp. 3533-3562, 2003.

4.   G. Marko-Varga, J. Nilsson, and T. Laurell, "New directions of miniaturization within the proteomics research area," Electrophoresis, vol. 24, pp. 3521-3532, 2003.

5.   S. Mocellin, C. R. Rossi, P. Traldi, D. Nitti, and M. Lise, "Molecular oncology in the post-genomic era: the challenge of proteomics," Trends in Molecular Medicine, vol. 10, pp. 24-32, 2004.

6.   M. Rothmund, A. Schutz, A. Brecht, G. Gauglitz, G. Berthel, and D. Grafe, "Label free binding assay with spectroscopic detection for pharmaceutical screening," Fresenius Journal of Analytical Chemistry, vol. 359, pp. 15-22, 1997.

7.   J. R. Heath, M. E. Phelps, and L. Hood, "NanoSystems Biology," Molecular Imaging and Biology, vol. 5, pp. 312-325, 2003.

8.   B. B. Haab and R. A. Mathies, "Single-molecule detection of DNA separations in microfabricated capillary electrophoresis chips employing focused molecular streams," Analytical Chemistry, vol. 71, pp. 5137-5145, 1999.

9.   M. D. Barnes, W. B. Whitten, and J. M. Ramsey, "Detecting Single Molecules in Liquids," Analytical Chemistry, vol. 67, pp. A418-A423, 1995.

10.   J. C. Fister, S. C. Jacobson, L. M. Davis, and J. M. Ramsey, "Counting single chromophore molecules for ultrasensitive analysis and separations on microchip devices," Analytical Chemistry, vol. 70, pp. 431-437, 1998.

11.   J. J. Lundquist and E. J. Toone, "The cluster glycoside effect," Chemical Reviews, vol. 102, pp. 555-578, 2002.

12.   B. A. Williams, M. C. Chervenak, and E. J. Toone, "Energetics of Lectin-Carbohydrate Binding: A Microcalorimetric Investigation of Concanavalin A-Oligomannoside Complexation," Journal of Biological Chemistry, vol. 267, pp. 22907-22911, 1992.

13. D. K. Mandal, N. Kishore, and C. F. Brewer, "Thermodynamics of Lectin-Carbohydrate Interactions - Titration Microcalorimetry Measurements of the Binding of N-Linked Carbohydrates and Ovalbumin to Concanavalin-A," Biochemistry, vol. 33, pp. 1149-1156, 1994.

14. T. K. Dam, S. Oscarson, J. C. Sacchettini, and C. F. Brewer, "Differential solvation of "core" trimannoside complexes of the Dioclea grandiflora lectin and concanavalin A detected by primary solvent isotope effects in isothermal titration microcalorimetry," Journal of Biological Chemistry, vol. 273, pp. 32826-32832, 1998.

15. R. Wimmer, F. L. Aachmann, K. L. Larsen, and S. B. Petersen, "NMR diffusion as a novel tool for measuring the association constant between cyclodextrin and guest molecules," Carbohydrate Research, vol. 337, pp. 841-849, 2002.

16. T. Drakenberg, S. Forsen, E. Thulin, and H. J. Vogel, "The Binding of Ca-2+, Mg-2+, and Cd-2+ to Tryptic Fragments of Skeletal-Muscle Troponin-C - Cd-113 and Proton Nmr-Studies," Journal of Biological Chemistry, vol. 262, pp. 672-678, 1987.

17. H. T. Hu, J. H. Sheehan, and W. J. Chazin, "The mode of action of centrin - Binding of Ca2+ and a peptide fragment of Kar1p to the C-terminal domain," Journal of Biological Chemistry, vol. 279, pp. 50895-50903, 2004.

18. J. Danielsson, J. Jarvet, P. Damberg, and A. Graslund, "Two-site binding of beta-cyclodextrin to the Alzheimer A beta(1-40) peptide measured with combined PFG-NMR diffusion and induced chemical shifts," Biochemistry, vol. 43, pp. 6261-6269, 2004.

19. R. S. Luo, M. L. Liu, and X. A. Mao, "NMR diffusion and relaxation study of drug-protein interaction," Spectrochimica Acta Part a-Molecular and Biomolecular Spectroscopy, vol. 55, pp. 1897-1901, 1999.

20. G. Veglia, M. Delfini, M. R. Del Giudice, E. Gaggelli, and G. Valensin, "H-1 NMR studies on the interaction of beta-carboline derivatives with human serum albumin," Journal of Magnetic Resonance, vol. 130, pp. 281-286, 1998.

21. C. Dalvit, M. Flocco, S. Knapp, M. Mostardini, R. Perego, B. J. Stockman, M. Veronesi, and M. Varasi, "High-throughput NMR-based screening with competition binding experiments," Journal of the American Chemical Society, vol. 124, pp. 7702-7709, 2002.

22. M. L. Liu, J. K. Nicholson, and J. C. Lindon, "Analysis of drug-protein binding using nuclear magnetic resonance based molecular diffusion measurements," Analytical Communications, vol. 34, pp. 225-228, 1997.

23. R. L. Rich, Y. S. N. Day, T. A. Morton, and D. G. Myszka, "High-resolution and high-throughput protocols for measuring drug/human serum albumin interactions using BIACORE," Analytical Biochemistry, vol. 296, pp. 197-207, 2001.

24. E. C. de Macario, U. H. Rudofsky, and A. J. L. Macario, "Surface plasmon resonance for measuring TBP-promoter interaction," Biochemical and Biophysical Research Communications, vol. 298, pp. 625-631, 2002.

25. A. J. Thiel, A. G. Frutos, C. E. Jordan, R. M. Corn, and L. M. Smith, "In situ surface plasmon resonance imaging detection of DNA hybridization to oligonucleotide arrays on gold surfaces," Analytical Chemistry, vol. 69, pp. 4948-4956, 1997.

26. G. J. Wegner, N. J. Lee, G. Marriott, and R. M. Corn, "Fabrication of histidine-tagged fusion protein arrays for surface plasmon resonance imaging studies of protein-protein and protein-DNA interactions," Analytical Chemistry, vol. 75, pp. 4740-4746, 2003.

27. E. A. Smith, W. D. Thomas, L. L. Kiessling, and R. M. Corn, "Surface plasmon resonance imaging studies of protein-carbohydrate interactions," Journal of the American Chemical Society, vol. 125, pp. 6140-6148, 2003.

28. D. A. Mann, M. Kanai, D. J. Maly, and L. L. Kiessling, "Probing low affinity and multivalent interactions with surface plasmon resonance: Ligands for concanavalin A," Journal of the American Chemical Society, vol. 120, pp. 10575-10582, 1998.

29. H. Sota, Y. Hasegawa, and M. Iwakura, "Detection of conformational changes in an immobilized protein using surface plasmon resonance," Analytical Chemistry, vol. 70, pp. 2019-2024, 1998.

30. B. P. Nelson, T. E. Grimsrud, M. R. Liles, R. M. Goodman, and R. M. Corn, "Surface plasmon resonance imaging measurements of DNA and RNA hybridization adsorption onto DNA microarrays," Analytical Chemistry, vol. 73, pp. 1-7, 2001.

31. C. E. Jordan, A. G. Frutos, A. J. Thiel, and R. M. Corn, "Surface plasmon resonance imaging measurements of DNA hybridization adsorption and streptavidin/DNA multilayer formation at chemically modified gold surfaces," Analytical Chemistry, vol. 69, pp. 4939-4947, 1997.

32. S. Boussaad, J. Pean, and N. J. Tao, "High-resolution multiwavelength surface plasmon resonance spectroscopy for probing conformational and electronic changes in redox proteins," Analytical Chemistry, vol. 72, pp. 222-226, 2000.

33. H. J. Lee, T. T. Goodrich, and R. M. Corn, "SPR imaging measurements of 1-D and 2-D DNA microarrays created from microfluidic channels on gold thin films," Analytical Chemistry, vol. 73, pp. 5525-5531, 2001.

34.	F. P. Schwarz, K. D. Puri, R. G. Bhat, and A. Surolia, "Thermodynamics of Monosaccharide Binding to Concanavalin-a, Pea (Pisum-Sativum) Lectin, and Lentil (Lens-Culinaris) Lectin," Journal of Biological Chemistry, vol. 268, pp. 7668-7677, 1993.

35.	R. V. Weatherman, K. I. Mortell, M. Chervenak, L. L. Kiessling, and E. J. Toone, "Specificity of C-glycoside complexation by mannose glucose specific lectins," Biochemistry, vol. 35, pp. 3619-3624, 1996.

36.	L. Neumann, T. Wohland, R. J. Whelan, R. N. Zare, and B. K. Kobilka, "Functional immobilization of a ligand-activated G-protein-coupled receptor," Chembiochem, vol. 3, pp. 993-998, 2002.

37.	S. R. Haseley, P. Talaga, J. P. Kamerling, and J. F. G. Vliegenthart, "Characterization of the carbohydrate binding specificity and kinetic parameters of lectins by using surface plasmon resonance," Analytical Biochemistry, vol. 274, pp. 203-210, 1999.

38.	E. Duverger, N. Frison, A. C. Roche, and M. Monsigny, "Carbohydrate-lectin interactions assessed by surface plasmon resonance," Biochimie, vol. 85, pp. 167-179, 2003.

39.	J. Rickert, A. Brecht, and W. Gopal, "QCM operation in liquids: Constant sensitivity during formation of extended protein multilayers by affinity," Analytical Chemistry, vol. 69, pp. 1441-1448, 1997.

40.	K. A. Marx, T. A. Zhou, A. Montrone, H. Schulze, and S. J. Braunhut, "A quartz crystal microbalance cell biosensor: detection of microtubule alterations in living cells at nM nocodazole concentrations," Biosensors & Bioelectronics, vol. 16, pp. 773-782, 2001.

41.	A. Janshoff, H. J. Galla, and C. Steinem, "Piezoelectric mass-sensing devices as biosensors - An alternative to optical biosensors?," Angewandte Chemie-International Edition, vol. 39, pp. 4004-4032, 2000.

42.	M. Rodahl, F. Hook, and B. Kasemo, "QCM operation in liquids: An explanation of measured variations in frequency and Q factor with liquid conductivity," Analytical Chemistry, vol. 68, pp. 2219-2227, 1996.

43.	J. L. Cole and J. C. Hansen, "Analytical Ultracentrifugation as a Contemporary Biomolecular Reseach Tool," Journal of Biomolecular Techniques, vol. 10, pp. 163-176, 1999.

44.	G. J. Howlett, A. P. Minton, and G. Rivas, "Analytical ultracentrifugation for association and assembly the study of protein," Current Opinion in Chemical Biology, vol. 10, pp. 430-436, 2006.

45.   J. Lebowitz, M. S. Lewis, and P. Schuck, "Modern analytical ultracentrifugation in protein science: A tutorial review," Protein Science, vol. 11, pp. 2067-2079, 2002.

46.   M. Le Maire, B. Arnou, C. Olesen, D. Georgin, C. Ebel, and J. V. Moller, "Gel chromatography and analytical ultracentrifugation to determine the extent of detergent binding and aggregation, and Stokes radius of membrane proteins using sarcoplasmic reticulum Ca2+-ATPase as an example," Nature Protocols, vol. 3, pp. 1782-1795, 2008.

47.   J. P. Gabrielson, K. K. Arthur, B. S. Kendrick, T. W. Randolph, and M. R. Stoner, "Common Excipients Impair Detection of Protein Aggregates during Sedimentation Velocity Analytical Ultracentrifugation," Journal of Pharmaceutical Sciences, vol. 98, pp. 50-62, 2009.

48.   X. D. Fan, I. M. White, S. I. Shopoua, H. Y. Zhu, J. D. Suter, and Y. Z. Sun, "Sensitive optical biosensors for unlabeled targets: A review," Analytica Chimica Acta, vol. 620, pp. 8-26, 2008.

49.   F. Brosinger, H. Freimuth, M. Lacher, W. Ehrfeld, E. Gedig, A. Katerkamp, F. Spener, and K. Cammann, "A label-free affinity sensor with compensation of unspecific protein interaction by a highly sensitive integrated optical Mach-Zehnder interferometer on silicon," Sensors and Actuators B-Chemical, vol. 44, pp. 350-355, 1997.

50.   F. Prieto, B. Sepulveda, A. Calle, A. Llobera, C. Dominguez, A. Abad, A. Montoya, and L. M. Lechuga, "An integrated optical interferometric nanodevice based on silicon technology for biosensor applications," Nanotechnology, vol. 14, pp. 907-912, 2003.

51.   F. Prieto, B. Sepulveda, A. Calle, A. Llobera, C. Dominguez, and L. M. Lechuga, "Integrated Mach-Zehnder interferometer based on ARROW structures for biosensor applications," Sensors and Actuators B-Chemical, vol. 92, pp. 151-158, 2003.

52.   E. F. Schipper, A. M. Brugman, C. Dominguez, L. M. Lechuga, R. P. H. Kooyman, and J. Greve, "The realization of an integrated Mach-Zehnder waveguide immunosensor in silicon technology," Sensors and Actuators B-Chemical, vol. 40, pp. 147-153, 1997.

53.   A. Ymeti, J. S. Kanger, J. Greve, P. V. Lambeck, R. Wijn, and R. G. Heideman, "Realization of a multichannel integrated Young interferometer chemical sensor," Applied Optics, vol. 42, pp. 5649-5660, 2003.

54.   D. Hradetzky, C. Mueller, and H. Reinecke, "Interferometric label-free biomolecular detection system," Journal of Optics a-Pure and Applied Optics, vol. 8, pp. S360-S364, 2006.

55. K. Schmitt, B. Schirmer, C. Hoffmann, A. Brandenburg, and P. Meyrueis, "Interferometric biosensor based on planar optical waveguide sensor chips for label-free detection of surface bound bioreactions," Biosensors & Bioelectronics, vol. 22, pp. 2591-2597, 2007.

56. B. H. Schneider, J. G. Edwards, and N. F. Hartman, "Hartman interferometer: versatile integrated optic sensor for label-free, real-time quantification of nucleic acids, proteins, and pathogens," Clinical Chemistry, vol. 43, pp. 1757-1763, 1997.

57. B. H. Schneider, E. L. Dickinson, M. D. Vach, J. V. Hoijer, and L. V. Howard, "Highly sensitive optical chip immunoassays in human serum," Biosensors & Bioelectronics, vol. 15, pp. 13-22, 2000.

58. B. H. Schneider, E. L. Dickinson, M. D. Vach, J. V. Hoijer, and L. V. Howard, "Optical chip immunoassay for hCG in human whole blood," Biosensors & Bioelectronics, vol. 15, pp. 597-604, 2000.

59. P. M. St John, R. Davis, N. Cady, J. Czajka, C. A. Batt, and H. G. Craighead, "Diffraction-based cell detection using a microcontact printed antibody grating," Analytical Chemistry, vol. 70, pp. 1108-1111, 1998.

60. J. B. Goh, R. W. Loo, and M. C. Goh, "Label-free monitoring of multiple biomolecular binding interactions in real-time with diffraction-based sensing," Sensors and Actuators B-Chemical, vol. 106, pp. 243-248, 2005.

61. J. Houle and S. Kumaraswamy, "Solving the Multiplexing-Dynamic Range Conundrum with Diffractive Optics Technology," Nature Methods, vol. 4, pp. i-ii, 2007.

62. G. Acharya, C. L. Chang, D. D. Doorneweerd, E. Vlashi, W. A. Henne, L. C. Hartmann, P. S. Low, and C. A. Savran, "Immunomagnetic diffractometry for detection of diagnostic serum markers," Journal of the American Chemical Society, vol. 129, pp. 15824-15829, 2007.

63. G. Acharya, C. L. Chang, D. P. Holland, D. H. Thompson, and C. A. Savran, "Rapid detection of S-adenosyl homocysteine using self-assembled optical diffraction gratings," Angewandte Chemie-International Edition, vol. 47, pp. 1051-1053, 2008.

64. M. J. Swann, L. L. Peel, S. Carrington, and N. J. Freeman, "Dual-polarization interferometry: an analytical technique to measure changes in protein structure in real time, to determine the stoichiometry of binding events, and to differentiate between specific and nonspecific interactions," Analytical Biochemistry, vol. 329, pp. 190-198, 2004.

65. S. M. Lin, C. K. Lee, Y. H. Lin, S. Y. Lee, B. C. Sheu, J. C. Tsai, and S. M. Hsu, "Homopolyvalent antibody-antigen interaction kinetic studies with use of a dual-

polarization interferometric biosensor," Biosensors & Bioelectronics, vol. 22, pp. 715-721, 2006.

66.   S. Ricard-Blum, L. L. Peel, F. Ruggiero, and N. J. Freeman, "Dual polarization interferometry characterization of carbohydrate-protein interactions," Analytical Biochemistry, vol. 352, pp. 252-259, 2006.

67.   J. Wang, X. W. Xu, Z. X. Zhang, F. Yang, and X. R. Yang, "Real-Time Study of Genomic DNA Structural Changes upon Interaction with Small Molecules Using Dual-Polarization Interferometry," Analytical Chemistry, vol. 81, pp. 4914-4921, 2009.

68.   C. L. Baird and D. G. Myszka, "Current and emerging commercial optical biosensors," Journal of Molecular Recognition, vol. 14, pp. 261-268, 2001.

69.   www.farfield-group.com.

70.   V. S. Y. Lin, K. Motesharei, K. P. S. Dancil, M. J. Sailor, and M. R. Ghadiri, "A porous silicon-based optical interferometric biosensor," Science, vol. 278, pp. 840-843, 1997.

71.   K. P. S. Dancil, D. P. Greiner, and M. J. Sailor, "A porous silicon optical biosensor: Detection of reversible binding of IgG to a protein A-modified surface," Journal of the American Chemical Society, vol. 121, pp. 7925-7930, 1999.

72.   Y. Y. Li, F. Cunin, J. R. Link, T. Gao, R. E. Betts, S. H. Reiver, V. Chin, S. N. Bhatia, and M. J. Sailor, "Polymer replicas of photonic porous silicon for sensing and drug delivery applications," Science, vol. 299, pp. 2045-2047, 2003.

73.   M. M. Varma, H. D. Inerowicz, F. E. Regnier, and D. D. Nolte, "High-speed label-free detection by spinning-disk micro-interferometry," Biosensors & Bioelectronics, vol. 19, pp. 1371-1376, 2004.

74.   M. M. Varma, D. D. Nolte, H. D. Inerowicz, and F. E. Regnier, "Spinning-disk self-referencing interferometry of antigen-antibody recognition," Optics Letters, vol. 29, pp. 950-952, 2004.

75.   M. Zhao, D. Nolte, W. R. Cho, F. Regnier, M. Varma, G. Lawrence, and J. Pasqua, "High-speed interferometric detection of label-free immunoassays on the biological compact disc," Clinical Chemistry, vol. 52, pp. 2135-2140, 2006.

76.   X. F. Wang, M. Zhao, and D. D. Nolte, "Prostate-specific antigen immunoassays on the BioCD," Analytical and Bioanalytical Chemistry, vol. 393, pp. 1151-1156, 2009.

77.   E. Ozkumur, J. W. Needham, D. A. Bergstein, R. Gonzalez, M. Cabodi, J. M. Gershoni, B. B. Goldberg, and M. S. Unlu, "Label-free and dynamic detection of

biomolecular interactions for high-throughput microarray applications," Proceedings of the National Academy of Sciences of the United States of America, vol. 105, pp. 7988-7992, 2008.

78. E. Özkumur, A. Yalçin, M. Cretich, C. A. Lopez, D. A. Bergstein, B. B. Goldberg, M. Chiari, and M. S. Ünlü, "Quantification of DNA and protein adsorption by optical phase shift," Biosensors & Bioelectronics, vol. 25, pp. 167-172, 2009.

79. O. Birkert and G. Gauglitz, "Development of an assay for label-free high-throughput screening of thrombin inhibitors by use of reflectometric interference spectroscopy," Analytical and Bioanalytical Chemistry, vol. 372, pp. 141-147, 2002.

80. O. Birkert, R. Tunnernann, G. Jung, and G. Gauglitz, "Label-free parallel screening of combinatorial triazine libraries using reflectometric interference spectroscopy," Analytical Chemistry, vol. 74, pp. 834-840, 2002.

81. D. J. Bornhop, "Microvolume Index of Refraction Determinations by Interferometric Backscatter," Applied Optics, vol. 34, pp. 3234-3239, 1995.

82. K. Swinney and D. J. Bornhop, "A chip-scale universal detector for electrophoresis based on backscattering interferometry," Analyst, vol. 125, pp. 1713-1717, 2000.

83. K. Swinney and D. J. Bornhop, "Detection in capillary electrophoresis," Electrophoresis, vol. 21, pp. 1239-1250, 2000.

84. K. Swinney and D. J. Bornhop, "Quantification and evaluation of Joule heating in on-chip capillary electrophoresis," Electrophoresis, vol. 23, pp. 613-620, 2002.

85. K. Swinney and D. J. Bornhop, "Noninvasive picoliter volume thermometry based on backscatter interferometry," Electrophoresis, vol. 22, pp. 2032-2036, 2001.

86. D. A. Markov and D. J. Bornhop, "Nanoliter-scale non-invasive flow-rate quantification using micro-interferometric back-scatter and phase detection," Fresenius Journal of Analytical Chemistry, vol. 371, pp. 234-237, 2001.

87. D. A. Markov, S. Dotson, S. Wood, and D. J. Bornhop, "Noninvasive fluid flow measurements in microfluidic channels with backscatter interferometry," Electrophoresis, vol. 25, pp. 3805-3809, 2004.

88. K. Swinney, D. Markov, and D. J. Bornhop, "Chip-scale universal detection based on backscatter interferometry," Analytical Chemistry, vol. 72, pp. 2690-2695, 2000.

89.   Z. L. Wang, K. Swinney, and D. J. Bornhop, "Attomole sensitivity for unlabeled proteins and polypeptides with on-chip capillary electrophoresis and universal detection by interferometric backscatter," Electrophoresis, vol. 24, pp. 865-873, 2003.

90.   D. A. Markov, K. Swinney, and D. J. Bornhop, "Label-free molecular interaction determinations with nanoscale interferometry," Journal of the American Chemical Society, vol. 126, pp. 16659-16664, 2004.

91.   D. J. Bornhop, J. C. Latham, A. Kussrow, D. A. Markov, R. D. Jones, and H. S. Sorensen, "Free-solution, label-free molecular interactions studied by back-scattering interferometry," Science, vol. 317, pp. 1732-1736, 2007.

92.   D. Markov, D. Begari, and D. J. Bornhop, "Breaking the 10(-7) barrier for RI measurements in nanoliter volumes," Analytical Chemistry, vol. 74, pp. 5438-5441, 2002.

93.   J. C. Latham, D. A. Markov, H. S. Sorensen, and D. J. Bornhop, "Photobiotin surface chemistry improves label-free interferometric sensing of biochemical interactions," Angewandte Chemie-International Edition, vol. 45, pp. 955-958, 2006.

94.   A. K. Abbas and A. H. Lichtman, Cellular and Molecular Immunology, Fifth ed. Philadelphia: Saunders, 2003.

95.   J. Theze, P. M. Alzari, and J. Bertoglio, "Interleukin 2 and its receptors: Recent advances and new immunological functions," Immunology Today, vol. 17, pp. 481-486, 1996.

96.   G. H. Reem, N. H. Yeh, D. L. Urdal, P. L. Kilian, and J. J. Farrar, "Induction and up-Regulation by Interleukin-2 of High-Affinity Interleukin 2-Receptors on Thymocytes and T-Cells," Proceedings of the National Academy of Sciences of the United States of America, vol. 82, pp. 8663-8666, 1985.

97.   H. Lis and N. Sharon, "Lectins: Carbohydrate-specific proteins that mediate cellular recognition," Chemical Reviews, vol. 98, pp. 637-674, 1998.

98.   C. R. Bertozzi and L. L. Kiessling, "Chemical glycobiology," Science, vol. 291, pp. 2357-2364, 2001.

99.   A. Varki, "Biological Roles of Oligosaccharides - All of the Theories Are Correct," Glycobiology, vol. 3, pp. 97-130, 1993.

100.   S. M. Dimick, S. C. Powell, S. A. McMahon, D. N. Moothoo, J. H. Naismith, and E. J. Toone, "On the meaning of affinity: Cluster glycoside effects and concanavalin A," Journal of the American Chemical Society, vol. 121, pp. 10286-10296, 1999.

101.   S. Howorka, J. Nam, H. Bayley, and D. Kahne, "Stochastic detection of monovalent and bivalent protein-ligand interactions," Angewandte Chemie-International Edition, vol. 43, pp. 842-846, 2004.

102.   A. Velazquez-Campoy and E. Freire, "ITC in the post-genomic era... ? Priceless," Biophysical Chemistry, vol. 115, pp. 115-124, 2005.

103.   A. Ababou and J. E. Ladbury, "Survey of the year 2005: literature on applications of isothermal titration calorimetry," Journal of Molecular Recognition, vol. 20, pp. 4-14, 2007.

104.   S. Leavitt and E. Freire, "Direct measurement of protein binding energetics by isothermal titration calorimetry," Current Opinion in Structural Biology, vol. 11, pp. 560-566, 2001.

105.   F. E. Torres, P. Kuhnt, D. De Bruyker, A. G. Bell, M. V. Wolkin, E. Peeters, J. R. Williamson, G. B. Anderson, G. P. Schmitz, M. I. Recht, S. Schweizer, L. G. Scott, J. H. Ho, S. A. Elrod, P. G. Schultz, R. A. Lerner, and R. H. Bruce, "Enthalpy arrays," Proceedings of the National Academy of Sciences of the United States of America, vol. 101, pp. 9517-9522, 2004.

106.   M. B. Kerby, R. S. Legge, and A. Tripathi, "Measurements of kinetic parameters in a microfluidic reactor," Analytical Chemistry, vol. 78, pp. 8273-8280, 2006.

107.   D. C. Duffy, J. C. McDonald, O. J. A. Schueller, and G. M. Whitesides, "Rapid prototyping of microfluidic systems in poly(dimethylsiloxane)," Analytical Chemistry, vol. 70, pp. 4974-4984, 1998.

108.   G. M. Whitesides, E. Ostuni, S. Takayama, X. Y. Jiang, and D. E. Ingber, "Soft lithography in biology and biochemistry," Annual Review of Biomedical Engineering, vol. 3, pp. 335-373, 2001.

109.   Y. C. Lee and R. T. Lee, "Carbohydrate-Protein Interactions - Basis of Glycobiology," Accounts of Chemical Research, vol. 28, pp. 321-327, 1995.

110.   B. E. Collins and J. C. Paulson, "Cell surface biology mediated by low affinity multivalent protein-glycan interactions," Current Opinion in Chemical Biology, vol. 8, pp. 617-625, 2004.

111.   H. J. Gabius, H. C. Siebert, S. Andre, J. Jimenez-Barbero, and H. Rudiger, "Chemical biology of the sugar code," Chembiochem, vol. 5, pp. 741-764, 2004.

112.   D. H. Dube and C. R. Bertozzi, "Glycans in cancer and inflammation. Potential for therapeutics and diagnostics," Nature Reviews Drug Discovery, vol. 4, pp. 477-488, 2005.

113.   N. Sharon, "Lectins: Carbohydrate-specific reagents and biological recognition molecules," Journal of Biological Chemistry, vol. 282, pp. 2753-2764, 2007.

114.   www.functionalglycomics.org.

115.   M. Kapoor, C. J. Thomas, K. Bachhawat-Sikder, S. Sharma, and A. Surolia, "Exploring kinetics and mechanism of protein-sugar recognition by surface plasmon resonance," Recognition of Carbohydrates in Biological Systems Pt A: General Procedures, vol. 362, pp. 312-329, 2003.

116.   H. Sota, R. T. Lee, Y. C. Lee, and Y. Shinohara, "Quantitative lectin-carbohydrate interaction analysis on solid-phase surfaces using biosensor based on surface plasmon resonance," Recognition of Carbohydrates in Biological Systems Pt A: General Procedures, vol. 362, pp. 330-340, 2003.

117.   I. Okazaki, "BIACORE applications for glycoconjugate research," Trends in Glycoscience and Glycotechnology, vol. 10, pp. 321-329, 1998.

118.   E. Jule, Y. Nagasaki, and K. Kataoka, "Lactose-installed poly(ethylene glycol)-poly(D,L-lactide) block copolymer micelles exhibit fast-rate binding and high affinity toward a protein bed simulating a cell surface. A surface plasmon resonance study," Bioconjugate Chemistry, vol. 14, pp. 177-186, 2003.

119.   Y. Zhang, S. Z. Luo, Y. J. Tang, L. Yu, K. Y. Hou, J. P. Cheng, X. Q. Zeng, and P. G. Wang, "Carbohydrate-protein interactions by "clicked" carbohydrate self-assembled monolayers," Analytical Chemistry, vol. 78, pp. 2001-2008, 2006.

120.   W. Vornholt, M. Hartmann, and M. Keusgen, "SPR studies of carbohydrate-lectin interactions as useful tool for screening on lectin sources," Biosensors & Bioelectronics, vol. 22, pp. 2983-2988, 2007.

121.   M. J. Linman, J. D. Taylor, H. Yu, X. Chen, and Q. Cheng, "Surface plasmon resonance study of protein-carbohydrate interactions using biotinylated sialosides," Analytical Chemistry, vol. 80, pp. 4007-4013, 2008.

122.   Z. C. Pei, H. Anderson, T. Aastrup, and O. Ramstrom, "Study of real-time lectin-carbohydrate interactions on the surface of a quartz crystal microbalance," Biosensors & Bioelectronics, vol. 21, pp. 60-66, 2005.

123.   K. Lebed, A. J. Kulik, L. Forro, and M. Lekka, "Lectin-carbohydrate affinity measured using a quartz crystal microbalance," Journal of Colloid and Interface Science, vol. 299, pp. 41-48, 2006.

124.   Z. H. Shen, M. C. Huang, C. D. Xiao, Y. Zhang, X. Q. Zeng, and P. G. Wang, "Nonlabeled quartz crystal microbalance biosensor for bacterial detection using carbohydrate and lectin recognitions," Analytical Chemistry, vol. 79, pp. 2312-2319, 2007.

125.   M. C. Chervenak and E. J. Toone, "Calorimetric Analysis of the Binding of Lectins with Overlapping Carbohydrate-Binding Ligand Specificities," Biochemistry, vol. 34, pp. 5685-5695, 1995.

126. J. B. Corbell, J. J. Lundquist, and E. J. Toone, "A comparison of biological and calorimetric analyses of multivalent glycodendrimer ligands for concanavalin A," Tetrahedron-Asymmetry, vol. 11, pp. 95-111, 2000.

127. B. W. Sigurskjold, "Exact analysis of competition ligand binding by displacement isothermal titration calorimetry," Analytical Biochemistry, vol. 277, pp. 260-266, 2000.

128. T. Christensen and E. J. Toone, "Calorimetric evaluation of protein-carbohydrate affinities," Recognition of Carbohydrates in Biological Systems Pt A: General Procedures, vol. 362, pp. 486-504, 2003.

129. T. Weimar, B. Haase, and T. Kohli, "Low affinity carbohydrate lectin interactions examined with surface plasmon resonance," Journal of Carbohydrate Chemistry, vol. 19, pp. 1083-1089, 2000.

130. I. Blikstad, L. G. Fagerstam, R. Bhikhabhai, and H. Lindblom, "Detection and characterization of oligosaccharides in column effluents using surface plasmon resonance," Analytical Biochemistry, vol. 233, pp. 42-49, 1996.

131. C. Jungar, M. Strandh, S. Ohlson, and C. F. Mandenius, "Analysis of carbohydrates using liquid chromatography-surface plasmon resonance immunosensing systems," Analytical Biochemistry, vol. 281, pp. 151-158, 2000.

132. S. Ohlson, C. Jungar, M. Strandh, and C. F. Mandenius, "Continuous weak-affinity immunosensing," Trends in Biotechnology, vol. 18, pp. 49-52, 2000.

133. A. R. Patil, C. J. Thomas, and A. Surolia, "Kinetics and the mechanism of interaction of the endoplasmic reticulum chaperone, calreticulin, with monoglucosylated (Glc(1)Man(9)GlcNAc(2)) substrate," Journal of Biological Chemistry, vol. 275, pp. 24348-24356, 2000.

134. D. Beccati, K. M. Halkes, G. D. Batema, G. Guillena, A. C. de Souza, G. van Koten, and J. P. Kamerling, "SPR studies of carbohydrate-protein interactions: Signal enhancement of low-molecular-mass analytes by organoplatinum(II)-labeling," Chembiochem, vol. 6, pp. 1196-1203, 2005.

135. T. Taguchi, H. Takeyama, and T. Matsunaga, "Immuno-capture of Cryptosporidium parvum using micro-well array," Biosensors & Bioelectronics, vol. 20, pp. 2276-2282, 2005.

136. A. Kussrow, E. Kaltgrad, M. L. Wolfenden, M. J. Cloninger, M. G. Finn, and D. J. Bornhop, "Measurement of Monovalent and Polyvalent Carbohydrate-Lectin Binding by Back-Scattering Interferometry," Analytical Chemistry, vol. 81, pp. 4889-4897, 2009.

137. T. W. Lin, C. Porta, G. Lomonossoff, and J. E. Johnson, "Structure-based design of peptide presentation on a viral surface: The crystal structure of a plant/animal

virus chimera at 2.8 angstrom resolution," Folding & Design, vol. 1, pp. 179-187, 1996.

138. Q. Wang, T. W. Lin, L. Tang, J. E. Johnson, and M. G. Finn, "Icosahedral virus particles as addressable nanoscale building blocks," Angewandte Chemie-International Edition, vol. 41, pp. 459-462, 2002.

139. T. M. Kozlovska, I. Cielens, D. Dreilinna, A. Dislers, V. Baumanis, V. Ose, and P. Pumpens, "Recombinant Rna Phage Q-Beta Capsid Particles Synthesized and Self-Assembled in Escherichia-Coli," Gene, vol. 137, pp. 133-137, 1993.

140. D. E. Prasuhn, R. M. Yeh, A. Obenaus, M. Manchester, and M. G. Finn, "Viral MRI contrast agents: coordination of Gd by native virions and attachment of Gd complexes by azide-alkyne cycloaddition," Chemical Communications, pp. 1269-1271, 2007.

141. T. W. Lin, Z. G. Chen, R. Usha, C. V. Stauffacher, J. B. Dai, T. Schmidt, and J. E. Johnson, "The refined crystal structure of cowpea mosaic virus at 2.8 angstrom resolution," Virology, vol. 265, pp. 20-34, 1999.

142. R. Golmohammadi, K. Fridborg, M. Bundule, K. Valegard, and L. Liljas, "The crystal structure of bacteriophage Q beta at 3.5 angstrom resolution," Structure, vol. 4, pp. 543-554, 1996.

143. Q. Wang, E. Kaltgrad, T. W. Lin, J. E. Johnson, and M. G. Finn, "Natural supramolecular building blocks: Wild-type cowpea mosaic virus," Chemistry & Biology, vol. 9, pp. 805-811, 2002.

144. A. Chatterji, W. F. Ochoa, M. Paine, B. R. Ratna, J. E. Johnson, and T. W. Lin, "New addresses on an addressable virus nanoblock: Uniquely reactive lys residues on cowpea mosaic virus," Chemistry & Biology, vol. 11, pp. 855-863, 2004.

145. E. Strable, D. E. Prasuhn, A. K. Udit, S. Brown, A. J. Link, J. T. Ngo, G. Lander, J. Quispe, C. S. Potter, B. Carragher, D. A. Tirrell, and M. G. Finn, "Unnatural amino acid incorporation into virus-like particles," Bioconjugate Chemistry, vol. 19, pp. 866-875, 2008.

146. M. L. Wolfenden and M. J. Cloninger, "Carbohydrate-functionalized dendrimers to investigate the predictable tunability of multivalent interactions," Bioconjugate Chemistry, vol. 17, pp. 958-966, 2006.

147. L. A. Murphy and I. J. Goldstein, "5 Alpha-D-Galactopyranosyl-Binding Isolectins from Bandeiraea-Simplicifolia Seeds," Journal of Biological Chemistry, vol. 252, pp. 4739-4742, 1977.

148. C. E. Hayes and Goldstei.Ij, "Alpha-D-Galactosyl-Binding Lectin from Bandeiraea-Simplicifolia Seeds - Isolation by Affinity Chromatography and

Characterization," Journal of Biological Chemistry, vol. 249, pp. 1904-1914, 1974.

149.   C. J. Arnusch, S. Andre, P. Valentini, M. Lensch, R. Russwurm, H. C. Siebert, M. J. E. Fischer, H. J. Gabius, and R. J. Pieters, "Interference of the galactose-dependent binding of lectins by novel pentapeptide ligands," Bioorganic & Medicinal Chemistry Letters, vol. 14, pp. 1437-1440, 2004.

150.   I. J. Goldstein, D. A. Blake, S. Ebisu, T. J. Williams, and L. A. Murphy, "Carbohydrate Binding-Studies on the Bandeiraea-Simplicifolia-I Isolectins - Lectins Which Are Monovalent,Divalent,Trivalent and Tetravalent for N-Acetyl-D-Galactosamine," Journal of Biological Chemistry, vol. 256, pp. 3890-3893, 1981.

151.   T. K. Dam, R. Roy, D. Page, and C. F. Brewer, "Thermodynamic binding parameters of individual epitopes of multivalent carbohydrates to concanavalin a as determined by "reverse" isothermal titration microcalorimetry," Biochemistry, vol. 41, pp. 1359-1363, 2002.

152.   K. S. Raja, Q. Wang, and M. G. Finn, "Icosahedral virus particles as polyvalent carbohydrate display platforms," Chembiochem, vol. 4, pp. 1348-1351, 2003.

153.   S. Sen Gupta, K. S. Raja, E. Kaltgrad, E. Strable, and M. G. Finn, "Virus-glycopolymer conjugates by copper(I) catalysis of atom transfer radical polymerization and azide-alkyne cycloaddition," Chemical Communications, pp. 4315-4317, 2005.

154.   E. Kaltgrad, S. Sen Gupta, S. Punna, C. Y. Huang, A. Chang, C. H. Wong, M. G. Finn, and O. Blixt, "Anti-carbohydrate antibodies elicited by polyvalent display on a viral scaffold," Chembiochem, vol. 8, pp. 1455-1462, 2007.

155.   E. K. Woller and M. J. Cloninger, "The lectin-binding properties of six generations of mannose-functionalized dendrimers," Organic Letters, vol. 4, pp. 7-10, 2002.

156.   E. K. Woller, E. D. Walter, J. R. Morgan, D. J. Singel, and M. J. Cloninger, "Altering the strength of lectin binding interactions and controlling the amount of lectin clustering using mannose/hydroxyl-functionalized dendrimers," Journal of the American Chemical Society, vol. 125, pp. 8820-8826, 2003.

157.   M. Kanai, K. H. Mortell, and L. L. Kiessling, "Varying the size of multivalent ligands: The dependence of concanavalin a binding on neoglycopolymer length," Journal of the American Chemical Society, vol. 119, pp. 9931-9932, 1997.

158.   O. Livnah, E. A. Bayer, M. Wilchek, and J. L. Sussman, "3-Dimensional Structures of Avidin and the Avidin-Biotin Complex," Proceedings of the National Academy of Sciences of the United States of America, vol. 90, pp. 5076-5080, 1993.

159. N. Misawa, S. Yamamura, K. Yong-Hoon, R. Tero, Y. Nonogaki, and T. Urisu, "Orientation of avidin molecules immobilized on COOH-modified SiO2/Si(100) surfaces," Chemical Physics Letters, vol. 419, pp. 86-90, 2006.

160. H. S. Sorensen, H. Pranov, N. B. Larsen, D. J. Bornhop, and P. E. Andersen, "Absolute refractive index determination by microinterferometric backscatter detection," Analytical Chemistry, vol. 75, pp. 1946-1953, 2003.

161. Z. L. Wang and D. J. Bornhop, "Dual-capillary backscatter interferometry for high-sensitivity nanoliter-volume refractive index detection with density gradient compensation," Analytical Chemistry, vol. 77, pp. 7872-7877, 2005.

162. J. C. Latham, R. A. Stein, D. J. Bornhop, and H. S. Mchaourab, "Free-Solution Label-Free Detection of alpha-Crystallin Chaperone Interactions by Back-Scattering Interferometry," Analytical Chemistry, vol. 81, pp. 1865-1871, 2009.

163. T. Polifke and P. Rauch, "Avoiding interference in immunoassays," Genetic Engineering & Biotechnology News, vol. 28, pp. 43-45, 2008.

164. M. Domeika, I. Litvinenko, T. Smirnova, O. Gaivaronskaya, A. Savicheva, E. Sokolovskiy, R. C. Ballard, and M. Unemo, "Laboratory diagnostics for non-viral sexually transmitted infections in St. Petersburg, Russia: current situation and hallmarks for improvements," Journal of the European Academy of Dermatology and Venereology, vol. 22, pp. 1094-1100, 2008.

165. D. Bhardwaj, S. Bhatt, B. M. Khamar, R. I. Modi, and P. K. Ghosh, "Recombinant HIV-1 p24 protein: cloning, expression, purification and use in the development of ELISA kits," Current Science, vol. 91, pp. 913-917, 2006.

166. K. Sugata, K. Taniguchi, A. Yui, F. Miyake, S. Suga, Y. Asano, M. Ohashi, K. Suzuki, N. Nishimura, T. Ozaki, and T. Yoshikawa, "Analysis of rotavirus antigenemia and extraintestinal manifestations in children with rotavirus gastroenteritis," Pediatrics, vol. 122, pp. 392-397, 2008.

167. S. A. Larsen, V. Pope, R. E. Johnson, and E. J. K. Jr., "A Manual of Tests for Syphilis," 9th ed. Washington D.C.: American Public Health Association, 1998.

168. M. E. Kent and F. Romanelli, "Reexamining syphilis: An update on epidemiology, clinical manifestations, and management," Annals of Pharmacotherapy, vol. 42, pp. 226-236, 2008.

169. M. R. Golden, C. M. Marra, and K. K. Holmes, "Update on syphilis - Resurgence of an old problem," Jama-Journal of the American Medical Association, vol. 290, pp. 1510-1514, 2003.

170. www.leeds.ac.uk.

171.   M. F. Krummel and M. M. Davis, "Dynamics of the immunological synapse: finding, establishing and solidifying a connection," Current Opinion in Immunology, vol. 14, pp. 66-74, 2002.

172.   J. P. Overington, B. Al-Lazikani, and A. L. Hopkins, "Opinion - How many drug targets are there?," Nature Reviews Drug Discovery, vol. 5, pp. 993-996, 2006.

173.   A. Wise, K. Gearing, and S. Rees, "Target validation of G-protein coupled receptors," Drug Discovery Today, vol. 7, pp. 235-246, 2002.

174.   P. S. Cremer and S. G. Boxer, "Formation and spreading of lipid bilayers on planar glass supports," Journal of Physical Chemistry B, vol. 103, pp. 2554-2559, 1999.

175.   B. W. Koenig, S. Kruger, W. J. Orts, C. F. Majkrzak, N. F. Berk, J. V. Silverton, and K. Gawrisch, "Neutron reflectivity and atomic force microscopy studies of a lipid bilayer in water adsorbed to the surface of a silicon single crystal," Langmuir, vol. 12, pp. 1343-1350, 1996.

176.   G. M. Kuziemko, M. Stroh, and R. C. Stevens, "Cholera toxin binding affinity and specificity for gangliosides determined by surface plasmon resonance," Biochemistry, vol. 35, pp. 6375-6384, 1996.

177.   M. Masserini, E. Freire, P. Palestini, E. Calappi, and G. Tettamanti, "Fuc-Gm1 Ganglioside Mimics the Receptor Function of Gm1 for Cholera-Toxin," Biochemistry, vol. 31, pp. 2422-2426, 1992.

178.   Y. Fang, A. G. Frutos, and J. Lahiri, "Ganglioside microarrays for toxin detection," Langmuir, vol. 19, pp. 1500-1505, 2003.

179.   P. Hinterdorfer, G. Baber, and L. K. Tamm, "Reconstituted Influenza Hemagglutinin in Supported Planar Lipid Bilayers Selectively Binds Target Lipid Vesicles and Induces Membrane-Fusion at Low Ph," Biophysical Journal, vol. 66, pp. A6-a6, 1994.

180.   J. Jass, T. Tjarnhage, and G. Puu, "From liposomes to supported, planar bilayer structures on hydrophilic and hydrophobic surfaces: An atomic force microscopy study," Biophysical Journal, vol. 79, pp. 3153-3163, 2000.

181.   A. A. Brian and H. M. Mcconnell, "Allogeneic Stimulation of Cyto-Toxic T-Cells by Supported Planar Membranes," Proceedings of the National Academy of Sciences of the United States of America-Biological Sciences, vol. 81, pp. 6159-6163, 1984.

182.   P. S. Cremer and T. L. Yang, "Creating spatially addressed arrays of planar supported fluid phospholipid membranes," Journal of the American Chemical Society, vol. 121, pp. 8130-8131, 1999.

183. L. L. Kiessling, J. E. Gestwicki, and L. E. Strong, "Synthetic multivalent ligands in the exploration of cell-surface interactions," Current Opinion in Chemical Biology, vol. 4, pp. 696-703, 2000.

184. K. D. Mossman, G. Campi, J. T. Groves, and M. L. Dustin, "Altered TCR signaling from geometrically repatterned immunological synapses," Science, vol. 310, pp. 1191-1193, 2005.

185. B. F. Cravatt, D. K. Giang, S. P. Mayfield, D. L. Boger, R. A. Lerner, and N. B. Gilula, "Molecular characterization of an enzyme that degrades neuromodulatory fatty-acid amides," Nature, vol. 384, pp. 83-87, 1996.

186. B. F. Cravatt and A. H. Lichtman, "Fatty acid amide hydrolase: an emerging therapeutic target in the endocannabinoid system," Current Opinion in Chemical Biology, vol. 7, pp. 469-475, 2003.

187. M. K. McKinney and B. F. Cravatt, "Structure and function of fatty acid amide hydrolase," Annual Review of Biochemistry, vol. 74, pp. 411-432, 2005.

188. G. Schwoch and H. Passow, "Preparation and Properties of Human Erythrocyte-Ghosts," Molecular and Cellular Biochemistry, vol. 2, pp. 197-218, 1973.

189. M. Tanaka, A. P. Wong, F. Rehfeldt, M. Tutus, and S. Kaufmann, "Selective deposition of native cell membranes on biocompatible micropatterns," Journal of the American Chemical Society, vol. 126, pp. 3257-3260, 2004.

190. B. Bettler and J. Y. H. Tiao, "Molecular diversity, trafficking and subcellular localization of GABA(B) receptors," Pharmacology & Therapeutics, vol. 110, pp. 533-543, 2006.

191. D. Ulrich and B. Bettler, "GABA(B) receptors: synaptic functions and mechanisms of diversity," Current Opinion in Neurobiology, vol. 17, pp. 298-303, 2007.

192. N. G. Bowery, "GABA(B) receptor: a site of therapeutic benefit," Current Opinion in Pharmacology, vol. 6, pp. 37-43, 2006.

193. J. K. DeMartino, J. Garfunkle, D. G. Hochstatter, B. F. Cravatt, and D. L. Boger, "Exploration of a fundamental substituent effect of alpha-ketoheterocycle enzyme inhibitors: Potent and selective inhibitors of fatty acid amide hydrolase," Bioorganic & Medicinal Chemistry Letters, vol. 18, pp. 5842-5846, 2008.

194. W. Froestl, S. J. Mickel, R. G. Hall, G. Vonsprecher, D. Strub, P. A. Baumann, F. Brugger, C. Gentsch, J. Jaekel, H. R. Olpe, G. Rihs, A. Vassout, P. C. Waldmeier, and H. Bittiger, "Phosphinic Acid Analogs of Gaba .1. New Potent and Selective Gaba(B) Agonists," Journal of Medicinal Chemistry, vol. 38, pp. 3297-3312, 1995.

195. K. Kaupmann, K. Huggel, J. Heid, P. J. Flor, S. Bischoff, S. J. Mickel, G. McMaster, C. Angst, H. Bittiger, W. Froestl, and B. Bettler, "Expression cloning of GABA(B) receptors uncovers similarity to metabotropic glutamate receptors," Nature, vol. 386, pp. 239-246, 1997.

196. H. R. Hoogenboom, "Selecting and screening recombinant antibody libraries," Nature Biotechnology, vol. 23, pp. 1105-1116, 2005.

197. R. S. Yalow and S. A. Berson, "Assay of Plasma Insulin in Human Subjects by Immunological Methods," Nature, vol. 184, pp. 1648-1649, 1959.

198. G. Kohler and C. Milstein, "Continuous Cultures of Fused Cells Secreting Antibody of Predefined Specificity," Nature, vol. 256, pp. 495-497, 1975.

199. G. A. Canziani, S. Klakamp, and D. G. Myszka, "Kinetic screening of antibodies from crude hybridoma samples using Biacore," Analytical Biochemistry, vol. 325, pp. 301-307, 2004.

200. S. F. Kingsmore, "Multiplexed protein measurement: technologies and applications of protein and antibody arrays," Nature Reviews Drug Discovery, vol. 5, pp. 310-320, 2006.

201. C. Milstein, "The hybridoma revolution: an offshoot of basic research," Bioessays, vol. 21, pp. 966-973, 1999.

202. C. A. K. Borrebaeck, "Antibodies in diagnostics - from immunoassays to protein chips," Immunology Today, vol. 21, pp. 379-382, 2000.

203. A. J. Haes, L. Chang, W. L. Klein, and R. P. Van Duyne, "Detection of a biomarker for Alzheimer's disease from synthetic and clinical samples using a nanoscale optical biosensor," Journal of the American Chemical Society, vol. 127, pp. 2264-2271, 2005.

204. A. Lueking, D. J. Cahill, and S. Mullner, "Protein biochips: a new and versatile platform technology for molecular medicine," Drug Discovery Today, vol. 10, pp. 789-794, 2005.

205. J. C. Miller, H. P. Zhou, J. Kwekel, R. Cavallo, J. Burke, E. B. Butler, B. S. Teh, and B. B. Haab, "Antibody microarray profiling of human prostate cancer sera: Antibody screening and identification of potential biomarkers," Proteomics, vol. 3, pp. 56-63, 2003.

206. R. Orchekowski, D. Hamelinck, L. Li, E. Gliwa, M. VanBrocklin, J. A. Marrero, G. F. V. Woude, Z. D. Feng, R. Brand, and B. B. Haab, "Antibody microarray profiling reveals individual and combined serum proteins associated with pancreatic cancer," Cancer Research, vol. 65, pp. 11193-11202, 2005.

207. M. Sanchez-Carbayo, N. D. Socci, J. J. Lozano, B. B. Haab, and C. Cordon-Cardo, "Profiling bladder cancer using targeted antibody arrays," American Journal of Pathology, vol. 168, pp. 93-103, 2006.

208. L. J. Fanning, A. M. Connor, and G. E. Wu, "Development of the immunoglobulin repertoire," Clinical Immunology and Immunopathology, vol. 79, pp. 1-14, 1996.

209. G. Winter and C. Milstein, "Man-Made Antibodies," Nature, vol. 349, pp. 293-299, 1991.

210. E. Eleuteri, A. Di Stefano, F. L. M. Ricciardolo, F. Magno, I. Gnemmi, M. Colombo, R. Anzalone, F. Cappello, G. La Rocca, F. T. Genta, G. Zummo, and P. Giannuzzi, "Increased nitrotyrosine plasma levels in relation to systemic markers of inflammation and myeloperoxidase in chronic heart failure," International Journal of Cardiology, vol. 135, pp. 386-390, 2009.

211. I. Mohiuddin, H. Chai, P. H. Lin, A. B. Lumsden, Q. Z. Yao, and C. Y. Chen, "Nitrotyrosine and chlorotyrosine: Clinical significance and biological functions in the vascular system," Journal of Surgical Research, vol. 133, pp. 143-149, 2006.

212. I. T. Mohiuddin, H. Chai, P. Lin, A. Lumsden, Q. H. Yao, and C. Y. Chen, "Effect of nitrotyrosine on endothelial cell dysfunction: a novel mechanism," Journal of the American College of Surgeons, vol. 201, pp. S100-S100, 2005.

213. P. Chazot, F. Shenton, W. Schunack, D. Grandi, and G. Morini, "Influence of (R)-alpha-Methylhistamine on the histamine H-3 receptor in the rat gastrointestinal tract," Inflammation Research, vol. 56, pp. S19-S20, 2007.

214. H. L. Haas, O. A. Sergeeva, and O. Selbach, "Histamine in the nervous system," Physiological Reviews, vol. 88, pp. 1183-1241, 2008.

215. M. Jutel, K. Blaser, and C. A. Akdis, "Histamine in allergic inflammation and immune modulation," International Archives of Allergy and Immunology, vol. 137, pp. 82-92, 2005.

216. M. Berger, J. A. Gray, and B. L. Roth, "The Expanded Biology of Serotonin," Annual Review of Medicine, vol. 60, pp. 355-366, 2009.

217. www.abcam.com.

218. www.scbt.com.

219. A. D. Ellington and J. W. Szostak, "Invitro Selection of Rna Molecules That Bind Specific Ligands," Nature, vol. 346, pp. 818-822, 1990.

220. C. Tuerk and L. Gold, "Systematic Evolution of Ligands by Exponential Enrichment - Rna Ligands to Bacteriophage-T4 DNA-Polymerase," Science, vol. 249, pp. 505-510, 1990.

221. S. D. Jayasena, "Aptamers: An emerging class of molecules that rival antibodies in diagnostics," Clinical Chemistry, vol. 45, pp. 1628-1650, 1999.

222. R. D. Jenison, S. C. Gill, A. Pardi, and B. Polisky, "High-Resolution Molecular Discrimination by Rna," Science, vol. 263, pp. 1425-1429, 1994.

223. L. Gold, "Oligonucleotides as Research, Diagnostic, and Therapeutic Agents," Journal of Biological Chemistry, vol. 270, pp. 13581-13584, 1995.

224. D. Proske, M. Blank, R. Buhmann, and A. Resch, "Aptamers - basic research, drug development, and clinical applications," Applied Microbiology and Biotechnology, vol. 69, pp. 367-374, 2005.

225. S. Tombelli, A. Minunni, and A. Mascini, "Analytical applications of aptamers," Biosensors & Bioelectronics, vol. 20, pp. 2424-2434, 2005.

226. C. Bourne, S. Lee, B. Venkataiah, A. Lee, B. Korba, M. G. Finn, and A. Zlotnick, "Small-Molecule Effectors of Hepatitis B Virus Capsid Assembly Give Insight into Virus Life Cycle," Journal of Virology, vol. 82, pp. 10262-10270, 2008.

227. C. R. Bourne, M. G. Finn, and A. Zlotnick, "Global structural changes in hepatitis B virus capsids induced by the assembly effector HAP1," Journal of Virology, vol. 80, pp. 11055-11061, 2006.

228. S. J. Stray, C. R. Bourne, S. Punna, W. G. Lewis, M. G. Finn, and A. Zlotnick, "A heteroaryldihydropyrimidine activates and can misdirect hepatitis B virus capsid assembly," Proceedings of the National Academy of Sciences of the United States of America, vol. 102, pp. 8138-8143, 2005.

229. J. M. Carothers, S. C. Oestreich, and J. W. Szostak, "Aptamers selected for higher-affinity binding are not more specific for the target ligand," Journal of the American Chemical Society, vol. 128, pp. 7929-7937, 2006.

230. D. P. King, N. Montague, K. Ebert, S. M. Reid, J. P. Dukes, L. Schadlich, G. J. Belsham, and G. P. Lomonossoff, "Development of a novel recombinant encapsidated RNA particle: Evaluation as an internal control for diagnostic RT-PCR," Journal of Virological Methods, vol. 146, pp. 218-225, 2007.

231. W. L. Brown, R. A. Mastico, M. Wu, K. G. Heal, C. J. Adams, J. B. Murray, J. C. Simpson, J. M. Lord, A. W. Taylor-Robinson, and P. G. Stockley, "RNA bacteriophage capsid-mediated drug delivery and epitope presentation," Intervirology, vol. 45, pp. 371-380, 2002.

232. D. Legendre and J. Fastrez, "Production in Saccharomyces cerevisiae of MS2 virus-like particles packaging functional heterologous mRNAs," Journal of Biotechnology, vol. 117, pp. 183-194, 2005.

233. B. L. Pasloske, C. R. Walkerpeach, R. D. Obermoeller, M. Winkler, and D. B. DuBois, "Armored RNA technology for production of ribonuclease-resistant viral RNA controls and standards," Journal of Clinical Microbiology, vol. 36, pp. 3590-3594, 1998.

234. B. Wei, Y. X. Wei, K. Zhang, J. Wang, R. H. Xu, S. Zhan, G. G. Lin, W. Wang, M. Liu, J. N. Wang, R. Zhang, and J. M. Li, "Development of an antisense RNA delivery system using conjugates of the MS2 bacteriophage capsids and HIV-1 TAT cell penetrating peptide," Biomedicine & Pharmacotherapy, vol. 63, pp. 313-318, 2009.

235. D. J. Siler, J. Babcock, and G. Bruening, "Electrophoretic Mobility and Enhanced Infectivity of a Mutant of Cowpea Mosaic-Virus," Virology, vol. 71, pp. 560-567, 1976.

236. O. H. Lowry, N. J. Rosebrough, A. L. Farr, and R. J. Randall, "Protein Measurement with the Folin Phenol Reagent," The Journal of biological chemistry, vol. 193, pp. 265-275, 1951.

237. A. Y. Chernyak, G. V. M. Sharma, L. O. Kononov, P. R. Krishna, A. B. Levinsky, N. K. Kochetkov, and A. V. R. Rao, "2-Azidoethyl Glycosides - Glycosides Potentially Useful for the Preparation of Neoglycoconjugates," Carbohydrate Research, vol. 223, pp. 303-309, 1992.

238. T. K. Lindhorst, S. Kotter, U. Krallmann-Wenzel, and S. Ehlers, "Trivalent alpha-D-mannoside clusters as inhibitors of type-1 fimbriae-mediated adhesion of Escherichia coli: structural variation and biotinylation," Journal of the Chemical Society-Perkin Transactions 1, pp. 823-831, 2001.

239. A. K. Sanki and L. K. Mahal, "A one-step synthesis of azide-tagged carbohydrates: Versatile intermediates for glycotechnology," Synlett, pp. 455-459, 2006.

240. S. Sen Gupta, J. Kuzelka, P. Singh, W. G. Lewis, M. Manchester, and M. G. Finn, "Accelerated bioorthogonal conjugation: A practical method for the Ligation of diverse functional molecules to a polyvalent virus scaffold," Bioconjugate Chemistry, vol. 16, pp. 1572-1579, 2005.